THE CRUSTAL AND UPPER MANTLE SHEAR WAVE VELOCITY STRUCTURE BENEATH EASTERN TURKEY USING INVERSION OF SURFACE WAVE DISPERSION

by

BİRSEN CAN

B.S., Geophysical Engineering, İstanbul Technical University

Submitted to

Boğaziçi University

Kandilli Observatory and Earthquake Research Institute

in partial fulfillment of

the requirements for the degree of

Master of Science

in

Geophysics

Boğaziçi University

2006

ACKNOWLEDGEMENTS

I dedicate this dissertation to those who have been with me on this thesis, helping me, supporting me and encouraging me. I would like to express my special thanks to my adviser Prof. Dr. Cemil Gürbüz, for his guidance throughout this study, giving me the opportunity to study this subject and for his contributions to this thesis. I also thank to the members of my Committee.

I thank all the faculty members, staff and students of the Boğaziçi University Department of Geophysics for their dedication, friendship and support. Their strong support and patience was very crucial for finishing my study. Thanks for sharing with me these years. I thank to Fatih Bulut, Tülay Kaya and Özlem Kurtuluş for being my friend and for their valuable advices. To Tuna Eken, for those afternoons sitting around a cup of coffee and discussing seismology. To Korhan Umut Şemin, Tuğçe Afacan Ergün and Doğan Aksarı for helping me when I needed. The final outcome documented here has benefited from such an enthusiastic exchange of scientific views of all of them. I must recognize their valuable comments and reviews.

Finally, nothing I can say would be enough to express my appreciation to my family for their concern and encouragement in realizing this goal. I shall always remain grateful to my father, mother and brother who motivated me for this career.

ABSTRACT

In this study, shear wave velocity structure of the crust and upper mantle across a portion of Eastern Turkey was obtained with one station method, using group and phase velocity dispersion of fundamental mode Rayleigh and Love waves.

The S wave velocity structure of the Eastern Turkey is estimated beneath the 29 broadband seismological stations that were deployed during the 1999/2001 ETSE experiment.

Rayleigh wave phase velocity is measured between 10 and 85 second periods. Phase velocity is 2.75 km/s for 10 second period and it is 3.9 km/s for 85 second period. On the other hand, Love wave phase velocity is measured between 10 and 50 second periods. Phase velocity is 2.8 km/s for 10 second period and 4.40 km/s for 50 second period.

According to the results of S wave velocity inversion, it is found that; between 20 and 30 km depth there is a low velocity layer, which has S wave velocity of approximately 3.4 km/s. The thickness of the crust is calculated as 45 km. S wave velocity, gradually increases between 30 km and 45km.

ÖZET

Bu çalışmada, Doğu Anadolu Bölgesi'nin bir bölümünün kabuk ve üst manto S dalgası hız yapısı, tek istasyon yöntemi ile, Rayleigh ve Love dalgası esas modu grup ve faz hızı dispersiyonu kullanılarak elde edilmiştir.

Doğu Anadolu Bölgesi'nin S dalgası hız yapısı, 1999 / 2001 yılları arasında ETSE deneyi sırasında yerleştirilmiş 29 adet sismolojik istasyon ile hesaplanmıştır.

Rayleigh dalgası faz hızı 10 ile 85 saniye periyotları arasında ölçülmüştür. Faz hızı 10 saniye periyodu için 2.75 km/s ve 85 saniye periyodu için 3.9 km/s 'dir. Diğer taraftan, Love dalgası faz hızı 10 ile 50 saniye periyotları arasında ölçülmüştür. Faz hızı 10 saniye periyodu için 2.8 km/s ve 50 saniye periyodu için 4.40 km/s 'dır.

S dalgası hızı ters çözümleri sonuçlarına göre, 20 ile 30 km derinlikleri arasında, S dalgası hızı yaklaşık olarak 3.4 km/s olan, bir düşük hız zonu vardır. Kabuk kalınlığı 45 km olarak ölçülmüştür. S dalgası hızı, 30 ile 45 km arasında kademeli olarak artmaktadır.

TABLE OF CONTENTS

Page No

LIST OF FIGURES

Page No

LIST OF TABLES

Page No

1. INTRODUCTION

1.1. Introduction

In this study, shear wave velocity structure of the crust and upper mantle across a portion of Eastern Turkey was obtained, with one station method, using group and phase velocity information from the dispersion of fundamental mode Rayleigh and Love waves.

Delineation of elastic, or velocity, structure of the Earth has long been a goal of the seismologists. Knowledge of seismic velocity structure of the crust and the upper mantle is important for several reasons. These include; accurate location of earthquakes and understanding them, determination of the composition and thickness of the layers of the earth and origin of them and improvement of the ability to discriminate nuclear explosions from earthquakes and interpretation of large scale tectonics.

Among the oldest and most fundamental problems in seismology are determining the velocity depth relation accurately, understanding the nature of discontinuities within the Earth, and translating this information into knowledge of the materials that constitute the interior of the earth. There are large variations in fundamental properties such as crustal and upper mantle velocity structure and the depth to the lithospheric / asthenospheric boundary.

The Eastern Anatolian region is important because it is one of the most seismically active regions of the world. This study is a step towards determination of the shear wave velocity structure of the crust and uppermost mantle of a portion of this region.

In this present work, group and phase velocity dispersion curves for fundamental mode Rayleigh and Love waves were obtained from the events recorded with the Eastern Turkey Seismic Experiment (ETSE) network. The lithospheric structure of the Eastern Turkey is estimated beneath the 29 broadband seismological stations that were deployed during the 1999 / 2001 ETSE experiment.

Chapter 1 introduces the previous studies, geology and tectonics of Eastern Turkey. Chapter 2 gives an overview on surface waves and their dispersion properties. In Chapter 3, the theoretical bases for the group velocity measurement; Multiple Filter Technique and Phase Matched Filter Technique, and (p-w) stacking are introduced. Then, Chapter 4 is concerned with the theory of inversion of dispersion curves. Chapter 5, presents the surface wave analysis and results, respectively. Finally, in Chapter 6 results are discussed.

The purpose of this dissertation is to obtain the S wave velocity distribution with depth at places, defined by the location of a temporal broadband array deployed during the ETSE experiment. The results may provide new insights that further researchers can use to advance our understanding of the origin and evolution of the Anatolian Plateau, as well as obtaining a S wave velocity model of a portion of the region.

1.2. Previous Studies

Studies related to the ETSE data comprises a wide variety of techniques for imaging and understanding earth structure and evolution, including high temperature geochemistry, seismic tomography, seismic anisotropy, waveform modeling and seismotectonic studies. The results of these studies yield a clear picture of the lithospheric structure and deformation beneath the Northern Arabian Plate and the Anatolian Plateau. This picture and its interpretation are critical to improving our understanding of how continental collision works.

Hypocentral locations and the crustal model were tested and calibrated by using a 12 ton controlled source explosion that took place in Eastern Turkey on June 5, 2001 (Gürbüz et al., 2004). The travel time data from this explosion was used to obtain average crustal structure and site correction terms for the stations.

ETSE data was also used to locate local and regional events (Türkelli et al., 2003). From this study all hypocenter locations were classified into four different categories based on the reliability of the locations.

The findings show that the entire region is seismically very active. The seismic activity clusters along the North and East Anatolian Faults. It was observed that the EAFZ seismic activitiy continues into the easternmost portion of the Anatolian Plateau. The hypocenters of well located events indicate that there were no subcrustal earthquakes in Eastern Anatolia. The majority of earthquakes occured in a depth range between 2-10 km. The deepest event that was located was 32 km on the Bitlis Suture Zone. A correlation between active faults and epicenter locations was found (Türkelli et al., 2003).

The crustal structure of Eastern Turkey has also been analyzed using receiver functions obtained from the teleseismic recordings (Zor et al.,2003). In this study, the receiver functions were analyzed in order to obtain S wave velocity structure.

No significant crustal root beneath the western portion of the array was found, but some evidence of crustal thickening in the north was noticed. The crust thickens from 44 km in the southern part of the Bitlis Suture Zone to 50 km towards the northern end of the array in the vicinity of the North Anatolian Fault. A low velocity zone was found in the crust beneath the middle part of the array where the crustal thickness is around 46-48 km. In the eastern part of the array crustal thickness increases from the southern tip of the array and it is 40 km to the middle section of the array where the thickness reaches 48 km. The average crustal P wave velocities are higher in the east and reach 6.25-6.40 km/s. The crustal thickness in the Arabian Plate, south of the Bitlis Zagros Suture Zone is between 38-45 km. with the highest average velocities observed (6.40-6.60 km/s) (Zor et al., 2003).

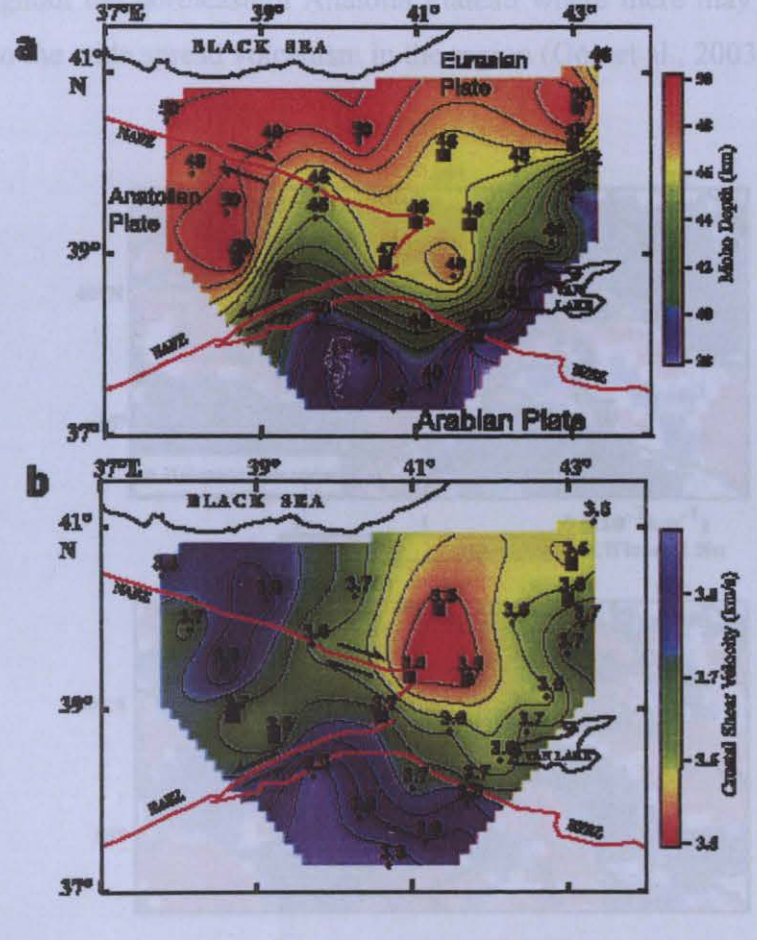

Figure 1.1. Maps showing (a) the Moho depth variation in km (contour interval is 1 km) and (b) the average crustal shear velocity in km/s (contour interval is 0.04 km/s) for each station. Black squares indicate stations which may have a low velocity layer. Red lines indicate the three plate boundaries (Zor et al.,2003).

During the study of the propagation characteristics of regional shear waves, Sn and Lg, have been used to constrain lithospheric structure and provide insights into the ongoing tectonics of the Eastern Anatolia (Gök et al., 2003). The propagation efficiencies of Sn and Lg phases were examined and ranked by their amplitude and frequency content. Attenuation maps are then tomographically constructed using the ranks of propagation efficiency.

Results show that Sn is not observed in Eastern Turkey while highly attenuated for paths that cross the Dead Sea Fault Zone. Efficient Sn along the Zagros fold and thrust belt has been observed. Results are consistent with there being a region of thin hot lithospheric mantle beneath the Anatolian and Iranian plateaus. Lg is observed to be less efficient in the relatively stable Arabian platform and for paths that cross the Dead Sea fault zone. Lg is blocked throughout the northeastern Anatolia Plateau where there may be partial melt in the crust due to the wide spread volcanism in the region (Gök et al., 2003).

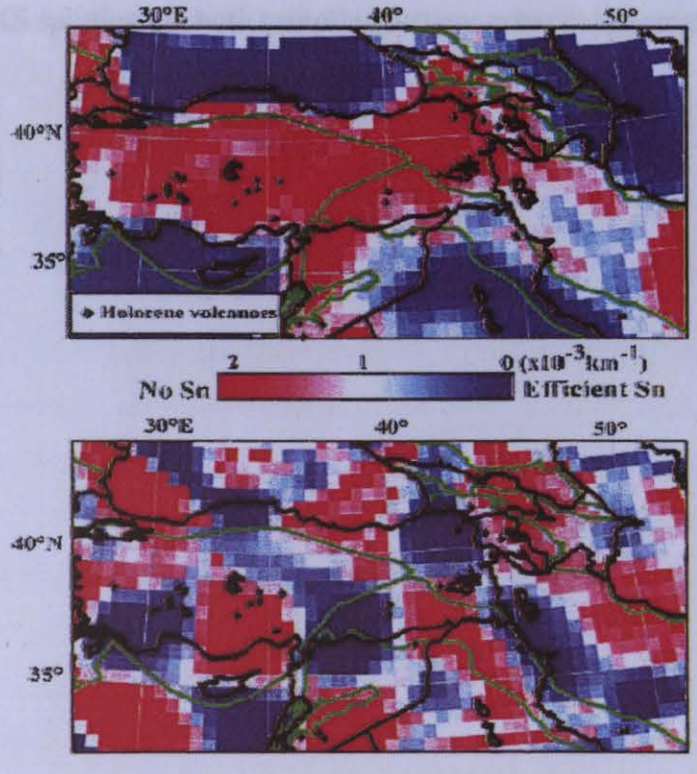

Figure 1.2. (a) Map showing Sn efficiency tomography results. Green lines are major tectonic boundaries and coast lines, black lines are national boundaries. (b) Resolution test using a synthetic checkerboard for extinction path length of 350 km (Q = 100) (Gök et al., 2003).

In the Pn study, Pn wave velocity and anisotropy beneath the Arabian, Eurasian and African plates' junction have been mapped (Al-Lazki et al., 2003).

Two types of low Pn velocity anomalies have been found. A broader scale (~500 km) low Pn velocity zone (< 8.0 km/s) underlies regions within and nearby the Arabian Plate boundaries and beneath most of the Anatolian Plate. Smaller scale (~200 km) very low Pn velocity (< 7.8 km/s) zones were found to underlie the Lesser Caucasus, southern Syria and northern Jordan, the Isparta Angle, central Turkey and the northern Aegean Sea backarc region. The broad low velocity zone beneath İran, Eastern Turkey and the Anatolian plate may be in part the result of subducted Tethyan oceanic lithosphere beneath Eurasia. In Eastern Anatolia, they observed a localized very low Pn velocity zone. The mapped Pn azimuthal anisotropy also showed coherency in orientations in the same zone (Al-Lazki et al.,2003). Moreover, the Pn anisotropy orientations were similar to observed orientations of polarization anisotropy based on shear wave (SKS) splitting analysis (Sandvol et al., 2003). This implies a thinned or absent mantle lid in Eastern Anatolia and that Pn anisotropy and SKS splitting are both sampling asthenospheric deformation.

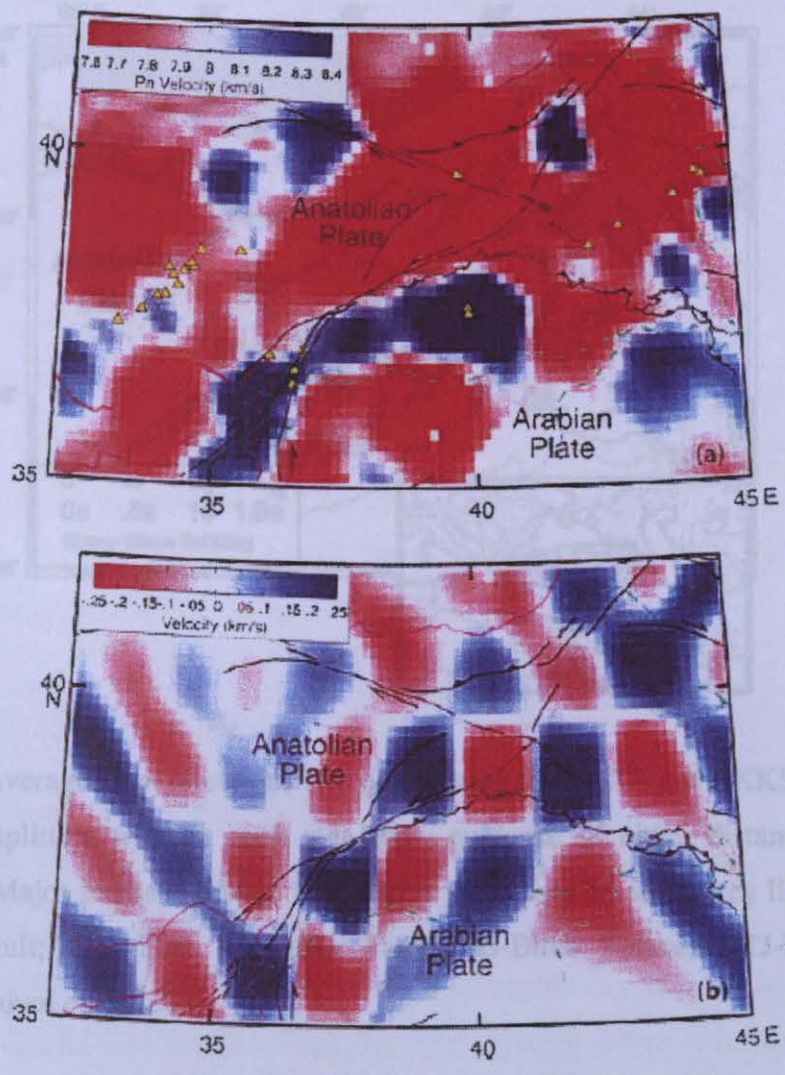

Figure 1.3. (a) Map showing tomographic image of Pn velocity using only the data picked and read. The upper bounds of high Pn velocity zone along the EAF and the eastern BS are used to define the northern extent of the Arabian plate boundary. (b) A map showing 1.5 x 1.5 checkerboard test results inverted using the same stations and events distribution. The best resolution is along the EAF, eastern BS zones and at the intersection zone between the EAF and NAF zones (Al-Lazki et al.,2003).

Shear wave splitting analysis (Sandvol et al.,2003) indicates that there is no significant change in upper mantle polarization anisotropy across the Bitlis suture or the EAFZ. There also appears to be some correlation between very slow mantle lid velocity and large splitting lag times across the eastern portion of the Anatolian Plateau (Sandvol et al.,2003).

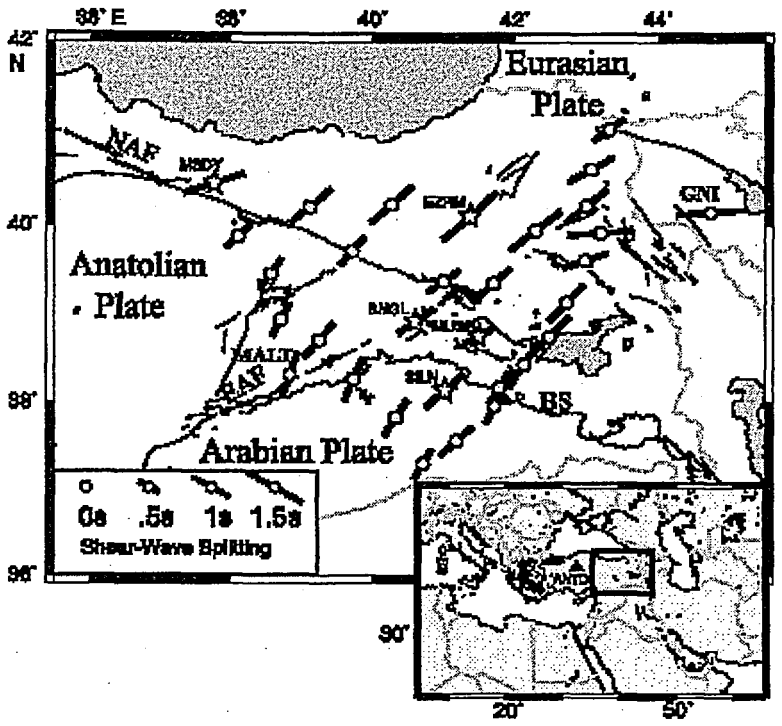

Figure 1.4. Averaged fast directions and delay times from SKS and SKKS measurements. Shear wave splitting with an open star show evidence of either distance or azimuthal dependence. Major Faults and plate boundaries are shown by solid grey lines. NAF-North Anatolian Fault; EAF-East Anatolian Fault; BS-Bitlis Suture; KTJ-Karlıova Triple Junction (Sandvol et al.,2003).

Source properties of small to moderate magnitude events in Eastern Turkey were studied using waveform data (Örgülü et al.,2003). A data set of fault plane solutions was obtained for the earthquakes. Most of the events studied had strike slip mechanisms in agreement with nearby local fault structures. Reverse mechanisms were restricted to certain areas, such as the Eastern Anatolian Plateau and southwest of the Karlıova Junction along the Arabian Plate boundary (Örgülü et al., 2003). Results indicate a difference in the deformational style east and west of the Karlıova Junction. This results in internal deformation in the east and westward extrusion of the Anatolian Plate with no or very little internal deformation in the west. Results also suggest that in Eastern Turkey, most of the collision is taken up by strike slip faults of varying types and sizes (Örgülü et al., 2003).

A new model for magma genesis was proposed which is slab steepening and breakoff beneath a large subduction accretion complex (Keskin, 2003). According to this model, a northward subducting oceanic lithosphere beneath the Eastern Anatolian Accretionary

Prism gets steepened and detached from the continental lithosphere of the Bitlis Pötürge Massif, following the continent accretionary complex collision. This brings the asthenospheric mantle in contact with the accretionary complex at shallow depths, resulting in rapid regional uplift and extensive melting which leads to collisional volcanism (Keskin, 2003).

According to Şengör, et al.,2003, the East Anatolian High Plateau is a region exhibiting active diffuse N-S shortening and widespread Pliocene to recent volcanism. Most of the East Anatolian High Plateau is devoid of mantle lithosphere. The absence of mantle lithosphere is ascribed to break off of northward subducted slab beneath the prism and the widespread volcanism to melting its lower levels because of direct contact with hot asthenosphere. The East Anatolian High Plateau is supported not by thick crust, but by hot mantle (Şengör, et al.,2003).

1.3. Tectonics and Geology of Eastern Turkey

1.3.1. Tectonics of Eastern Turkey

The East Anatolian High Plateau is a region of average ~2 km elevation exhibiting active diffuse N-S shortening and widespread Pliocene to recent volcanism. The results of ETSE shows that most of the East Anatolian High Plateau is devoid of mantle lithosphere. The absence of mantle lithosphere is because of the break off of northward subducted slab beneath the prism. Because of direct contact with hot asthenosphere there is widespread volcanism (Figure 1.5). The East Anatolian High Plateau is thus supported not by thick crust, but by hot mantle (Şengör, et al.,2003).

The Bitlis suture / thrust zone and the East Anatolian Fault system (EAF) mark a distributed, irregular and young continental collision zone. The NAF and EAF have been active since the Miocene (Allen,1975; Ambraseys,1970; Barka and Kadinsky-Cade,1988) and are associated with large pull apart basins, such as the Karlıova Basin located at the junction of these two fault systems (Hempton, 1985) (Figure 1.5). The area to the east of Karlıova triple junction is characterized by a N-S compressional tectonic regime and conjugate strike slip faults of dextral and sinistral character, mostly paralleling the NAF and EAF which are the dominant structural elements of the region.

1.3.2. Geology of Eastern Turkey

The Anatolian Iranian Plateau extends from Eastern Anatolia to Eastern Iran, and typically has an elevation of about 1.5–2 km in Eastern Anatolia. The basement of the Anatolian Iranian Plateau is made up of micro continents, accreted to each other during the Late Cretaceous to Early Tertiary. These micro continents are separated from each other by ophiolite belts and accretionary complexes. Five different tectonic blocks are recognized in North Eastern Anatolia; The Eastern Rhodope Pontide fragment in the northwest of the region. It underlies the south western and north eastern parts of the Erzurum Kars Plateau. The Northwest Iranian fragment. The eastern part of the Erzurum Kars Plateau (Horasan, Aladağ, Kagızman, Kars areas and Mt.Ararat) overlies this tectonic block (Keskin et al., 1998). The Eastern Anatolian Accretionary Complex in the middle of the region located between the Aras River and the Bitlis Pötürge Massif, The Bitlis Pötürge unit which is exposed along the Taurus belt, and Autochthonous units of the Arabian continent or foreland. Except for The Eastern Anatolian Accretionary Complex, all the tectonic blocks correspond to the mentioned micro continents.

The Eastern Anatolian Accretionary Complex forms a 150-180 km wide, NW-SE extending belt in the middle of the region. It represents the remnant of a huge subduction accretion complex formed on a north dipping subduction zone located between the Rhodop Pontide in the north and the Bitlis Pötürge microcontinent in the south in a period between the Late Cretaceous and Oligocene (Şengör et al., 2003).

An ophiolitic melange of Late Cretaceous age and Paleocene to Late Oligocene flysch sequences incorporated into the ophiolitic melange as north dipping tectonic slices. These flysch slices become younger from north to south and shallower from the Cretaceous to the Oligocene (Şengör et al., 2003). This observation is consistent with the polarity of the subduction zone that is thought to have created the Eastern Anatolian accretionary prism by underthrusting.

Collision related volcanic units, unconformably overlie both the five tectonic blocks and the marine deposits, masking the basement units over great distances.

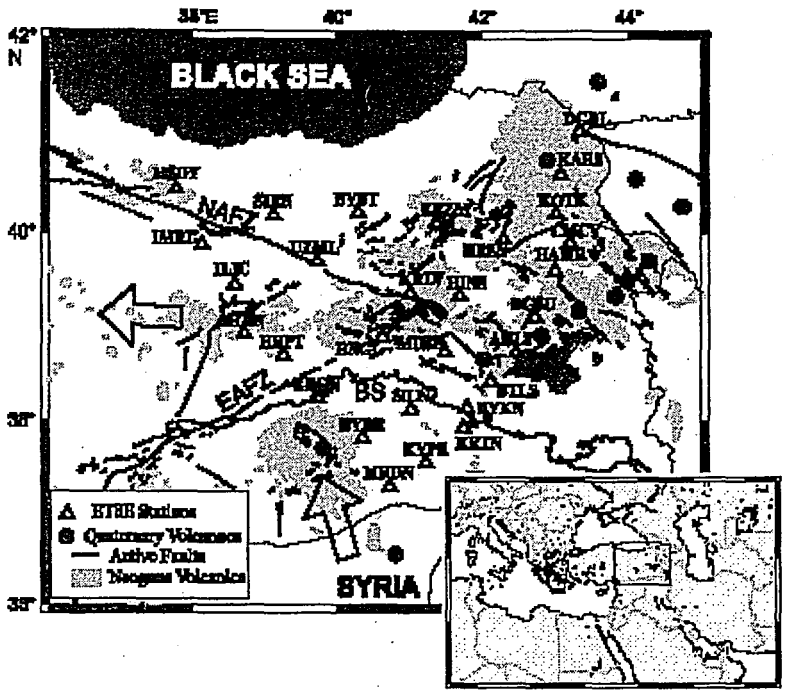

Figure 1.5. Map showing the 29 three component PASSCAL broadband stations (triangles) used in the Eastern Turkey Seismic Experiment (ETSE). Filled circles indicate Quaternary volcanoes and the gray shaded area shows Neogene volcanics. Arrows indicate the direction of the plate and fault motions. BS, NAFZ and EAFZ are the Bitlis Zagros Suture Zone, North Anatolian Fault Zone and East Anatolian Fault Zone, respectively (Zor et al.,2003).

2. SURFACE WAVES AND EARTH STRUCTURE

2. 1. Introduction

Knowledge of the Earth's structure with depth is a challenging problem. The almost unique source of information for structures located at intermediate and deep depths comes from the record of seismic signals. Among these, surface waves play a principal role. As its name states, surface waves are signals associated with the presence of a free surface (or, more generally, a discontinuity surface). They are characterized by the simultaneous interaction of wave fronts with a traction free boundary as a response of the layered structure. Surface waves result from different body wave phases interacting at the free surface. At the Earth's surface, both incident and reflected seismic waves instantaneously coexist, and the entire motion involves the sum of their respective amplitudes.

Their amplitudes decrease inversely with the distance from the source, in contrast to the quadratic decrease of P and S wave amplitudes. Surface waves travel more slowly and decay less with distance than body waves. This results from the 2D geometric spreading of the surface wave relative to the 3D spreading that affects the body waves.

For this reason, surface waves form the longest and the strongest portion of the seismic records excited by explosions and shallow earthquakes. Surface wave motions are generally the strongest and the largest of any arrivals recorded on the seismogram. The longer the wavelength of a surface wave the deeper it samples the Earth's structure, and the faster is its propagation velocity.

Large earthquakes excite surface waves that appear as the highest amplitude waves on a broadband seismogram. At teleseismic distances they provide some of the best constraints on the Earth's crust and upper mantle structure.

Within the surface waves, information about the Earth's structure is encoded in the form of their dispersion curves. The data are the dispersion curves and the model parameters are the elastic constants and density.

There are two types of surface waves known as Love and Rayleigh waves. For both Rayleigh and Love waves, the displacement amplitude decays exponentially with depth in the half space. They provide information on the properties of the crust and upper mantle in the various regions of the Earth (Mitchell and Herrmann, 1979). Both Love and Rayleigh waves

are used to estimate shear wave velocity variations in the crust and upper mantle. Because of their sensitivity to shear wave velocity structure, they provide information that is often difficult to obtain from body wave studies.

The study of surface waves covers long paths and yields information on a range of depths in the upper mantle that may be difficult to determine by body wave techniques in the presence of a low velocity channel (Brune and Dorman, 1963).

2.2. Rayleigh and Love Waves

The solution of the wave equation in a stratified media has been studied for the presence of seismic waves that propagate with specific characteristics. A waveguide is produced when a ray strikes a reflecting horizon at post critical angels, then all the energy is trapped within this waveguide.

In 1887, Lord Rayleigh found a particular solution of the wave equation in an elastic body, which corresponds to a wave that propagates along the surface of the body. Twenty two years later, Love; in 1911 showed that another particular solution exists in a body in which a low velocity superficial layer rests on top its bulk (Love, A. E. H., 1911).

In fact, a solution for which the displacement field is larger at the free surface than within the body and whose particle motion is transversely polarized, corresponds to the Love wave. Love waves are formed by the constructive interference of reflected SH wave energy of reverberations trapped, when the velocity structure turns the energy toward the surface, at the free surface due to internal layering of the earth, (between the surface of the structure and a half space) whose S wave velocity is higher than that of the overlying materials. Love waves require a wave guide to exist. The SH component of the S wave has displacements parallel to the surface and can only have total reflections from the free surface (Lay and Wallace,1995).

Because Love wave particle motion is parallel to the surface, a complete separation of Rayleigh and Love wave surface motion occurs in isotropic media. Love wave dispersion values are measured on the transverse components. Love waves travel faster than Rayleigh waves and arrive ahead of the Rayleigh wave slightly before them. Love waves are more sensitive to lateral structural heterogeneities than are Rayleigh waves (Lysmer and Drake, 1971) and they are more greatly affected by scattering and multipathing than the latter.

Rayleigh waves are obtained by looking for the solution of the wave equation for which amplitudes decrease with depth, and transverse displacement vanishes at the free surface.

Such solution corresponds to an elliptically polarized wave whose particle motion changes from retrograde at the surface to prograde somewhere at depth. Rayleigh particle motion is retrograde elliptical in the direction of propogation to a depth L/5 (L is the wavelength of the Rayleigh wave) where then it goes to zero. Below this depth, elliptical particle motion becomes prograde.

Fundamental mode Rayleigh waves travel along the surface with a retrograde elliptical particle motion at the surface and change to prograde with depth, passing through a node when there is no radial motion at all. Rayleigh waves can exist in a homogeneous half space, as they are the result of the interaction of incident P and SV plane wave interference at the free surface and travel along the surface. Rayleigh waves also exist in a multilayered media. A Rayleigh wave is found in the vertical plane with no tangential motion. Rayleigh waves arrive on the vertical and radial components, so Rayleigh wave dispersion curves are obtained with the vertical and radial seismograms while Love wave dispersion values were measured on the corresponding transverse components. Rayleigh and Love waves are known to be sensitive mainly to the shear wave velocity.

For both, Love and Rayleigh waves, the displacement amplitude decays exponentially with depth in the half space and the solution exists as a fundamental mode and a finite number of modes for which amplitudes become zero, before the entire wavefield vanishes, at a number of points (nodes) that is equal to the overtone number minus one. Modes other than the fundamental are called higher modes, and they are characterized by traveling faster than the fundamental mode.

2.2.1. Rayleigh Waves

Extrapolating the form of a plane wave to the case in which some of the direction cosines; $\hat{k}_x$, $\hat{k}_y$, $\hat{k}_z$ are greater than zero, leaving the relation $\hat{k}_x^2+\hat{k}_y^2+\hat{k}_z^2=1$ unchanged, an evanescent form for the displacement fields is obtained;

$$\vec{u}_P = A\left(a_x \pm i\gamma_\alpha \hat{a}_z \right)\exp\left[\mp(w/c)\gamma_\alpha z\right]\exp\left[iwt - i(w/c)x\right] \qquad (2.1)$$

$$\vec{u}_{SV} = B\left(\mp i\gamma_\beta \hat{a}_x + \hat{a}_z\right)\exp\left[\mp(w/c)\gamma_\beta z\right]\exp\left[iwt - i(w/c)x\right] \tag{2.2}$$

$$\vec{u}_{SH} = C\hat{a}_y \exp\left[\mp(w/c)\gamma_\beta z\right]\exp\left[iwt - i(w/c)x\right] \tag{2.3}$$

where;

$$\gamma_\alpha = \left(1 - \frac{c^2}{\alpha^2}\right)^{1/2} \tag{2.4}$$

and

$$\gamma_\beta = \left(1 - \frac{c^2}{\beta^2}\right)^{1/2} \tag{2.5}$$

There is only a regular solution that satisfies the free surface boundary condition. This solution is a combination of evanescent P and SV waves traveling along the x axis;

$$\vec{u} = A\left(\overrightarrow{a_x} - i\gamma_\alpha \overrightarrow{a_z}\right)\exp\left[-(w/c)\gamma_\alpha z\right]\exp\left[iwt - i(w/c)x\right] \tag{2.6}$$

$$+B\left(i\gamma_\beta \overrightarrow{a_x} + \overrightarrow{a_z}\right)\exp\left[-(w/c)\gamma_\beta z\right]\exp\left[iwt - i(w/c)x\right]$$

This will represent waves traveling in the positive x direction with phase velocity c. Its evanescent character can be seen in the decaying exponentially with increasing z (provided $\gamma_\alpha, \gamma_\beta$ are real), that is, $c < \beta$. Applying the boundary condition on the free surface (Ben-Menahem and Singh, 1981), the relations are obtained;

$$2\gamma_\alpha A + i\left(2 - \frac{c^2}{\beta^2}\right)B = 0 \tag{2.7}$$

$$-i\left(2-\frac{c^2}{\beta^2}\right)A+2\gamma_\beta B=0 \tag{2.8}$$

and therefore, the condition;

$$\left(2-\frac{c^2}{\beta^2}\right)^2-4\gamma_\alpha\gamma_\beta=0 \tag{2.9}$$

This condition is known as the Rayleigh equation. It can be shown that, provided that, $\beta<\alpha$, a $c<\beta$ exists (and independent of w) that satisfies the Rayleigh equation.

A real representation of a Rayleigh wave configuration can be written as;

$$\vec{u}=A\left\{\hat{a}_x D_x(z)\sin\left[wt-(w/c)x\right]+\gamma_\alpha \hat{a}_z D_z(z)\sin\left[wt-(w/c)x\right]\right\} \tag{2.10}$$

with depth functions $D_x(z)$ and $D_z(z)$ of the form;

$$D_x(z)=\exp\left[-(w/c)\gamma_\alpha z\right]-\left(1-\frac{c^2}{2\beta^2}\right)\exp\left[-(w/c)\gamma_\beta z\right] \tag{2.11}$$

$$D_z(z)=-\exp\left[-(w/c)\gamma_\alpha z\right]+\left(1-\frac{c^2}{2\beta^2}\right)^{-1}\exp\left[-(w/c)\gamma_\beta z\right] \tag{2.12}$$

They are inhomogeneous plane waves with vanishing amplitude at greater and greater depths. Their polarization can be described as retrograde elliptical at the surface. At a depth $h=1-\left(c^2/\beta^2\right)$, where $D_x(z)$ goes through a zero, they change this behaviour to prograde elliptical.

If the simple case of a single layer over a half space model is considered, the generalization of the Rayleigh wave configurations to this case gives rise to new phenomenology. The different solutions can be classified into branches $(M_1, M_2, ...)$ and these branches into modes $(M_{11}, M_{12}, ..., M_{21}, ...)$ (Ben-Menahem and Singh, 1981). All these

solutions have a decaying behaviour in the half space. The part of the solutions inside the layer can have oscillatory behaviour or exponential (growing and decaying) behaviour. The "M_1 branch" term indicates oscillatory symmetric modes of the free surface. The energy of these configurations is concentrated mainly in the free surface. On the other hand, "M_2 branch" indicates antisymmetric modes of the free surface. In this case the energy is concentrated mainly in the interface. Within each branch, there are different solutions indicated by the symbols M_{11}, M_{12}, M_{13} and M_{21}, M_{22}, M_{23}. M_{11} and M_{21} are the fundamental modes of branch M_1 and M_2 respectively.

In this study, we will concentrate on the fundamental mode of the branch $M_1\left(M_{11}\right)$, that is the mode with major energy concentration in the free surface.

The most important feature of all these modes is that, on them the phase velocity c depends on the frequency w. This gives a dispersive character to the Rayleigh waves. The specific form of $c(w)$ for each mode depends on depth and properties of the layer with respect to the half space. In more general situations, one can have an earth model with multiple layers or even a continuously changing structure in depth. In these cases too, $c(w)$ will depend on the specific structure in depth of the earth. This is the crucial factor in this thesis. Information about the structure of the earth will be extracted by looking at the dispersion curves of Rayleigh and Love waves.

2.2.2. Love Waves

In a half space earth model there is no possibility of having an evanescent configuration. From equations (2.1), the displacement at any point of the medium is;

$$\vec{u}_{SH} = C\,\hat{a_y} \exp\left[\mp(w/c)\gamma_\beta z\right]\exp\left[iwt - i(w/c)x\right] \tag{2.13}$$

This confines the energy to propagate along the free surface with exponential decay away from the $z=0$. The stress free boundary condition at the surface $z=0$ yields;

$$\mu C(w/c)\gamma_\beta = 0 \tag{2.14}$$

Therefore, $C=0$ implies that in the case of a homogeneous half space medium Love waves do not exist.

However when a half space covered with a homogeneous layer of thickness H is considered. The free surface is taken as the plane $z=0$. From equations;

$$\bar{u}=\begin{cases}\hat{a}_y\left\{A\exp\left[-i(w/c)\eta_1 z\right]+B\exp i(w/c)\eta_1 z\right\}\times\exp\left[iwt-i(w/c)x\right] \\ (0<z<H) \\ C\hat{a}_y\exp\left[-(w/c)\gamma_2 kz\right]\times\exp\left[iwt-i(w/c)x\right] \\ (z>H)\end{cases} \tag{2.15}$$

where ;

$$\eta_1=\left(\frac{c^2}{\beta_1^2}-1\right)^{1/2} \tag{2.16}$$

and

$$\gamma_1=\left(1-\frac{c^2}{\beta_1^2}\right)^{1/2} \tag{2.17}$$

The traction at the free surface must be zero and the displacements and the tractions must be continuous across the interface. These conditions yield (Ben-Menahem and Singh, 1981);

$$A-B=0 \tag{2.18}$$

$$A\exp\left[-i(w/c)\eta_1 H\right]+B\exp\left[i(w/c)\eta_1 H\right]-C\exp\left[-(w/c)\gamma_2 H\right]=0 \tag{2.19}$$

$$A\exp\left[-i(w/c)\eta_1 H\right]-B\exp\left[i(w/c)\eta_1 H\right]+iC\frac{\mu_2\gamma_2}{\mu_1\gamma_1}\exp\left[-(w/c)\gamma_2 H\right]=0 \tag{2.20}$$

The solution of these equations leads to a dispersion relation, that gives the phase velocity as a function of the frequency (or period);

$$\tan\left((w/c)\eta_1 H\right)=\frac{\mu_2\gamma_2}{\mu_1\gamma_1} \tag{2.21}$$

Using the expressions of η and γ;

$$\tan\left(Hw\sqrt{\frac{1}{\beta_1^2}-\frac{1}{c^2}}\right)=\frac{\mu_2\sqrt{1/c^2-1/\beta_2^2}}{\mu_1\sqrt{1/\beta_2^2-1/c^2}} \tag{2.22}$$

and therefore a dispersion curve is $c=c(w)$.

It is clear that $c<\beta_2$, because otherwise, $\vec{u}$ will not tend to go zero as $z\to\infty$. Furthermore, if η_1 is purely imaginary, equations (2.16 and 2.17) becomes;

$$-\gamma_1\tanh\left((w/c)\gamma_1 H\right)=\left(\frac{\mu_2}{\mu_1}\right)\gamma_2 \tag{2.23}$$

which has no relevant solutions for $w>0$ because the two sides are of opposite signs. Therefore, η_1 is real, (i.e $\beta_1<c$). Then $\beta_1<c<\beta_2$, which implies that the shear wave velocity in the layer has to be less than the shear wave velocity in the half space. Only in this case (typical in real situations) Love waves occur.

Equation (2.21) or (2.22) is a transcendental equation. For any value of c in the interval $\beta_1<c<\beta_2$, it determines a set of possible values of $(w/c)\eta_1 H$, the first in the interval $(0,\pi/2)$, the second in the interval $(\pi,3\pi/2)$, and so on. As in the dispersive case of Rayleigh waves, different modes of propagation occurs. The dispersion equation shows that the phase velocity, c, of Love waves is not a fixed constant but depends on the particular value of w. Waves with different frequencies will have, in general, different phase velocities.

2.3. Phase and Group Velocity

In the Earth, faster materials are usually deeper than slower materials, as evidenced by the increasing character of surface wave phase velocities with period. In a layered half space earth model, (or with a continuously varying structure in depth), the structural $\lambda(z)$ and $\mu(z)$ can be encoded in the dispersive phase velocities; $c_R(w)$ and $c_L(w)$ of inhomogeneous plane Rayleigh and Love waves, respectively. Taking the traveling phase of surface inhomogeneous plane wave solutions;

$$\exp\left[iwt - i\left(w/c\right)x\right] \tag{2.24}$$

its wave number is;

$$k = \frac{w}{c(w)} \tag{2.25}$$

and from here, the relation is;

$$w = w(k) \tag{2.26}$$

From this relation, the phase velocity can be defined as;

$$c = w/k \tag{2.27}$$

The definition of group velocity is;

$$U = dw/dk \tag{2.28}$$

This definition can be written as;

$$\frac{1}{U(w)} = \frac{1}{c(w)} - \frac{w}{c^2(w)} \frac{dc(w)}{dw} \tag{2.29}$$

or

$$U(w) = c(w)\left[1 - \frac{w}{c(w)} \frac{dc(w)}{dw}\right]^{-1} = c(T)\left[1 - \frac{T}{c(T)} \frac{dc(T)}{dT}\right]^{-1} \tag{2.30}$$

If a plane wave is composed of the addition of a narrow Gaussian distribution of monochromatic waves around some fixed frequency w_0;

$$A = \int dk \frac{1}{\sqrt{2\pi}\sigma} \exp\left[-\left(\frac{k-k_0}{2\sigma^2}\right)\right] \exp\left[iw(k)t - ikx\right] \tag{2.31}$$

If the Gaussian function is narrow enough, the frequency can be approximated by a straight line;

$$w \approx w_0 + U(k_0)(k-k_0) \tag{2.32}$$

Then;

$$A = \int dk \frac{1}{\sqrt{2\pi}\sigma} \exp\left[-\left(\frac{k-k_0}{2\sigma^2}\right)\right] \exp\left[iw_0 t - ik_0 x\right] \exp\left[iU(k_0)(k-k_0 t) - i(k-k_0)x\right] \tag{2.33}$$

and integrating;

$$A = \exp\left[iw_0 t - ik_0 x\right] \exp\left[-\frac{\left[U(k_0)t - x\right]^2 \sigma^2}{2}\right] \tag{2.34}$$

A monochromatic plane wave is obtained, with frequency w_0 (the central frequency of the Gaussian distribution) and a phase moving at $c_0 = {w_0}/{k_0}$ velocity, modulated by a Gaussian envelope moving at a velocity $U(k_0)$, that is, at the group velocity for frequency w_0. The group velocity can be associated with the velocity of propagation of information by modulating a carrier frequency.

2.3.1. Phase Velocity

Surface waves in a stratified medium are characterized by having a frequency dependent velocity of propagation. The wave velocity at any of those frequencies is called phase velocity, and it describes the time difference of a peak or a trough as observed in two different points of the Earth's surface, separated a distance d, along the propagation path.

In general, phase velocity is a smooth function of frequency, so wave fronts with slightly different frequencies are expected to arrive to the station at slightly different times. However, as the wave fronts travel greater distances, the separation becomes larger and the waves spread out in a very particular fashion that characterize them and the path they are traveling. The phase velocity provides information on the long wavelength vertical averages of the shear wave velocity structure between any given station pair. The phase velocity of the surface waves has the advantage of being to first order a linear combination of the underlying 3D model (Nataf el al., 1986).

Measuring phase velocity is not always a simple task, as it involves the correct identification of a particular phase within the entire signal, and it requires a good knowledge of the phase of such signal at the source.

The observed phase of a seismic surface wave can be expressed as an initial phase from the source acted upon by a set of linear filters. Source phase, $\Phi_S(w)$, and observed phase, $\Phi_O(w)$, are related by;

$$\Phi_O(w) = \Phi_S(w) + \Phi_P(w) + \Phi_I(w) \tag{2.35}$$

where $w = 2\pi f$ (radian frequency), $\Phi_I(w)$ is the instrument phase and $\Phi_p(w)$ is the propagation phase. To estimate the phase velocity, the initial phase at the source, the origin time and the distance travelled must all be known. To calculate the initial phase, the faulting mechanism and the source depth must be known. The instrument response is known and can be removed when the seismogram is deconvolved to recover ground displacement. The propagation phase term depends on the phase velocity of the structure. The expression for the source and instrument corrected phase term is;

$$\Phi_p(w) = \frac{wr}{c(w)} \tag{2.36}$$

where;

$w = 2\pi f$ (radian frequency)

w = angular frequency

f = frequency

r = source receiver distance

$c(w)$ = phase velocity

Seismic sources usually excite a continuos spectrum of surface wave periods. Each harmonic component of an observed signal has a velocity, called phase velocity $c(w)$ defined by Dziewonski and Hales (1972) as the instantaneous velocity of the plane wave at a given frequency ;

$$c(w) = \frac{w}{k(w)} \tag{2.37}$$

where;

w = angular frequency

$w = 2\pi f$ (radian frequency)

f = frequency

$k(w)$ = wave number

$$k(w) = w / c(w) \tag{2.38}$$

For a given angular frequency (w), $c(w)$ depends on the medium parameters such as layer thickness (h), density (ρ), shear and compressional wave velocities (P and / or S).

Solving for the phase velocity, $c(w)$, introduces a $2\pi N$ uncertainty without changing the observed waveform. The $2\pi N$ term (N is a integer) represents the periodicty of the harmonic term in the phase velocities and is estimated using long period observations, which should converge to globally averaged values at long periods. (i.e estimated phase velocities are compared to reference velocities to determine the correct branch of the dispersion curve).

2.3.2. Group Velocity

The group velocity is the velocity associated with a packet of waves of a given frequency (Kovach, 1978). It is a dispersive characteristic where constructive patterns travel along the surface as wave packets.

An interesting phenomenon that occurs when waves at close frequencies travel at slightly different velocities is that, they mix together in a modulated trend whose frequency is the average of its constituents, and its envelope varies slower in amplitude with time. In such a case, the energy of the motion concentrates in packets that travel with a velocity known as the group velocity. It depends on the velocity of the individual waves and on how that velocity changes between them. Energy packets tend to separate with distance as they travel longer paths.

Wave disturbances with wide spectrum of periods interfere with each other producing constructive or destructive patterns that influence the total ground motion. Constructive patterns propagate along the surface as wave packets with well defined group velocities, which depend on the medium parameters and variation of phase velocity with frequency.

Group velocity is related to phase velocity with the equation;

$$U(w) = c(w) + k\frac{dc(w)}{dk} \tag{2.39}$$

where w is the angular frequency, $c(w)$ is the phase velocity, U is the group velocity, and k is the wave number;

$$k = wc(w)^{-1} \tag{2.40}$$

The group velocity, U, of a wave is defined by the angular frequency, w, and the wavenumber, k, as;

$$U = \frac{dw}{dk} \tag{2.41}$$

$$U = c + k\frac{dc}{dk} \tag{2.42}$$

where; c is the phase velocity.

When;

$k = \frac{w}{c}$ is subsituted ; (2.43)

$$\frac{dc}{dk} = \frac{dcdw}{dwdk} = \frac{dc}{dw}U \tag{2.44}$$

Then, at a particular frequency, the group velocity can be expressed as;

$$U = \frac{c}{1-(\frac{w}{c})(\frac{dc}{dw})} \tag{2.45}$$

Therefore, if the phase velocity dispersion, $c(w)$, is known across some frequency range, the group velocity, $U(w)$, can be easily calculated across that range (Larson and Ekstrom, 2001).

Group velocity is not a physical parameter of the medium, but a practical approach to the characterization of a dispersive signal. In addition to their simpler extraction from a seismogram, group velocities are slightly more sensitive to the medium parameters than phase velocities, which favors their use in a S wave velocity inversion study. Knowledge of the group velocity dispersion curve is useful by itself, as they may be used in inversion processes to obtain shear wave velocity structures (Keilis-Borok, 1986).

The group velocity provides information on the long wavelength vertical averages of the shear wave structure between any given station pair. Group velocities of surface waves are very useful for estimating the elastic properties of the Earth, and their variation both vertically and horizontally. Also, comparison of calculated and observed group velocities represents a test of the validity of a model.

Still, as those velocities can be regarded as the result of applying a smoothing filter acting on the actual structure of the Earth, some information is lost and only partial properties can be recovered by the study of those velocities.

2.4. Dispersion

When the elastic parameters vary with depth surface waves are dispersive, that is the velocity of propagation of a surface wave depends on the frequency considered. This phenomenon is called dispersion, because energy packets tend to separate with distance as they travel longer paths. Dispersion is observed in the frequency dependent travel times of surface waves, resulting from the increase of velocity with depth. In general, short period surface waves travel slower than long period waves. Long periods are more sensitive to the faster velocities found deeper part of the earth. Longer wavelengths penetrate deeper within the body, and so propagation velocities of surface waves are modified by the properties of the medium to a depth that increases with period.

Interpreting surface wave dispersion measurements provides an important method for determining the shear wave velocity variation in the Earth. Additionally, looking at Rayleigh

or Love wave dispersion curves separately is not plausible, especially in regions where anisotropy is significant.

Dispersion curves do not provide enough information to accurately constrain the geometry of deep structures. Surface wave dispersion depends upon the absolute averages of the model parameters rather than on their variation.

Dispersion curves are sensitive to the average velocity structure of the upper layers rather than to seismic discontinuities; therefore, they are very useful to obtain a picture of the Earth's interior.

Inversion of surface wave dispersion curves is used to obtain reasonable models of the S wave velocity distribution of the layers of the Earth. Surface wave dispersion measurements, for example, are very valuable in mapping the Earth's lateral heterogeneity (Ritzwoller and Levshin, 1998) through the use of teleseismic recordings.

In a homogeneous elastic half space with no damping, Rayleigh waves propagate along the surface of the body at a constant, frequency independent, phase velocity. For a homogeneous half space, the velocity of Rayleigh wave does not depend on frequency. In a layered or vertically heterogeneous half space, different frequency of surface waves propagate with different phase velocities and with different wavelengths.

All surface waves, except Rayleigh waves, in an isotropic half space, exhibit dispersion, with the apparent velocity along the surface depending on frequency (Lay and Wallace, 1995). Love waves are always dispersive because they require at least a low velocity layer over a half space to exist. Love wave dispersion contributes less information about the Earth structure than Rayleigh wave dispersion (Braile and Keller, 1975).

Both group and phase velocity are identical if the media is non dispersive and the seismic pulse that propagates outward from the source will travel without a change in shape. In contrast, when the media is dispersive, each frequency component will travel with its own characteristic velocity. Both phase and group velocity dispersion curves contribute generally the same information about the earth structure (Der et al., 1970; Wiggins, 1972). However, due to the nature of group velocity as it's beeing a differential of phase velocity, small perturbations in phase velocity show up as larger variations in group velocity.

The observed dispersion can be compared to theoretical dispersion to find the best fitting structure beneath an area of interest. The features of the sought model must satisfy the long wavelength constraints of the surface waves. Surface wave dispersion measurements constrain average of the absolute shear wave velocity that reach deeper structure with increasing period

(Julia et al., 2000). Dispersion curves has the averaging properties. A study of surface wave dispersion provides a much better determination of shear velocity structure compared to seismic refraction.

3. CALCULATION OF DISPERSION CURVES

3.1. Historical Development of Calculation of Dispersion Curves

Modern studies of surface waves and their application in structure interpretation were propelled by Haskell's (1953) matrix formulation of the multilayered system period equation, which made possible rapid and accurate computation of dispersion curves for complex models. Several studies on observations of surface waves are available for both global and regional models. Regional surface wave studies of the crust and upper mantle were reviewed by Kovach (1966); Ewing et al. (1972); Seidel and Müller (1977).

The peak and trough method, which is based on careful observation of the times of the arrival of individual crests and troughs in the dispersed wave train (Ewing, Jardetzky and Press 1957; Brune et al., 1960), often fails when the signal to noise ratio is small or when the signal is contaminated by other arrivals. Similar difficulties have been noted when the phase delay calculated by ordinary Fourier analysis (Sato 1955, 1956, 1958) are differentiated in order to obtain the group velocity (Dziewonski and Hales, 1972).

Block and Hales (1968), developed techniques to determine the phase velocities from the digitized seismograms from pairs of stations. One of these techniques is the Fourier analysis of the sum (or difference) of the two seismograms after time shifting in steps to correspond to steps in phase velocity. Another technique is to pass both seismograms through a narrow bandpass digital filter centered at various periods and form the cross product of the filtered seismogram after time shifting.

These techniques of phase velocity determination take advantage of much of the information contained in the surface waves train that the peak and trough method failed to exploit.

3.2. Theory of the Group Velocity Measurment

In obtaining the group velocity curves, the Multiple Filter and the Phase Matched Filter Techniques are used. The combination of these two techniques permits isolation of the fundamental mode to obtain cleaner group velocity dispersion curves. Once the fundamental

mode is isolated, the phase velocity dispersion curves are calculated with the (p - w) Technique.

Difficulties are often encountered in the analysis of surface wave seismograms. Disturbances, such as microseisms, sometimes tend to obscure the signal of interest. Several dispersive modes or several branches of the same mode may arrive simultaneously at the recording site. The measurement of dispersion curves, in general, is complicated because the seismogram consists of a complex sum of normal modes. Other factors that can affect the measurements of dispersion curves are multipathing and background noise.

These difficulties are especially severe for data at short periods. Because the surface wave spectrum for short periods is a superposition of many modal contributions, the resultant spectrum may be highly oscillatory, making analysis difficult (Dziewonski et al.,1969; Herrmann, 1973).

To study individual modes we need to be able to separate them in either time or frequency, in addition, the ability to extract and determine group velocity curve is a prerequisite of a realizable phase velocity measurement. The only way to do this exactly is by using a linear array of detectors spaced along the same azimuth from the source. Having this, wave number frequency analysis can be performed to recover both phase velocities and spectral amplitudes of the individual modes as a function of frequency (Herrmann, 1973). Such array data, however, are usually not available.

Dziewonski et al., (1969) developed the Multiple Filter Technique to determine group velocities of dispersed waves from the observations. Dziewonski et al., (1969) proposed Multiple Filter Technique (MFT) as an analytical method to compute and obtain group velocity dispersion curves for a specific mode from complex multimode dispersion signal. This technique converts an ordinary time series (amplitude versus time) into a two dimensional display of velocity (rows) versus period (columns) plane.

Multiple Filter Technique (Dziewonski et al., 1969; Herrmann, 1973) is performed when the displacements are computed. The amplitudes and phases of signals passed by an array of narrow band filters centered at selected frequencies can be used to measure group velocity as a function of period. A Gaussian filter with peak amplitude centered at the desired period is applied to the seismogram in the frequency domain. The peak of the envelope of the corresponding time domain signal is used to estimate the group travel time. The time of the peak is estimated by fitting a quadratic curve to the largest three values (allowing interpolation between time samples).

The technique (Dziewonski and Landisman, 1969) requires the application of a set of narrow bandpass filters to the displacement seismogram, centered at frequencies on which group velocity measurements are to be done. If the amplitude spectrum of the surface waves within the Gaussian window is relatively constant, the envelope of the so filtered signal will have a maximum at the group arrival time, which can be directly related to the group velocity.

The program MFT (II) (Herrmann,1987), searches for the four largest amplitude values of the envelope. In practice, the true period represented in the filtered signal may not correspond to the Gaussian filter's center period. To account for possible bias produced by changing spectral amplitudes, an instantaneous period is measured at the time of the envolope peak. The group velocity for a given period is estimated by dividing the distance between the station and source by the group arrival time. The process is repeated for each period in a specific range and is plotted versus group velocity.

After applying the MFT, the dispersion curves are used as an input for the PMF Technique proposed by Herrin and Gogorth (1977), which permits the isolation of the fundamental model and the cleaning of the signal. The goal is, to isolate the fundamental mode in order to calculate the cleanest group velocity curve. This allows to reapply the MFT and calculate a more accurate group velocity dispersion curve of the fundamental mode.

Application of this method of analysis to the recordings of mutually orthogonal detectors permits the separation of Love waves from Rayleigh waves. It is also useful in the identification of fundamental and higher modes. The Multiple Filter Technique is a fast and efficient method of analyzing multiply dispersed signals. MFT Technique is widely used and provides a sufficient number of group velocities to yield a continuous dispersion curve in an appropriate period interval from any dispersed wave train (Dziewonski et al., 1969; Herrmann, 1973; Bonner and Herrin, 1999). But the presence of multipathing in a surface wave train will bias conventional methods including MFT for estimating group velocities such that they will be determined slow (Jin and Herrin, 1980).

3.3. Multiple Filter Technique (MFT)

In this chapter, the theoretical basis for calculating the group velocity dispersion curve, the Multiple Filter Technique (MFT), and its development will be discussed together with limitations and improvement of this technique.

The basis of this method is the property of a dispersive signal that different frequency components arrive at different times. This method is the application of an array of narrow band filters to the complex seismic signal. These narrow band filters may resolve transient signals composed of several dominant periods that arrive at the recording station almost simultaneously. Using the filtered amplitude, the group velocity is calculated. It is assumed that the signal is a plane wave and the instrument response of the signal has been removed.

The Fourier transform of a signal $f(t)$ is defined as;

$$F(w) = \int_{-\infty}^{\infty} f(t) e^{-iwt} dt \tag{3.1}$$

The complex spectrum of the signal $F(w)$ can be represented by its amplitude and phase functions;

$$F(w) = |F(w)| e^{i\phi(r,w,\theta)} \tag{3.2}$$

where r is the distance and θ is the azimuth. The phase term for the propagating surface wave is composed of the initial phase (source phase), $\phi(w,\theta)$ and the propagation term $k(w)r$;

$$\phi(r,w,\theta) = -k(w)r + \phi(w,\theta) \tag{3.3}$$

Then a narrow band filter is applied to the signal. Dziewonski et al. (1969) used the following filter function;

$$H(w,w_n) = \exp\left[-\alpha\left(\frac{w-w_n}{w_n}\right)^2\right] \tag{3.4}$$

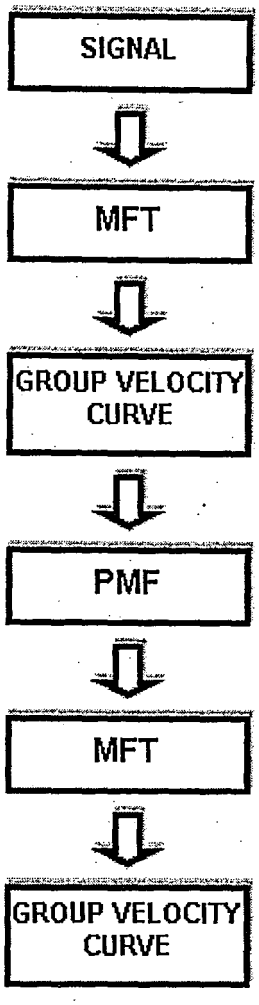

Figure 3.1. Flow chart of group velocity dispersion curve measurement. First the MFT is applied in order to obtain a provisional group velocity dispersion curve that is used as an input in the PMF to isolate the fundamental mode. Once the fundamental mode is obtained, the MFT is applied again to this clean signal, containing only the fundamental mode, and an improved group velocity is calculated.

which has cut off frequencies at $w = w_n \pm w_c$. This filter is a Gaussian filter centered at the frequency w_n, with the parameter α controlling the width. The expression of the filtered signal is ;

$$g_n(t) = \frac{1}{2\pi} \int_{w_n - w_c}^{w_n + w_c} F(w) H(w, w_n) e^{iwt} dw \tag{3.5}$$

where $g_n(t)$ is the resulting filtered signal. Substituting the definitions of $F(w)$ and $H(w)$, the expression for the filtered signal becomes;

$$g_n(t) = \frac{1}{2\pi} \int_{w_n - w_c}^{w_n + w_c} A(w) \exp[i(wt - k(w)r + \phi(w))] \exp\left[-\alpha\left(\frac{w - w_n}{w_n}\right)^2\right] \tag{3.6}$$

Following Bhattacharya (1983), it is assumed that, $A(w)$, $\phi(w)$ and $k(w)$ can be approximated in the vicinity of w_n by the first order Taylor series expansion;

$$A(w) = A(w_n) + \left(\frac{dA}{dw}\right)_{w=w_n} (w - w_n) = A_n + A_n'(w - w_n) \tag{3.7}$$

$$k(w) = k(w_n) + \left(\frac{dk}{dw}\right)_{w=w_n} (w - w_n) = k_n + k_n'(w - w_n) \tag{3.8}$$

$$\phi(w) = \phi(w_n) + \left(\frac{d\phi}{dw}\right)_{w=w_n} (w - w_n) = \phi_n + \phi_n'(w - w_n) \tag{3.9}$$

where;

$$k_n' = 1/U_n \tag{3.10}$$

and U_n is the group velocity.

$g_n(w)$ can be evaluated by substituting equations, with the variable change;

$$w - w_n = \bar{w} \tag{3.11}$$

$$g_n(t) = \frac{1}{2\pi} A_n \exp\left[i(w_n t) - k_n r + \phi_n\right] \times \int_{-w_c}^{w_c} (1 + p\bar{w}) \exp\left[i\beta\bar{w} - q\bar{w}^2\right] \tag{3.12}$$

where;

$$p = \frac{A_n^{'}}{A_n} \tag{3.13}$$

$$q = \frac{\alpha}{w_n^{\,2}} \tag{3.14}$$

$$\beta = \left(t - k_n^{'} r + \phi_n^{'}\right) \tag{3.15}$$

From Abramowitz and Stegun (1965);

$$\int \exp\left[-\left(ax^2 + 2bx^2 + c\right)\right] dx = \frac{1}{2}\sqrt{\frac{\pi}{a}} \exp\left[\frac{b^2 - ac}{a}\right] erf\left[\sqrt{ax} + \frac{b}{\sqrt{a}}\right] + \text{constant} \tag{3.16}$$

where erf is the error function. Then;

$$\int_{-R}^{R} (1 + px) \exp\left[-\left(ax^2 + 2bx + c\right)\right] dx = -\frac{p}{2a} \exp\left[-\left(ax^2 + 2bx + c\right)\right]\Big|_{-R}^{R} + \left(1 - \frac{pb}{a}\right) \mathrm{I}\Big|_{-R}^{R} \tag{3.17}$$

Thus;

$$\bar{\mathrm{I}} = \int_{-w_c}^{w_c} \left(1 + p\bar{w}\right) \exp\left[i\beta\bar{w} - q\bar{w}^2\right] d\bar{w} \tag{3.18}$$

$$\bar{\mathrm{I}} = -\frac{ip}{q} \exp\left[-qw_c^2\right] \sin\left(\beta w_c\right) + \frac{1}{2}\sqrt{\frac{\pi}{q}} \left(1 + \frac{ip\beta}{2q}\right) \exp\left[-\frac{\beta^2}{4q}\right] \tag{3.19}$$

$$\times \left[erf\left(\sqrt{q} w_c - i\frac{\beta}{2\sqrt{q}}\right) + erf\left(\sqrt{q} w_c + i\frac{\beta}{2\sqrt{q}}\right)\right]$$

using the relation;

$$erf(-z) = -erf(z) \tag{3.20}$$

Therefore the expression for $g_n(t)$ is;

$$g_n(t) = \frac{A_n}{2\pi}\exp\left[i\left(w_n t - k_n r + \phi_n\right)\right]\bar{I} \tag{3.21}$$

The series approximation of complex error function (Abramowitz and Stegun, 1965);

$$erf(x+iy) = erf(x) + \frac{\exp\left[-x^2\right]}{2\pi x}\left[1-\cos(2xy)+i\sin(2xy)\right]+..., \tag{3.22}$$

If q is large enough in the equation , the term with $1/\sqrt{q}$ can be neglected, using the first term in the above series approximation. Under this condition, $g_n(t)$ can be expressed as;

$$g_n(t) = \frac{A_n}{2\pi}\exp\left[i\left(w_n t - k_n r + \phi_n\right)\right] erf_c\left(\sqrt{q}w_c\right) \tag{3.23}$$

$$\times\left[-\frac{ip}{q}\exp\left[-qw_c^2\right]\sin(\beta w_c)+\frac{1}{2}\sqrt{\frac{\pi}{q}}\left(1+\frac{ip\beta}{2q}\right)\exp\left[-\frac{\beta^2}{4q}\right]\right]$$

Expressing $g_n(t)$ by its modulus and its phase;

$$g_n(t) = \left|g_n(t)\right|\exp\left[i\Theta_n\right] \tag{3.24}$$

where;

$$\left|g_n(t)\right| = \frac{A_n}{2\pi}\sqrt{\frac{\pi}{q}}\sqrt{1+\left(\frac{p\beta}{2q}\right)^2}\exp\left[-\frac{\beta^2}{4q}\right] erf\left(\sqrt{q}w_c\right) \tag{3.25}$$

$$\Theta_n = w_n t - k_n r + \phi_n + \arctan\left[\frac{p\beta}{2q}\right] \tag{3.26}$$

the extreme positions of $|g_n(t)|$ are given by;

$$\left(\frac{p}{2q}\right)^2 \beta^3 + \left(1 - \frac{p^2}{2p}\right)\beta = 0 \tag{3.27}$$

which has the solutions;

$$\beta = 0 \tag{3.28}$$

$$\beta = \pm\sqrt{2\left(1 - \frac{2q^2}{p^2}\right)} \tag{3.29}$$

If $2q^2/p^2 > 1$, then the only real solution is $\beta = 0$ and it is a maximum. Then the condition is in general satisfied. When measuring group velocities, it is assumed that, the only maximum corresponds to $\beta = 0$. Therefore, the group velocity can be obtained by following relation;

$$\beta = 0 = t - k_n' r + \phi_n' \tag{3.30}$$

Another assumption is that ϕ_n' is small enough that can be neglected in the analysis.

Therefore, the group velocity is the distance from the source to the receiver divided by the arrival time of the maximum of the envelope, $U_n = k_n' = r/t_n$, where t_n shows the arrival time of the maximum of the envelope for the n^{th} filter to the signal. The maximum of the envelope corresponds to the group travel time of the energy associated with the frequency. The equation was obtained using the first order expansion of $k(w)$, $A(w)$ and $\phi(w)$. Substitution of the second order terms leads to the form of $|g_n(t)|$ and the maximum of the envelope does not, in general, corresponds exactly to the group travel time.

For the precision of measurement of group velocity by a bandpass filtration technique the followings are assumed, either;

(i) filters are very narrow, which means that α is high and $1/\sqrt{q}$ may be neglected with respect to $\sqrt{q}$ and $\alpha / w_n^2 > A_n^{'} / A_n$, or

(ii) the approximations expressed in the equation are valid.

Problems arise when the variation of amplitude with frequency and the variation with frequency of the group velocity can not be neglected. Applying MFT to synthetic seismograms, Dziewonski and Hales (1972) showed that group velocity determination by MFT has systematic errors when the group velocity changes rapidly with frequency and these errors can be reduced with increase of α. Herrmann (1973) noted that the variation of group velocity with frequency causes an error in amplitude determination by MFT.

Also the use of the filtered output to estimate phase travel time will be affected by the shape of the signal amplitude spectrum. The magnitude of these errors, examining $\Theta_n(t)$, will depend on the group velocity and the rate of the slope and value of the spectral amplitude.

3.3.1. Why a Gaussian Filter?

One important thing to consider is the resolution of the filtering function in the immediate vicinity of each center frequency and velocity value. If the following integral is defined as a measure of the duration of a time signal,

$$D_t^2 = \int_{-\infty}^{\infty} t^2 |f(t)|^2 \, dt \tag{3.31}$$

and the frequency domain duration measure is;

$$D_w^2 = \int_{-\infty}^{\infty} w^2 |F(w)|^2 \, dw \tag{3.32}$$

then the uncertainity principle states for a time function, $f(t)$, vanishing at infinity faster than $t^{-1/2}$, that;

$$D_t^2 D_w^2 \geq \left(\frac{\pi}{2}\right)^{1/2} \tag{3.33}$$

The equality holds only for Gaussian signals (Percival and Walden,1993). D_t^2 and D_w^2 represent measures of the time and frequency domain resolution. The improvement of the time domain resolution can be achieved only at the expense of frequency domain resolution.

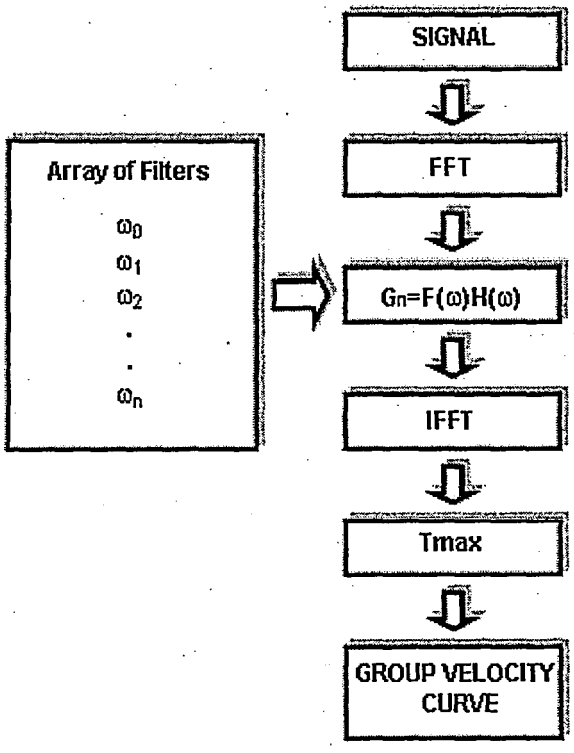

Figure 3.2. Flow chart of MFT. Following Fourier transform of the signal, an array of filters are convolved with the signal. After that, the inverse Fourier transform is applied to the filtered signal. The travel time of the maximum of the envelope is the group travel time. The group velocity is the distance dividing by this time.

It is seen, from the equation, that there is an advantage in using a filter for which this expense is the least.

If w_n denotes the center frequency for the Gaussian filter, in the frequency domain the Gaussian filter can be expressed as ;

$$H_n(w) = \exp\left[-\alpha\left(\frac{w-w_n}{w_n}\right)\right] \tag{3.34}$$

The inverse Fourier transform of $H_n(w)$ is;

$$h_n(t) = \frac{\sqrt{\pi}w_n}{2\alpha}\exp\left[-\frac{w_n^2 t^2}{4\alpha}\right]\cos(w_n t) \tag{3.35}$$

The resolution is controlled in both domains by the parameter α. Improved resolution in one domain causes the opposite effect in the other, but the value of the product of the RMS durations of the Gaussian function, $D_w.D_t$, remains constant. Selection of a particular filter width represents a compromise between the time and frequency domain resolution and depends on the level of noise, the character of the dispersion curve and the degree of contamination from energy belonging to other modes of propagation.

3.3.2. Effect of Modal Interference

Above, the theoretical discussion has been limited to the case in which only one mode is present in the signal. But the seismic signal is a complex signal, composed of different modes and noise. This complexity sets limitations to the problem.

At short periods, problems arise because of the presence of more than a single surface wave mode. Because the signal spectrum of these periods is a superposition of modal contributions, the resultant spectrum is highly oscillatory making analysis difficult(REF). Herrmann (1973) showed the limitation of the Multiple Filter Technique for the effect of modal interference.

Following Herrmann (1973), ignoring the source amplitude spectral shape, the filtered multimode signal can be expressed as;

$$g(t,r)=\frac{w_n}{2\pi}\sqrt{\frac{\pi}{\alpha}}\sum_{j=0}^{M}A_j(w_n,r)\exp\left[-\frac{w_n^2}{4\alpha}\left(t-\frac{r}{U_{nj}}\right)^2\right] \tag{3.36}$$

where the subscript j designates the value of a quantity for the j^{th} mode.

Dziewonski et al. (1969) stated that the individual maxima of the envelope correspond to the arrivals of the group velocities of each mode. Because the modulus of $g(t,r)$ is a very complicated function, the accurate determination of group velocities occurs when the envelope maxima are well separated.

The duration, t_d, of the resulting Gaussian envelope is defined as the time from the peak value until the amplitude decreases to $\exp(-\pi)$ of the original value. In terms of α and T_n (the characteristic filter period), the duration has the expression;

$$t_d=T_n\sqrt{\frac{\alpha}{\pi}} \tag{3.37}$$

Therefore, practically, when the two equal amplitude maxima are separated by a time greater than $2t_d$, it is assumed that the two modes do not interfere. If the different mode maxima are separated enough, determinations of spectral amplitude, group velocity, and instantaneous phase can be made using the equation for only one mode, rather than $t_d=T_n\sqrt{\frac{\alpha}{\pi}}$.

When the time separation of the arrivals of the two modes is less than $2t_d$, the maxima of the envelope will not correspond to the actual maxima of the individual modes. The resolution can be increased by decreasing the duration of the envelope of each mode by decreasing α. But, this would require more terms in the Taylor's expansion.

Narrow bandpass filtering of a dispersed surface wave can be used to determine the group velocities and spectral amplitudes of the various modes composing the signal under certain conditions. The group velocity arrivals of the individual modes are well enough separated in time that the contribution to the filtered signal do not interfere.

3.3.3. Including Higher Order in the Taylor's Expansion

Bhattacharya (1983) approximated $A(w)$, $k(w)$ and , $\phi(w)$ including higher order terms in the Taylor's series expansion than Dziewonski et al. (1969) did, by considering;

$$A(w) = A_n + A_n^{'}(w - w_n) \tag{3.38}$$

$$k(w) = k_n + \frac{1}{U_n}(w - w_n) + k_n^{"}\frac{1}{2}(w - w_n)^2 \tag{3.39}$$

$$\phi(w) = \phi_n + \phi_n^{'}(w - w_n) + \frac{1}{2}\phi_n^{"}(w - w_n)^2 \tag{3.40}$$

Substituting the above approximation into;

$$k_j^{\Gamma new} = k_j^{\Gamma} - \delta k \tag{3.41}$$

with the same p and β, but changing q by $q^{'}$, the new expression is;

$$g_n(t) = \frac{1}{2\pi} A_n \exp\left[i(w_n t - k_n r + \phi_n)\right] \times \int_{-w_c}^{w_c} (1 + p\overline{w}) \exp\left[i\beta\overline{w} - q^{'}\overline{w}^2\right] \tag{3.42}$$

where;

$$p = \frac{A_n^{'}}{A_n} \tag{3.43}$$

$$\beta = t - \frac{r}{U_n} + \phi_n^{'} \tag{3.44}$$

$$q^{'} = \frac{1}{2} i\left(r k_n^{"} - \phi_n^{"}\right) + \frac{\alpha}{w_n^2} \tag{3.45}$$

Writing;

$$q' = \rho \exp(i\psi) \tag{3.46}$$

with

$$\rho = \sqrt{\left[\left(\frac{\alpha}{w_n^2}\right) + \left(\frac{rk_n'' - \phi_n''}{2}\right)^2\right]} \tag{3.47}$$

$$\psi = \arctan \frac{\frac{1}{2}\left(rk_n'' - \phi_n''\right)}{\left(\frac{\alpha}{w_n^2}\right)} \tag{3.48}$$

the solution is;

$$g_n(t) = \frac{A_n}{2\pi} \exp\left[i\left(w_n t - k_n r + \phi_n\right)\right] \tag{3.49}$$

$$\times \left\{ -\frac{ip}{\rho} \exp\left[i\left(-\psi + \rho w_c^2 \sin\psi\right) + \rho w_c^2 \cos\psi\right] \sin\left(\beta w_c\right) \right\}$$

$$+ \frac{1}{2}\sqrt{\frac{\pi}{\rho}}\left(1 + \frac{p\beta}{2\rho}\sin\psi + \frac{ip\beta}{2\rho}\cos\psi\right)$$

$$\times \exp\left[i\left(-\left(\frac{\psi}{2}\right) + \left(\frac{\beta^2}{4\rho}\right)\sin\psi \right) - \left(\frac{\beta^2}{4\rho}\right)\cos\psi \right]$$

$$\times \left[erf\left(\xi_- + i\eta_-\right) + erf\left(\xi_+ + i\eta_+\right) \right]$$

where;

$$\xi_{\mp} = \sqrt{\rho} w_c \cos\left(\frac{1}{2}\Psi\right) \mp \frac{\beta}{2\sqrt{\rho}} \sin\left(\frac{1}{2}\Psi\right) \tag{3.50}$$

$$\eta_{\mp} = \sqrt{\rho} w_c \sin\left(\frac{1}{2}\Psi\right) \mp \frac{\beta}{2\sqrt{\rho}} \cos\left(\frac{1}{2}\Psi\right) \tag{3.51}$$

If ρ is large enough than, $1/\sqrt{\rho}$, can be neglected with respect to $\sqrt{\rho}$ and then the approximation described in (3.22) is applied, keeping the first term. Therefore;

$$g_n(t) = -\frac{pA_n}{2\rho\pi} \exp\left[-\rho w_c^2 \cos\Psi\right] \sin\left(\beta w_c^2\right) \tag{3.52}$$

$$\times \exp\left[i\left(w_n t - k_n r - \phi_n - \Psi - \rho w_c^2 \sin\Psi + \frac{2}{\pi} \right) \right]$$

$$+ \frac{A_n}{2\pi} \sqrt{\frac{\pi}{\rho}} \sqrt{\left[1 + \frac{p\beta}{\rho} \sin\Psi + \left(\frac{p\beta}{2\rho} \right)^2 \right]} \exp\left[-\left(\frac{\beta^2}{4\rho\cos\Psi} \right) \right]$$

$$\times erf\left[\sqrt{\rho} w_c \cos\left(\frac{1}{2}\Psi\right) \exp\left[i\left(w_n t - k_n r + x \right) \right] \right]$$

where;

$$x = \phi_n - \frac{\Psi}{2} + \frac{\beta^2}{4\rho} \sin\Psi + \lambda \tag{3.53}$$

and

$$\lambda = \arctan\left[\frac{\frac{p\beta}{2\rho}\cos\Psi}{\left(1+\frac{p\beta}{2\rho}\sin\Psi\right)}\right] \tag{3.54}$$

As before, the maximum of the envelope of $g_n(t)$ is searched. For that, the value of β at the point of the maximum is found. It is difficult to calculate the maximum of the envelope of $g_n(t)$ using both terms on the right side of the expression. So, it is simplified by neglecting the first term with respect to the second term when the envelope of the second term reaches maximum. If ρw_c^2 is large enough this can be done (Bhattacharya, 1983). Thus, near the maximum of second term, the filtered signal can be approximated by;

$$g_n(t) = \frac{A_n}{2\pi}\sqrt{\frac{\pi}{\rho}}\sqrt{\left[1+\left(\frac{p\beta}{\rho}\sin\Psi\right)+\left(\frac{p\beta}{2\rho}\right)^2\right]}\exp\left[-\left(\frac{\beta^2}{4\rho}\right)\cos\Psi\right] \tag{3.55}$$

$$\times erf\left(\sqrt{\rho}w_c\cos\left(\frac{1}{2}\Psi\right)\exp\left[i\left(w_n t - k_n r + x\right)\right]\right)$$

where the amplitude and phase of the above are, respectively;

$$\left|g_n(t)\right| = \frac{A_n}{2\pi}\sqrt{\frac{\pi}{\rho}}\sqrt{\left[1+\left(\frac{p\beta}{\rho}\sin\Psi\right)+\left(\frac{p\beta}{2\rho}\right)^2\right]}\exp\left[-\left(\frac{\beta^2}{4\rho}\right)\cos\Psi\right] \tag{3.56}$$

$$\times erf\left(\sqrt{\rho}w_c\cos\left(\frac{1}{2}\Psi\right)\right)$$

and

$$\Theta = w_n t - k_n r + x \tag{3.57}$$

The extreme positions of $|g_n(t)|$ are the solutions of the following equation;

$$\cos\Psi\left(\frac{p}{2\rho}\right)^2\beta^3+\left(\frac{p\sin\Psi\cos\Psi}{\rho}\right)\beta^2+\left(\cos\Psi-\frac{p^2}{2\rho}\right)\beta-p\sin\Psi=0 \tag{3.58}$$

or

$$\beta=\left[p\tan\Psi-\left(\beta^2\frac{p}{\rho}\sin\Psi+\beta^3\left(\frac{p}{2\rho}\right)^2\right)\right]\Big/\left(1-\frac{p^2}{2\rho\cos\Psi}\right) \tag{3.59}$$

Since, as it was assumed before that ρ is large then it may be taken as an initial approximation (Bhattacharya, 1983).

$$\beta=p\tan\Psi \tag{3.60}$$

The maximum of the envelope of the filtered signal occur at ;

$$t_m=\frac{r}{U_n}-\phi_n^{'}+p\tan\Psi \tag{3.61}$$

or

$$U_n=\frac{r}{t_m+\phi_n^{'}-p\tan\Psi} \tag{3.62}$$

Thus, if $(p\tan\Psi)$ is ignored, the above equation reveals that the measured group velocity by MFT will be higher than the true value if $(p\tan\Psi)$ is negative or lower than the true value if $(p\tan\Psi)$ is positive. For all combinations of signs of (Ψ) and (p), MFT distorts the computed group velocity to the group velocity of neighboring frequency at which the amplitude spectrum is rapidly changing.

3.3.4. Instantaneous Frequency

One way to improve the group velocity measurements when the amplitude changes with frequency, is to consider that the measured group velocity corresponds to the instantaneous frequency $(<w>)$ instead of the central filter frequency w_n.

If the complex signal in the time domain is;

$$g_n(t) = |g_n(t)| \exp[i\Theta(t)] \tag{3.63}$$

the instantaneous frequency is defined (Keilis-Borok, 1986) as;

$$\Omega(t) = \frac{d\Theta(t)}{dt} \tag{3.64}$$

The property below states that;

$$<\Omega> = <w> \tag{3.65}$$

According to (Keilis-Borok, 1986); when Ω is measured, an approximate value of the mean frequency around which the signal spectrum is concentrated, can be obtained. Only in the case when the slope in spectrum amplitude is equal to zero does the mean frequency coincide with the central frequency of the narrow band filter. The measurement can be improved by assuming that the mean instantaneous frequency is the frequency that corresponds to the value of the measured group velocity instead of the filter frequency.

$$\Omega(t) = \frac{d\Theta(t)}{dt} = w_n + \frac{1}{1+\left(\frac{p\beta}{2q}\right)^2}\left[\frac{p}{2q} + \frac{\beta}{2q}\frac{dp}{dt}\right] \tag{3.66}$$

If q is large it is assumed;

$$\frac{1}{1+\left(\frac{p\beta}{2q}\right)^2}\approx 1 \tag{3.67}$$

and neglecting;

$$p' = A_n'' / A_n' \tag{3.68}$$

term, the expression for the instantaneous frequency is;

$$\Omega(t) = w_n + \frac{p}{2q} \tag{3.69}$$

Examining the expressions;

$$p>0 \Rightarrow \begin{Bmatrix} U_n > U_n(measured) \\ \Omega > w_n \end{Bmatrix} \tag{3.70}$$

$$p<0 \Rightarrow \begin{Bmatrix} U_n < U_n(measured) \\ \Omega < w_n \end{Bmatrix} \tag{3.71}$$

this means that the instantaneous frequency is shifted toward a direction that compensates the error in the group velocity measurement.

3.4. Phase Matched Filter Technique (PMF)

Here; theoretical bases of the Phase Matched Filter (PMF) and isolating the fundamental mode with Phase Matched Filter Technique (PMF) are discussed. The goal is, to isolate the fundamental mode in order to calculate the cleanest group velocity curve. The Multiple Filter (MFT) and the Phase Matched Filter (PMF) Techniques are used to do this.

The presence of multipaths in a surface wave train, interfering with the great circle path arrival, will bias conventional methods for determining apparent group velocity dispersion curves such that the estimates will be too slow (ref). The effect of multipaths can be reduced using the process of Phase Match Filter Technique developed by Herrin and Goforth (1977). This method removes the bias mentioned above and thus improves the accuracy of the estimate of group velocity. The method developed based on the Matched Filter is defined by Turin (1960). Multipath interference can cause ripples and spectral holes, in addition to those caused by some effects, to appear in the signal spectrum. The removal of these effects of multipaths using Phase Matched Filter Technique provides Rayleigh and Love wave spectra which are much more closely related to source characteristics than are those obtained from Fourier transforms of the entire signal. At the same time results in a substantial improvement in the signal to noise ratio (Herrin and Goforth, 1977).

Once the group velocities are estimated, a mode isolation filter (Herrin and Goforth,1977) can be constructed and applied to the signal to isolate the fundamental mode from the signal generated and ambient Earth noise. Mode isolation provides smooth, stable spectral amplitudes and eases the estimation of signal phase. With the application of the PMF to the data set, we not only obtain an improvement of the group velocity dispersion curve but also isolate the fundamental mode. Then this simpler signal is used, in which the noise and the influence of higher modes is significantly reduced.

Herrin and Goforth (1977) proposed the Phase Matched Filter Technique (PMF) to remove the effect of noise and other modes from the seismic signal to isolate the fundamental mode. The PMF compresses the waveform into a narrow time window centered near zero time, allowing noise to be windowed out by taking the spectrum of this narrow window rather than the full signal time window. However, the amount of compression depends on how well the Phase Matched Filter matches the actual phase of the signal. The PMF can be used to remove multipathing effects, isolate the fundamental mode and improve the signal to noise ratio.

If the cross correlation of a signal, $f(t)$, with a time function, $h(t)$ is considered;

$$f(t)\otimes h(t)\Rightarrow\left|F(w)\right|\left|H(w)\right|\exp\left[i\left(\Phi(w)-\sigma(w)\right)\right] \tag{3.72}$$

Then a $h(t)$ is chosen such that the Fourier phase is the same as $f(t)$;

$$\sigma(w) = \Phi(w) \tag{3.73}$$

as a Phase Matched Filter with respect to the signal;

$$f(t) \otimes h(t) \Rightarrow |F(w)||H(w)| \tag{3.74}$$

There are different possible choices for $|H(w)|$;

a) $$|H(w)| = |F(w)| \tag{3.75}$$

This maximizes the signal to noise power ratio assuming "white noise". For a low level noise signal, this gives the best result.

b) $$|H(w)| = \frac{1}{|F(w)|} \tag{3.76}$$

The output after this filter becomes the impulse function in the time domain, which maximizes the time resolution of the function but greatly reduces the signal to noise ratio. This is a good choice for interfering signal.

c) $$|H(w)| = 1 \tag{3.77}$$

This is a compromise between the time resolution and the signal to noise ratio criteria. This one will be used in the measurements.

Herrin and Goforth (1977) refer to the zero phase time domain signal as the "pseudo autocorrelation function". Assuming that the seismogram is composed of propagating normal modes, the signal can be expressed as;

$$f(t) = \frac{1}{2\pi} \int_{-\infty}^{\infty} \sum_{m} |F_m(w)| \exp\left[wt - k_m(w) r + \phi_m(w)\right] dw \tag{3.78}$$

where $\phi_m(w)$ is source phase shift for the m^{th} mode.

When the PMF Technique is applied to the signal, $f(t)$, the pseudo autocorrelation function has the expression;

$$\psi_j(t) = \frac{1}{2\pi}\int_{-\infty}^{\infty} \exp\left[ik_j^{\square} r\right] \sum_m \left|F_m(w)\right| \exp\left[wt - k_m(w) r + \phi_m(w)\right] dw \tag{3.79}$$

where $k_j^{\square}$ is an estimate of dispersive wavenumber of the j^{th} mode of interest. Rewriting the above equation;

$$\psi_j(t) = \frac{1}{2\pi}\int_{-\infty}^{\infty} \left|F_j(w)\right| \exp\left[\left(k_j^{\square} - k_j(w)\right) r + \phi_j(w)\right] \exp\left[wt\right] dw \tag{3.80}$$

$$+\frac{1}{2\pi}\int_{-\infty}^{\infty} \sum_{m \neq j} \left|F_m(w)\right| \exp\left[wt - k_m(w) r + \phi_m(w)\right] dw$$

If the source effect is removed and $k_j^{\square} - k_j \approx 0$, the first integral in the right hand side will be approximately zero phase and will be concentrated around zero lag. Time windowing $\psi_j(t)$ with a symmetric and zero phase window, $w(t)$, will remove the contribution of the other modes and noise in the signal, provided that they are separated enough from the zero lag. Therefore;

$$\psi_j^{[]}(t) = w(t)\psi_j(t) \tag{3.81}$$

Taking the Fourier transform of the windowed pseudo autocorrelation function results in;

$$\left|F_j(w)\right| \exp\left[i\delta k_j r\right] = \int_{-\infty}^{\infty} w(t)\psi_j(t) \exp\left[iwt\right] dt \tag{3.82}$$

where;

$$\delta k = k_j^{\square} - k_j \tag{3.83}$$

or if the source phase shift is not removed;

$$\delta k = k_j^{\square} - k_j + \frac{\phi_j}{r} \tag{3.84}$$

When r, the distance between the source and the receiver, is large enough the source phase term can be neglected in the above expression. There may be a residual phase δkr depending on the accuracy of the initial estimate of the wavenumber dispersion curve. To improve that, an iterative process with a new estimate of the wavenumber dispersion curve can be used;

$$k_j^{\square new} = k_j^{\square} - \delta k \tag{3.85}$$

Then, this new value, $k_j^{\square new}$ is substituted and $\psi_j(t)$ equation is rewritten, and then the process is repeated again until the process converges.

A fundamental ambiguity is present in;

$$\left|F_j(w)\right| \exp\left[i\delta k_j r\right] = \int_{-\infty}^{\infty} w(t)\psi_j(t)\exp[iwt]dt \tag{3.86}$$

$$\exp\left[i\delta kr\right] = \exp\left[i\delta kr \pm i2n\pi\right] \tag{3.87}$$

Removing this ambiguity requires a priori knowledge of the location of the wavenumber at least at one frequency. This is possible if the data permits connecting the dispersion curve to global long period phase velocity dispersion curves.

Herrin and Goforth (1977) described the computer algorithm used in the PMF technique. To find a PMF for a given seismic signal, the following iterative process is used;

1) Input a trial group velocity dispersion curve and an amplitude spectrum for the filter. This trial group velocity dispersion curve is obtained from the Multiple Filter Technique.

2) The group delay and the Fourier phase of the signal are related (Keilis- Borok, 1989) by;

$$t_{gr}(w) = -\frac{d\Phi(w)}{dw} \tag{3.88}$$

where t_{gr} is the group delay and $\Phi(w)$ is the spectral phase, then;

$$\Phi(w_1) = \int_{w_0}^{w_1} t_{gr}(w)\,dw + \Phi(w_0) \tag{3.89}$$

This integral can have an additive constant without affecting the derivative group delay. Russell et al. (1987) shows that the windowed pseudo autocorrelation function is not biased by constant phase errors.

Using the epicentral distance and the dispersion curve, t_{gr}, is calculated. With group delay and $\Phi(w_1)$, the Fourier phase of the Phase Matched Filter is obtained.

3) Then, cross correlation of the signal with the Phase Matched Filter is performed,

$$\left(f(t) \otimes h(t) \Rightarrow |F(w)||H(w)|\right) \tag{3.90}$$

before calculating this in the frequency domain. The amplitude of the Phase Matched Filter is equal to unity $\left(|H(w)| = 1\right)$.

4) After that, the inverse Fourier transform to window the pseudo correlation function in the time domain is calculated. The window function that is used, is a Parzen window defined as;

$$w(t)=\begin{cases}1-6\left(\frac{t}{M}\right)^2+6\left(\frac{|t|}{M}\right)^3 & |t|\le M/2 \\ 2\left(1-\frac{|t|}{M}\right)^3 & M/2<|t|\le M \\ 0 & |t|>M\end{cases} \tag{3.91}$$

where M is the one sided width of the Parzen window. The window size is proportional to the longest period in the signal. Russell (1987) discusses the bias of the Parzen window function, showing that the PMF in an iterative process can remove residual bias in phase, but not the bias in the spectral amplitude, that can be quite biased when there is significant curvature $\left(\left|F''(w)\right|\right)$ in the amplitude spectrum.

5) Then, by taking this windowed pseudo correlation function, its spectral amplitude and phase is obtained.

6) And then, a first derivative smoothing condition is applied to the dispersion curve. This condition, with the approximations made, is the same as imposing a condition for continuity of the second derivative of the Fourier phase spectrum. This is used to correct the group delay of the trial filter ;

$$f(t)=\frac{1}{2\pi}\int_{-\infty}^{\infty}\sum_m\left|F_m(w)\right|\exp\left[wt-k_m(w)r+\phi_m(w)\right]dw \tag{3.92}$$

7) Return to the step 3, repeating the process until the phase spectra of the filter and the desired signal in the band of interest are identical.

3.5. (p-w) Stacking

McMechan and Yedlin, (1981), developed an alternate approach to surface wave analysis that consists of the transformation of the entire data wavefield into the slowness frequency $(p-w)$ domain, where the dispersion curve can be directly picked. This method is based on

the principle that; when two functions are in phase for a given frequency, their sum will reach the maximum and their difference will be the minimum value.

The $(p-w)$ stacking involves, searching for phase velocities that will produce constructive interference of monochromatic waves at a given frequency. A direct sum of many recordings at a given frequency will not, in general, constructively interfere, due to phase differences at different stations. However; if it is assumed that the seismic signal can be approximated by a sum of wave planes, the difference in phase between any two stations, having the same azimuth, $k(w)\Delta r$ will be equal to Δr, where Δr is the interstation distance. Here, Russell (1987) is followed for the determination of phase velocity, using the $(p-w)$ Technique, with discrete spatial sampling.

The expression for the wavenumber is;

$$k(w)=\frac{w}{c(w)}=wp(w) \tag{3.93}$$

where $p=1/c$ is the wave slowness. Therefore, either k, p or c can be treated as independent variables in searching, and they can be varied for the value (or values) where the phase adjusted sum of the recording reaches a maximum.

After applying the Phase Matched Filter, a signal containing a single mode, that is the fundamental mode is obtained. This simpler signals are used to obtain local phase velocity dispersion curves. Then, they can be expressed by;

$$f(t,r)=\int_{-\infty}^{\infty}A(r,w)\exp\left[i\left(wt+\phi(w,\theta)-k(w)r\right)\right]dw \tag{3.94}$$

where $\phi(w,\theta)$ is the source term, θ is the azimuth and r is the distance from the source to the receiver.

The $(p-w)$ stacking process involves two linear transformations; a slant stack followed by a Fourier transform. A slant stack is a linear operation that transforms a wavefield in the $(t-r)$ domain into the wavefield in the $(p-\tau)$ domain. Here p is the ray parameter

(horizontal slowness), and τ is projection of t to zero offset along a line of slope p through the point $(t-r)$ (McMechan and Ottolini, 1980).

The signal is normalized dividing the recorded seismograms by the signal belonging to the closed station to the source. With this normalization, the source phase and the contribution of the Earth's structure from the source to the closest station are removed. Then, the normalized signal has the expression;

$$\overline{f}(t,r_i)=\int_{-\infty}^{\infty}\frac{A(r,w)\exp\left[i\left(\phi(w,\theta)-k(w)r\right)\right]}{A(r_1,w)\exp\left[i\left(\phi(w,\theta)-k(w)r_1\right)\right]}\exp[iwt]dw \tag{3.95}$$

$$=\int_{-\infty}^{\infty}\frac{A(r,w)}{A(r_1,w)}\exp\left[i(w)t-k\Delta r_i\right]dw \tag{3.96}$$

where;

$$\Delta r_i=r_i-r_1 \tag{3.97}$$

i is the difference between station and the closest station.

After this normalization, the slant stack is performed, transforming from $\overline{f}(r,t)$ wavefield to $U(p',\tau)$, where;

$$U(p',\tau)=\sum_{n=1}^{N}\overline{f}(r_n,\tau+p'\Delta r_n) \tag{3.98}$$

N is the number of station. Substituting (3.95) into (3.98), we have;

$$U(p',\tau)=\sum_{n}\int_{-\infty}^{\infty}\hat{A}_n(r_n,w)\exp\left[i\left(w\tau+wp'\Delta r_n-wp(w)\Delta r_n\right)\right]dw \tag{3.99}$$

where;

$$\hat{A}_n(r_n,w)=\frac{A(r,w)}{A(r_1,w)} \tag{3.100}$$

The $(p-w)$ wavefield contains the same information that the original data does, but it is now decomposed into elements of equal phase velocity, c $1/p$. The slant stack introduces a desired phase distortion of the data (Chapman, 1978), but no frequency shift. Thus, the amplitude spectrum of the trace at a given p is identical to that associated with the corresponding phase velocity in the original data.

The second step is to perform a Fourier transform, that is;

$$U(p',w)=\sum_n \hat{A}_n(r_n,w)\exp\left[i\left(w(p'-p)\Delta r_n\right)\right] \tag{3.101}$$

The quantity $U(p',w)$ will have a maximum when $p'=p$. Then, the values of p' are searched that maximize the modulus of $U(p',w)$ at each frequency to find the phase velocity dispersion curve. If the signal amplitude is corrected by geometrical spreading and attenuation, the maximum value of $U(p',w)$ must be equal to the number of stations. If this value is less than N, then this can be attributed to some deviations from the assumptions, that all the station lie along the same azimuth and the signal can be approximated by plane waves. McMechan and R. Ottolini (1980) discuss the limitations of $(p-\tau)$ transform. The main limitations are;

1) The profiles are usually spatially aliased. In order to avoid spatial aliasing, the station must be placed at a distance from one another which is less than one half of the wavelength of the highest frequency wished to resolve. (For example, if at 20 s the phase velocity is around 3 km/s it is needed that the interstation distance to be less than 300 km).

2) Another limitation associated with the data is related with the coherency between sources when more than one source is used in the stacking process. This is not a problem when the sources are shots, but might be a problem if earthquake sources are used. Since slant stacking

depends on constructive interference to delineate the $(p-\tau)$ locus, it works well only when the apparent sources exhibit the same initial polarity. But, this problem is resolved when it is normalized by the closest station. In that way, the source dependence is removed.

3.6. Synthetic Examples of Multiple Filter and Phase Matched Filter Techniques

As an example of the techniques described in the previous sections, we applied them to some synthetic seismograms. These synthetic seismograms have been calculated using the mode summation code by R. B. Herrmann (Computer Programs in Seismology). To calculate synthetic seismograms a simple earth model is utilized, a layer over a half space and a strike slip source with strike $=0°$, rake $=0°$, and dip $=90°$, source and receivers are at 0° km depth. The recording azimuth is $45°$.

H (km)	Vp (km/s)	Vs (km/s)	RHO (g/cm^3)
40	6	3.5	2.8
0	8	4.7	3.3

Table 3.1. Earth model used in the synthetic surface wave computations.

In the Figures (3.3 and 3.11), the synthetic seismograms for eigth different distances (1000 km, 2000 km, 3000 km, 4000 km, 5000 km, 6000 km, 7000 km and 8000 km) are presented. The increased dispersion with distance is easily seen. The output of the MFT program is shown in Figures (3.8 and 3.16), where at the left, plot of the maximum values of the envelope amplitude per period, which are indicated with different symbols, is displayed. At the right side is the plot of group velocity with period where different colors represent different envelope amplitude values, with the highest amplitude in red. In the group velocity plot, the fundamental mode is clearly seen. For short periods the contributions of the higher modes are notable.

After picking the points that belong to the fundamental mode dispersion curve, these values are used as one of the input of the PMF Technique. With that, the fundamental mode is isolated.

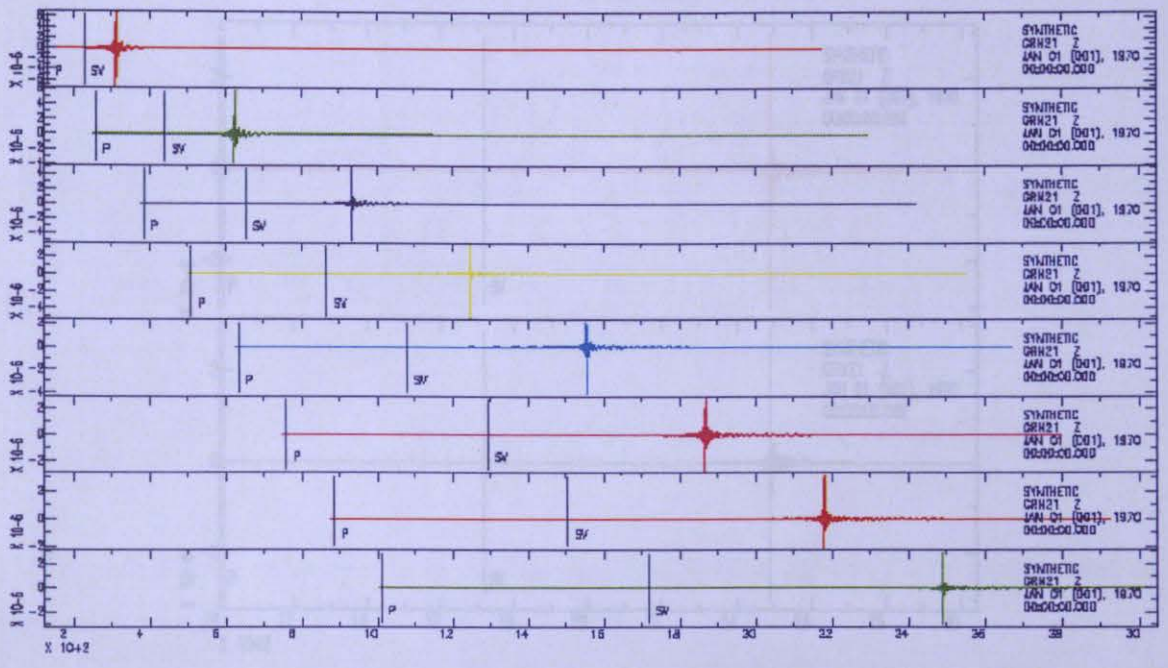

Figure 3.3. Synthetic Rayleigh waves at eigth different distances.

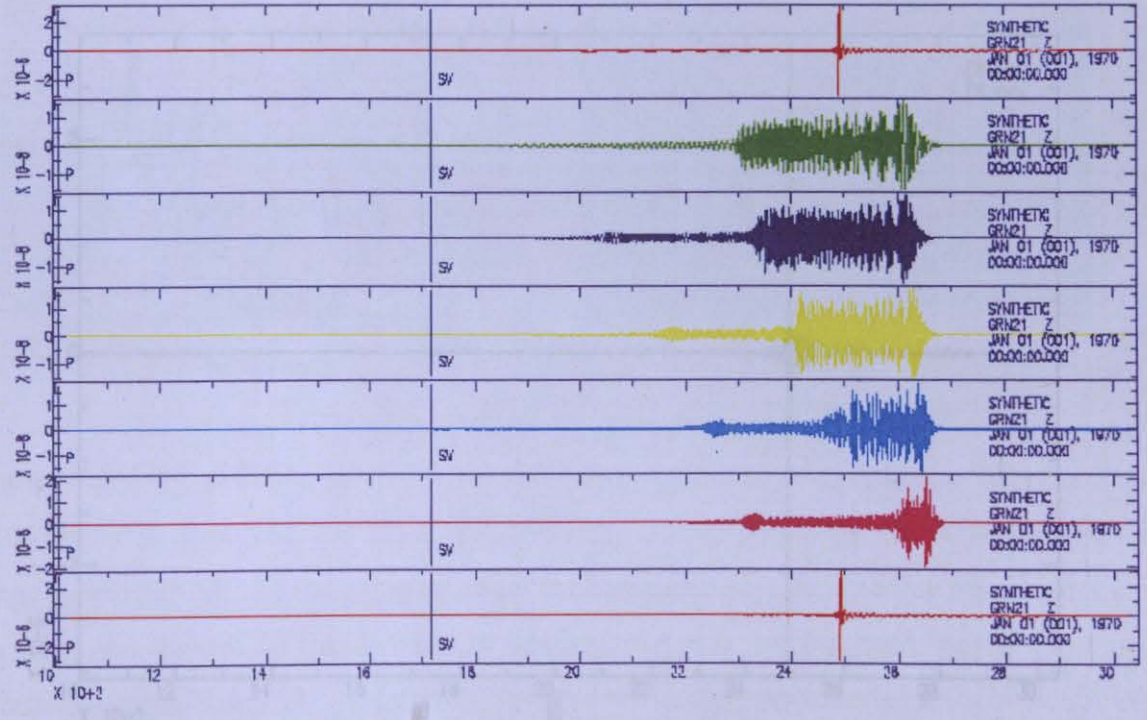

Figure 3.4. Fundamental mode, first five modes and the complete modal summation at 8000 km.

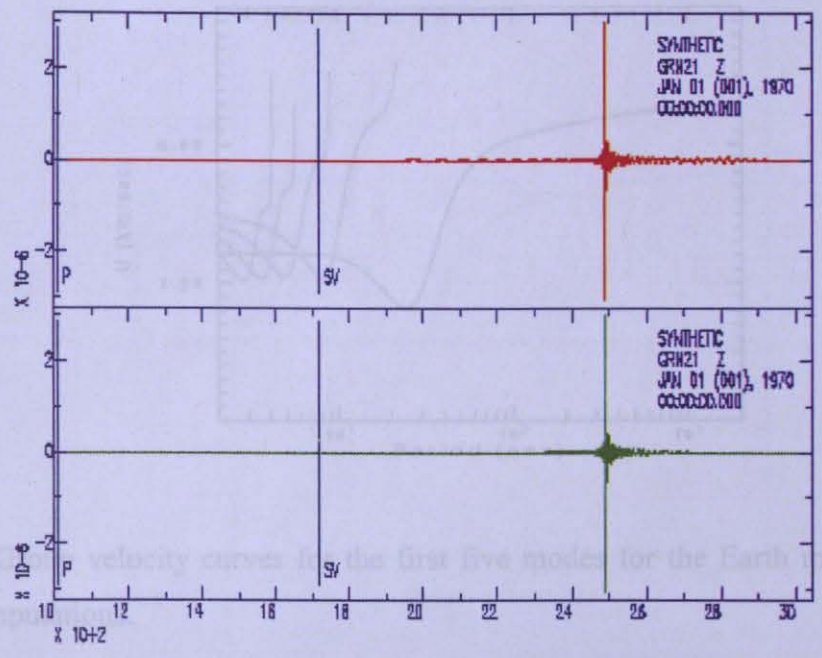

Figure 3.5. The original fundamental mode and the fundamental mode isolated by the PMF, for the signal at 8000 km.

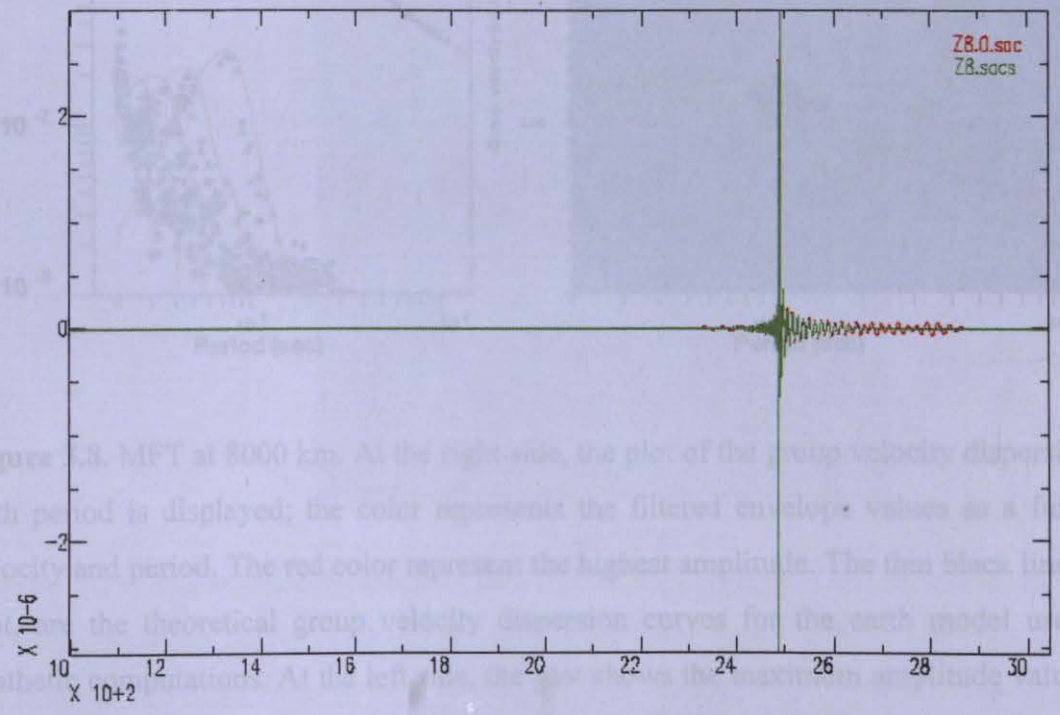

Figure 3.6. Superposition of the original fundamental mode and the output of PMF at 8000 km.

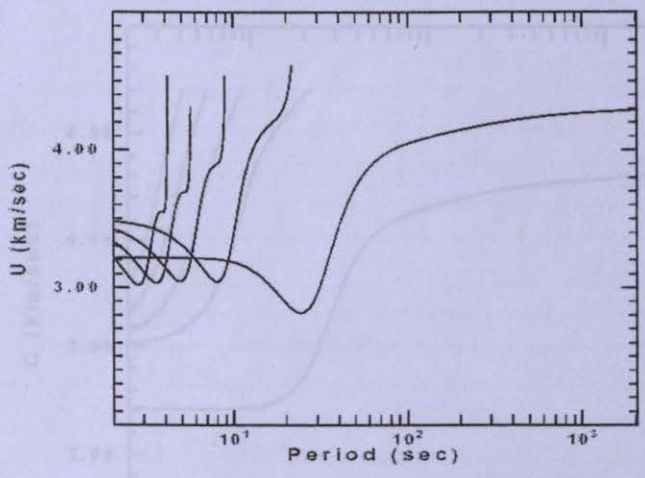

Figure 3.7. Group velocity curves for the first five modes for the Earth model used in the synthetic computations.

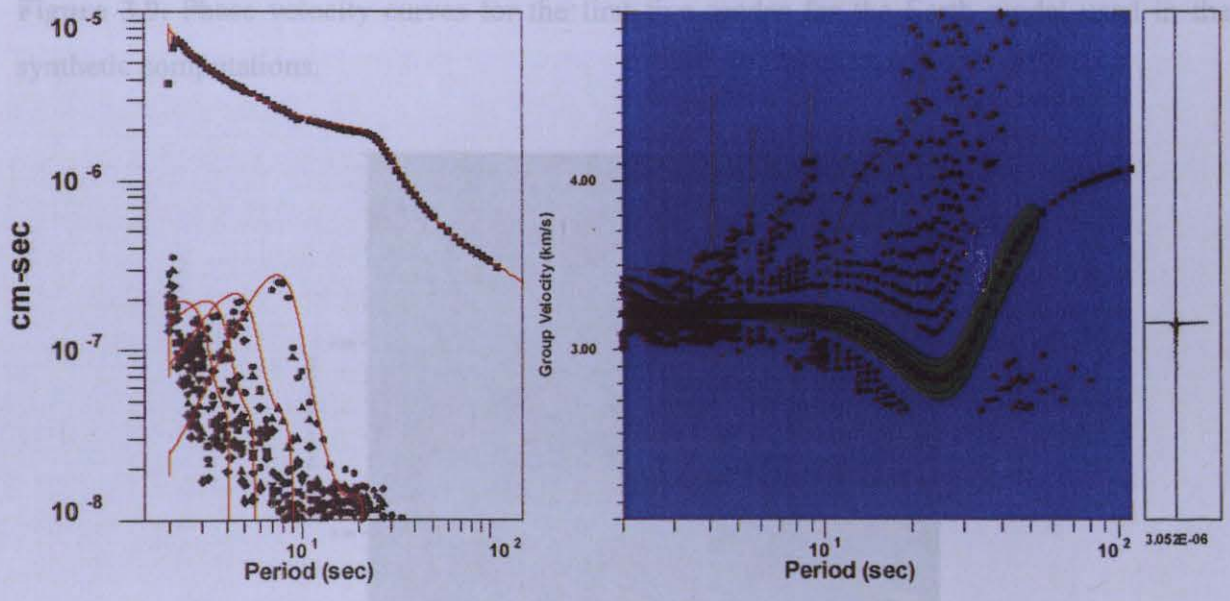

Figure 3.8. MFT at 8000 km. At the right side, the plot of the group velocity dispersion curve with period is displayed; the color represents the filtered envelope values as a function of velocity and period. The red color represent the highest amplitude. The thin black lines, in this plot, are the theoretical group velocity dispersion curves for the earth model used in the synthetic computations. At the left side, the plot shows the maximum amplitude values of the envelope (discrete symbol) per period. The red color lines show the amplitude of the different modes used in making the synthetic seismogram and with thin black line, the amplitude of the signal is plotted. The oscillation of the signal is due to the interferences of the higher modes.

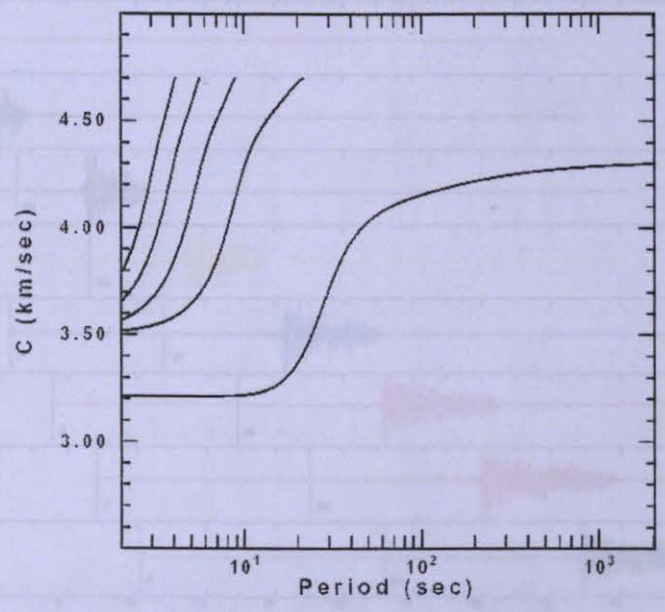

Figure 3.9. Phase velocity curves for the first five modes for the Earth model used in the synthetic computations.

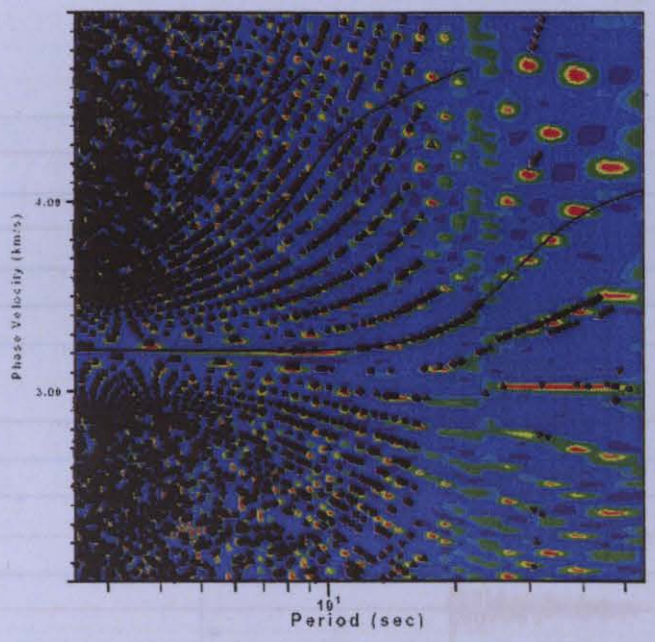

Figure 3.10. Phase velocity stack values overlain by synthetic model predicted phase velocity dispersion curves. The colors indicate the stack value, with red corresponding to the largest. The black symbol represents the chosen peaks. The thin black curves are the theoretical dispersion values. Note the difficulty in indentifying the higher modes.

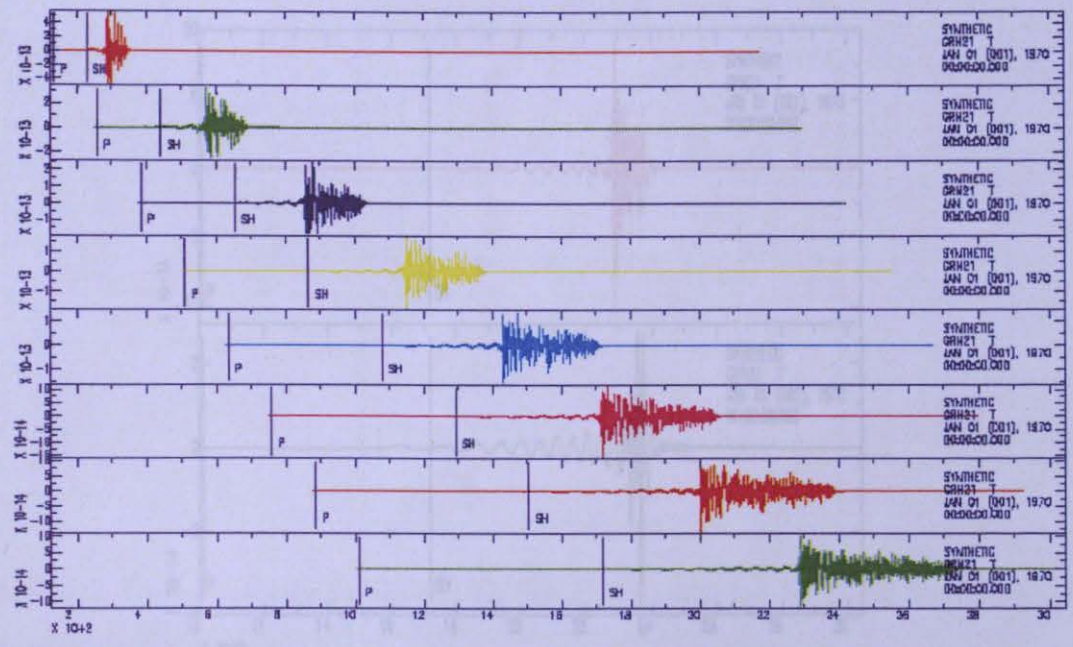

Figure 3.11. Synthetic Love waves at eigth different distances.

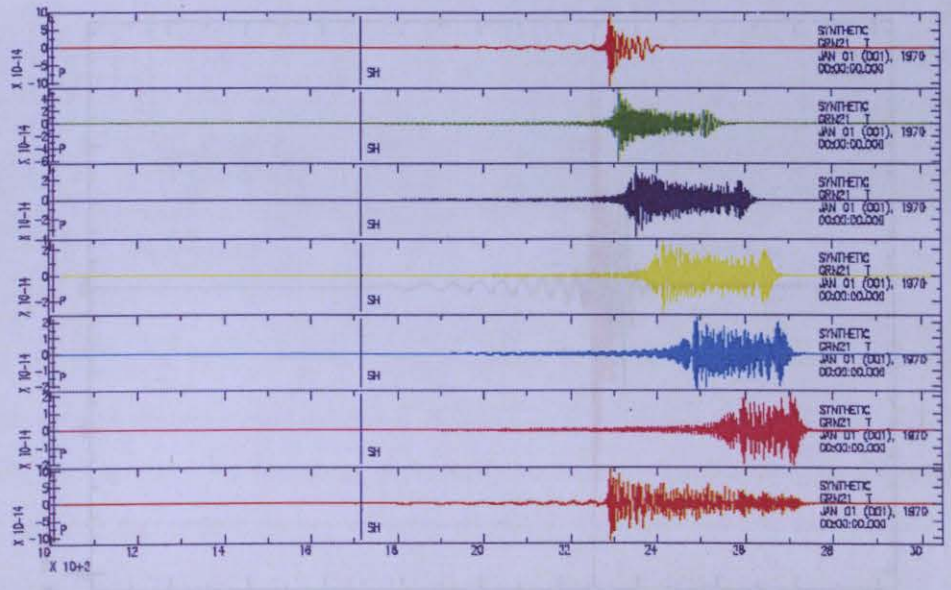

Figure 3.12. Fundamental mode, first five modes and the complete modal summation at 8000 km.

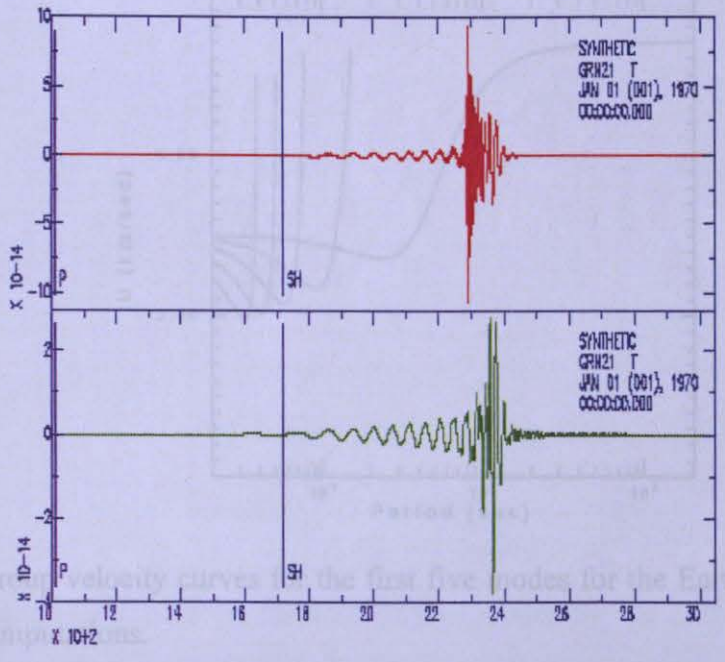

Figure 3.13. The original fundamental mode and the fundamental mode isolated by the PMF, for the signal at 8000 km.

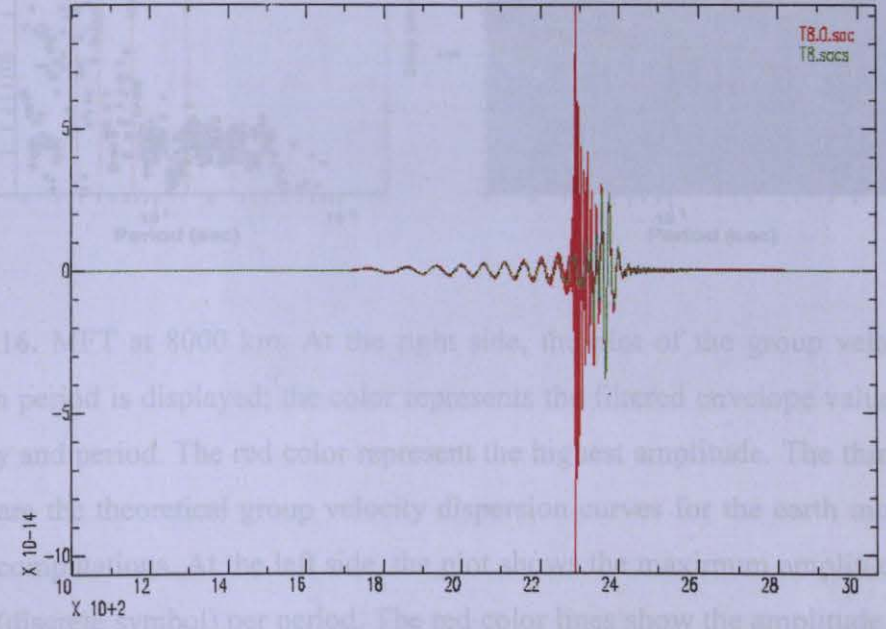

Figure 3.14. Superposition of the original fundamental mode and the output of PMF at 8000 km.

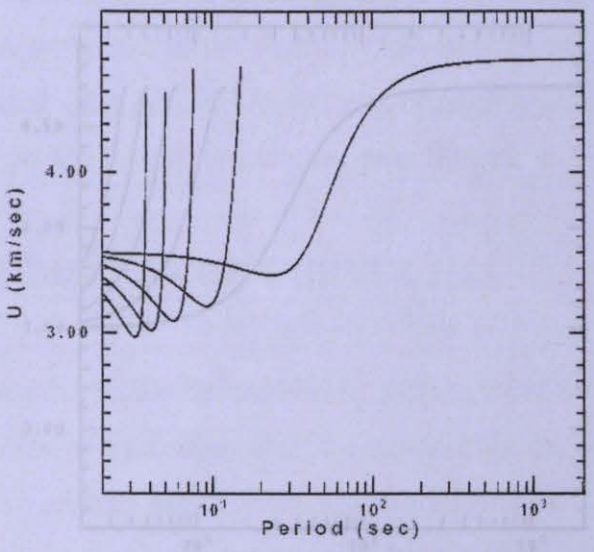

Figure 3.15. Group velocity curves for the first five modes for the Earth model used used in the synthetic computations.

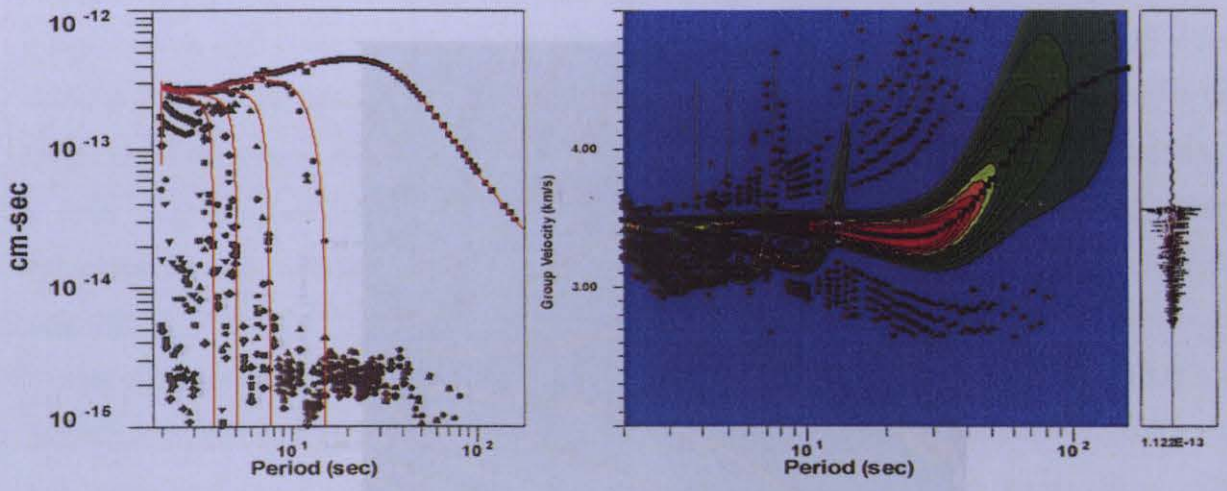

Figure 3.16. MFT at 8000 km. At the right side, the plot of the group velocity dispersion curve with period is displayed; the color represents the filtered envelope values as a function of velocity and period. The red color represent the highest amplitude. The thin black lines, in this plot, are the theoretical group velocity dispersion curves for the earth model used in the synthetic computations. At the left side, the plot shows the maximum amplitude values of the envelope (discrete symbol) per period. The red color lines show the amplitude of the different modes used in making the synthetic seismogram and with thin black line, the amplitude of the signal is plotted. The oscillation of the signal is due to the interferences of the higher modes.

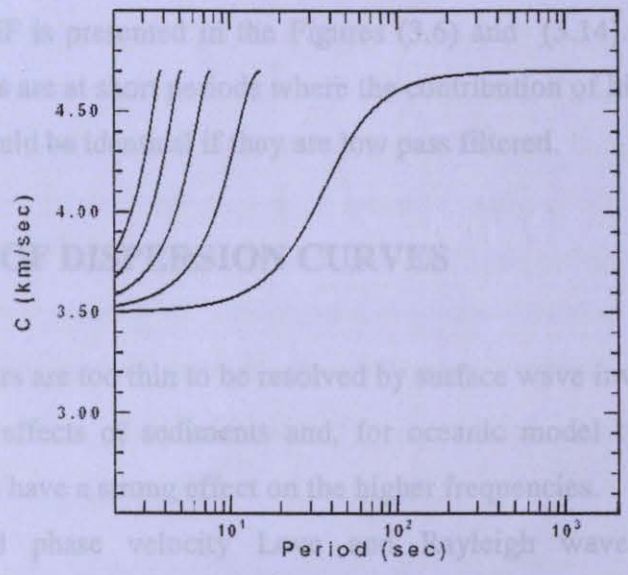

Figure 3.17. Phase velocity curves for the first five modes for the Earth model used used in the synthetic computations.

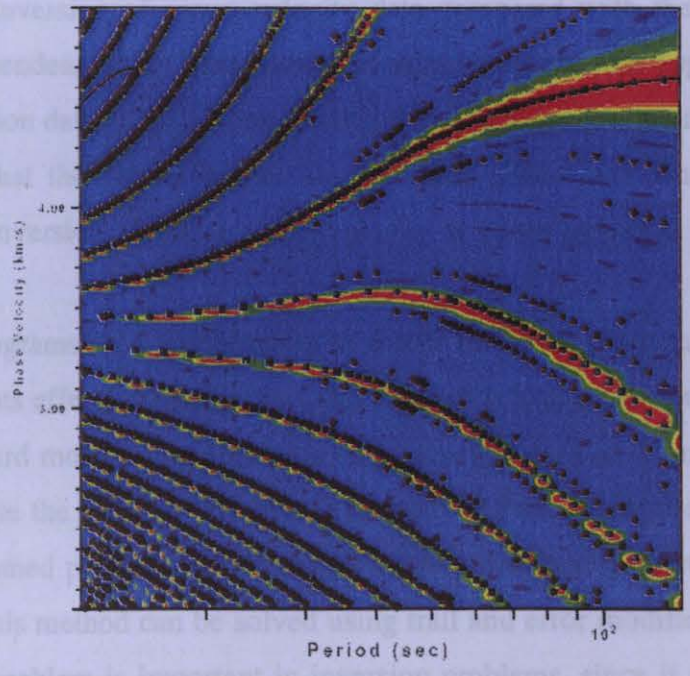

Figure 3.18. Phase velocity stack values overlain by synthetic model predicted phase velocity dispersion curves. The colors indicate the stack value, with red corresponding to the largest. The black symbol represents the chosen peaks. The thin black curve is the theoretical dispersion value.

The comparison between the synthetic fundamental mode and the isolated fundamental mode using the PMF is presented in the Figures (3.6) and (3.14). Most of the differences between both signals are at short periods where the contribution of higher modes is important. The two signals would be identical if they are low pass filtered.

4. INVERSION OF DISPERSION CURVES

The shallow layers are too thin to be resolved by surface wave inversion, but are important to account for the effects of sediments and, for oceanic model types, the water column, because these layers have a strong effect on the higher frequencies.

Both group and phase velocity Love and Rayleigh waves can be incorpareted simultaneously into shear wave velocity inversion. Group and phase velocity dispersion curves contribute generally the same information about a structural model (Bloch et al., 1969; Wiggins 1972, Yu and Mitchell, 1979). However, there exists an additional degree of non uniqueness in the inversion of group velocity data compared with the inversion of phase velocity data, independent of the other points of nonuniqueness that apply uniformly to the inversion of dispersion data of both types. If the group velocities for two regions are the same, it does not mean that the two structures are the same (Pilant and Knopoff, 1970). Phase velocities for the inversion of shear wave velocity is more powerful compared to group velocity.

Observed seismograms are a combination of source radiation, propagation path effects and recording instruments effects. Seismograms can be used to analyze the subsurface geology in two ways; by forward modeling or inversion of parameters derived from the waveform. The approach to compute the forward problem is to start with an approximate model and make changes to the assumed parameterization, until the observed and predicted seismograms are matched. Usually this method can be solved using trail and error modifications. On the other hand, the forward problem is important in inversion problems, since it provides the starting point for inversion.

For surface waves, the relationship between phase and / or group velocities at a specific frequency and the properties of the propagation path are not simple, so a numerical analysis must be performed to compute one from the other to invert for the earth model.

Obtaining a model from surface wave velocity data is neither direct nor unique, since this corresponds to the solution of a nonlinear inverse problem. A common approach to the

problem of estimating elastic properties of the Earth from seismological observations consists of assuming that the Earth is composed a finite number of horizontal homogeneous layers, and then inverting the observations for the seismic properties of each layer. Surface waves are mainly sensitive to variations in S wave velocities with depth, but such a complete variation can be done with the surface wave dispersion measurements to constrain the model.

Generally, inversion of a dispersion curve is a nonlinear process which can be linearized by applying Taylor's expansion to both phase and group velocities to a starting Earth model and neglecting higher order terms in the difference between observed phase velocity $c(\beta,\alpha,\rho)$ and predicted phase velocity $c(\beta_0,\alpha_0,\rho_0)$ to relate the difference between observed and model predicted phase velocity dispersion as;

$$c(\beta,\alpha,\rho)-c(\beta_0,\alpha_0,\rho_0)=\frac{\partial c}{\partial \beta}|_{\beta_0}(\Delta\beta)+\frac{\partial c}{\partial \alpha}|_{\alpha_0}(\Delta\alpha)+\frac{\partial c}{\partial \rho}|_{\rho_0}(\Delta\rho) \tag{4.1}$$

and between observed and predicted group velocity dispersion as;

$$U(\beta,\alpha,\rho)-U(\beta_0,\alpha_0,\rho_0)=\frac{\partial U}{\partial \beta}|_{\beta_0}(\Delta\beta)+\frac{\partial U}{\partial \alpha}|_{\alpha_0}(\Delta\alpha)+\frac{\partial U}{\partial \rho}|_{\rho_0}(\Delta\rho) \tag{4.2}$$

where;

c is the phase velocity

U is the group velocity

α_0, α is the P wave velocity

β_0, β is the S wave velocity

ρ is the density

The nonlinear inversion of the dispersion for a velocity model is easy because of the limited data sets usually used. The resulting model depends upon the starting model and constraints applied in the inversion. If the objective is that the model tells something about the Earth, it is necessary that the starting model be realistic at depth and that the model not be permitted to change in regions not controlled by the data set. The result of the inversion must

be carefully evaluated. Surface wave dispersion inversions do not exhibit the depth velocity trade off characteristic of body wave analysis, but lack of the resolution to identify velocity contrasts within the structure.

4.1. Resolution and Uniqueness

By using both group and phase velocity estimate in the inversion, we get a sense of how nonunique the modelling process is and that surface wave dispersion alone is not sufficient to fully describe the geologic structure at depth. Surface waves can not resolve thin layers.

Dispersion curves do not provide enough information to accurately constrain the geometry of deep structures. Rayleigh and Love waves are known to be sensitive mainly to the shear wave velocity and with longer wavelength they can penetrate the upper mantle, but lack the resolution to define crustal layers.

The vertical resolution of surface waves, is limited and their modeling capabilities are restricted to velocity averages rather than to vertical discontinuities.

Surface wave dispersion curves have been key to reveal the main features of the crust and upper mantle structure. As Molnar (1988) clearly states, surface wave analysis lacks the uniqueness and resolution to constrain unequivocally the distribution of S wave velocities under any region of the Earth.

Two important aspects of surface wave velocity inversions are their resolution and uniqueness. Resolution is defined as the ability of surface wave velocity information to recover the parameters of the media, and uniqueness as a qualitative measure of the number of models that could explain the observations. Both resolution and uniqueness depend on the data, and on the fineness of the details we are looking for. The discussion is limited to the resolution and uniqueness as seen from the generalized eigenvector analysis perspective (Jackson, 1972), operating in the case of a over parameterized idealization of the Earth.

Since estimating surface wave dispersion requires some important assumptions, potential sources of uncertainty must be evaluated to insure meaningful results during the shear wave velocity inversion process. Noise, scattering and errors in earthquake origin times can decrease the accuracy of the shear wave velocity and depth found during an inversion (Der et al.,1970).

Following Takeuchi and Saito (1972), surface wave velocities in a isotropic medium are sensitive to the elastic constants of the medium; that is, density, S wave velocity and P wave

velocity. Considering isotropy, the change on phase and group velocity at a given frequency due to small perturbations on the Earth properties can be written as;

$$\left(\frac{\delta c}{c}\right) = \int\left\{\frac{\delta\rho}{c}\frac{\partial c}{\partial\rho}\Big|_{\alpha,\beta,\rho} + \frac{\delta\alpha}{c}\frac{\delta c}{\delta\alpha}\Big|_{\alpha,\beta,\rho} + \frac{\delta\beta}{c}\frac{\delta c}{\delta\beta}\Big|_{\alpha,\beta,\rho}\right\}dz \tag{4.3}$$

$$\left(\frac{\delta U}{U}\right) = \int\left\{\frac{\delta\rho}{U}\frac{\partial U}{\partial\rho}\Big|_{\alpha,\beta,\rho} + \frac{\delta\alpha}{U}\frac{\delta U}{\delta\alpha}\Big|_{\alpha,\beta,\rho} + \frac{\delta\beta}{U}\frac{\delta U}{\delta\beta}\Big|_{\alpha,\beta,\rho}\right\}dz \tag{4.4}$$

where c is the phase velocity; U is the group velocity; α and β are the P and S wave velocities respectively, ρ is the density, and the symbol δ followed by a variable represents the change on the variable.

To inspect the sensitivity of the Rayleigh and Love wave phase and group velocities, A synthetic model was constructed for which the crust lies on top of a half space. The crust consists of three layers; a sedimentary cover, an upper crust, and lower crust. The thickness of the crustal layers was selected arbitrarily, but a finer discretization of 2 km per layer was used on the model. The effect of changes on surface wave velocities due to variations on the properties of the medium can be explored by looking at the partial derivatives of phase and group velocity with respect to each parameter.

Figures (4.1), (4.2), (4.3), and (4.4) show the model, Rayleigh and Love wave phase and group velocities, and the partial derivatives of those velocities with respect to the medium parameters (Vp, Vs, and density). In Figures (4.1) and (4.2) derivatives were computed for a period of 20 s while a period of 40 s was used on Figures (4.3) and (4.4). From all those figures we can draw the following observations;

Rayleigh and Love wave phase and group velocities, and the partial derivatives of those velocities with respect to the medium parameters (Vp, Vs, and density) change as follows;

1) Surface wave phase and group velocity are sensitive to changes on the medium parameters to a depth that increases with period. As the period increases the maximum value of the derivatives deepens and the general shape of the derivatives broadens.

2) The order of sensitivity of Rayleigh wave velocities is first to Vs, followed by density, and then Vp. The effects of Vp are more pronounced near the surface than at large depths.

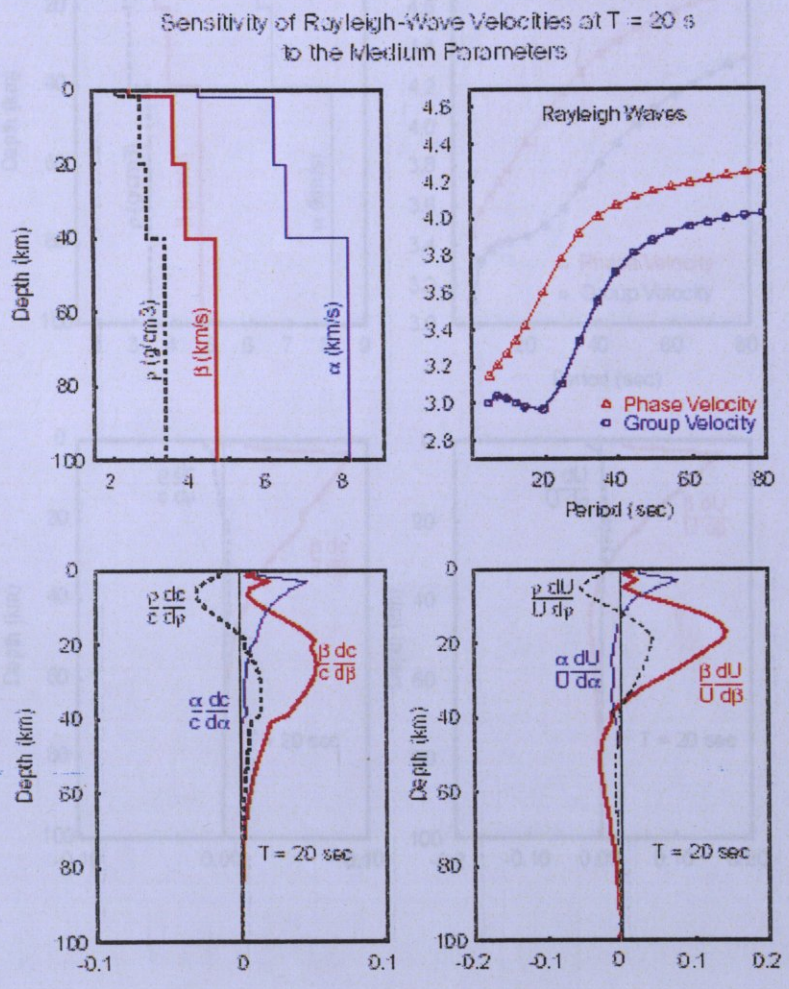

Figure 4.1. Partial derivatives of Rayleigh wave phase and group velocity at 20 s period with respect to P and S wave velocities, and density. Upper panels show the model used on this analysis (left), and the corresponding Rayleigh wave phase and group velocities (right). Bottom panels show the partial derivatives of the surface wave phase velocity (left) and group velocity (right) with respect to the model parameters. The horizontal scale is different on bottom panels, and that these derivatives are dimensionless.

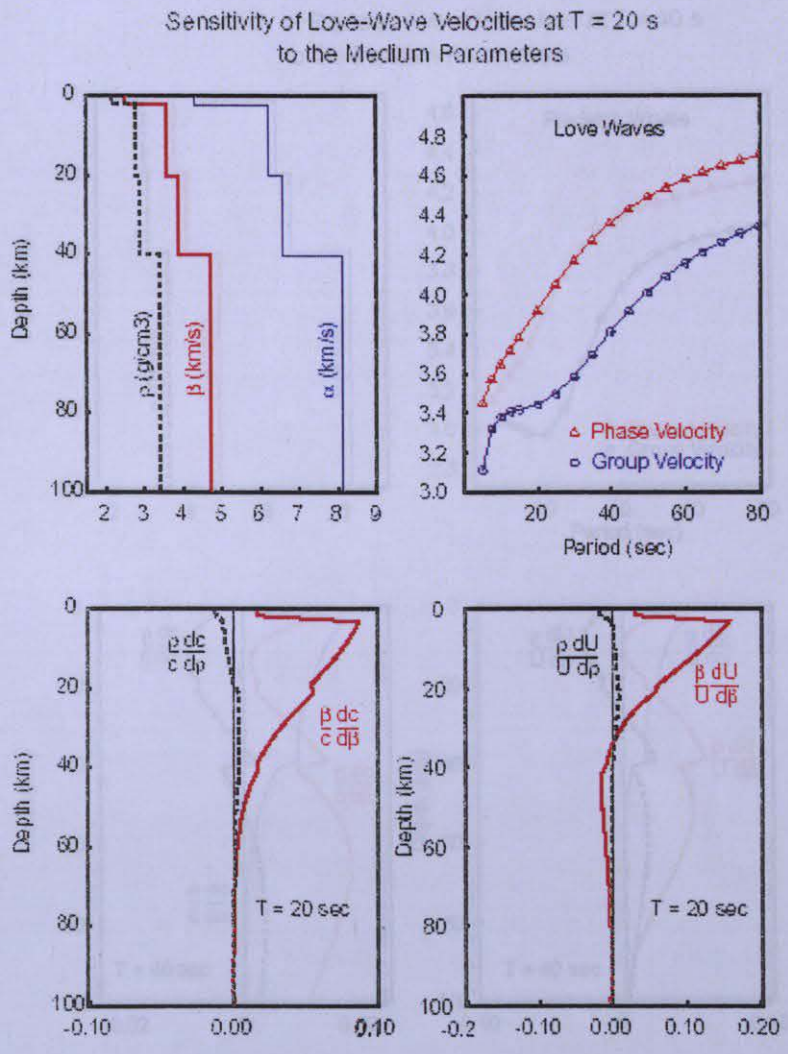

Figure 4.2. Partial derivatives of Love wave phase and group velocity at 20 s period with respect to S wave velocity and density. Upper panels show the model used on this analysis (left), and the corresponding Love wave phase and group velocities (right). Bottom panels show the partial derivatives of the surface wave phase velocity (left) and group velocity (right) with respect to the model parameters. The horizontal scale is different on bottom panels, and that these derivatives are dimensionless.

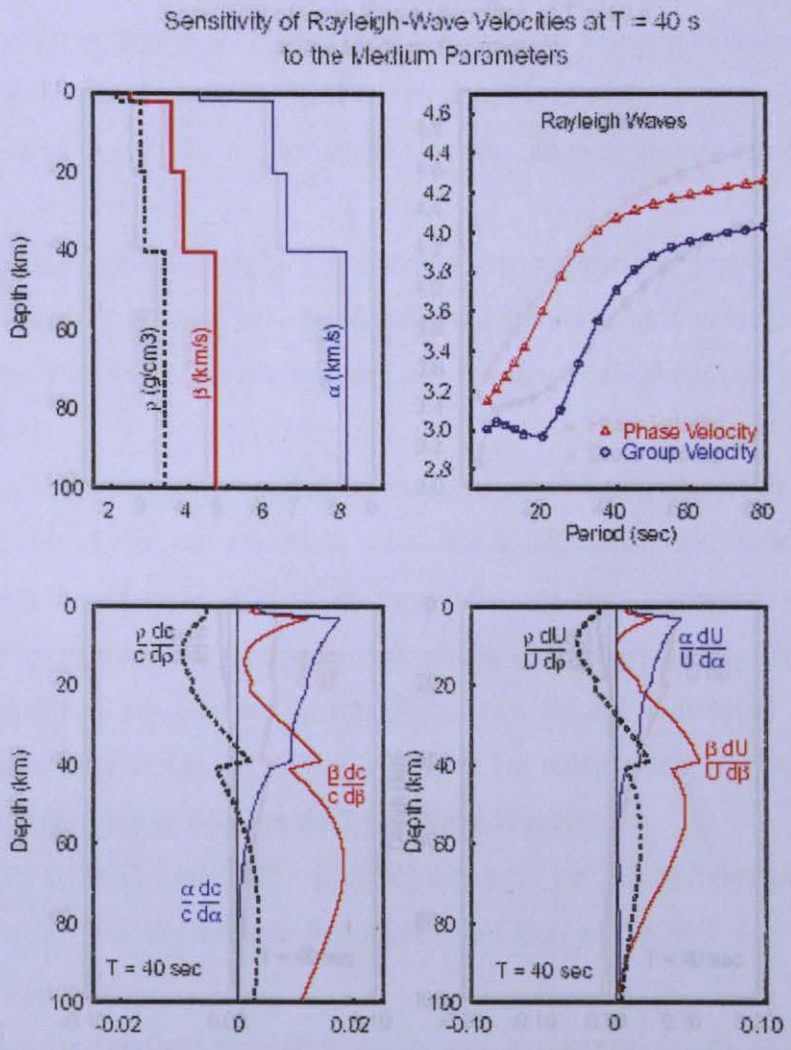

Figure 4.3. Partial derivatives of Rayleigh wave phase and group velocity at 40 s period with respect to P and S wave velocities, and density. Upper panels show the model used on this analysis (left), and the corresponding Rayleigh wave phase and group velocities (right). Bottom panels show the partial derivatives of the surface wave phase velocity (left) and group velocity (right) with respect to the model parameters. The horizontal scale is different on bottom panels, and that these derivatives are dimensionless.

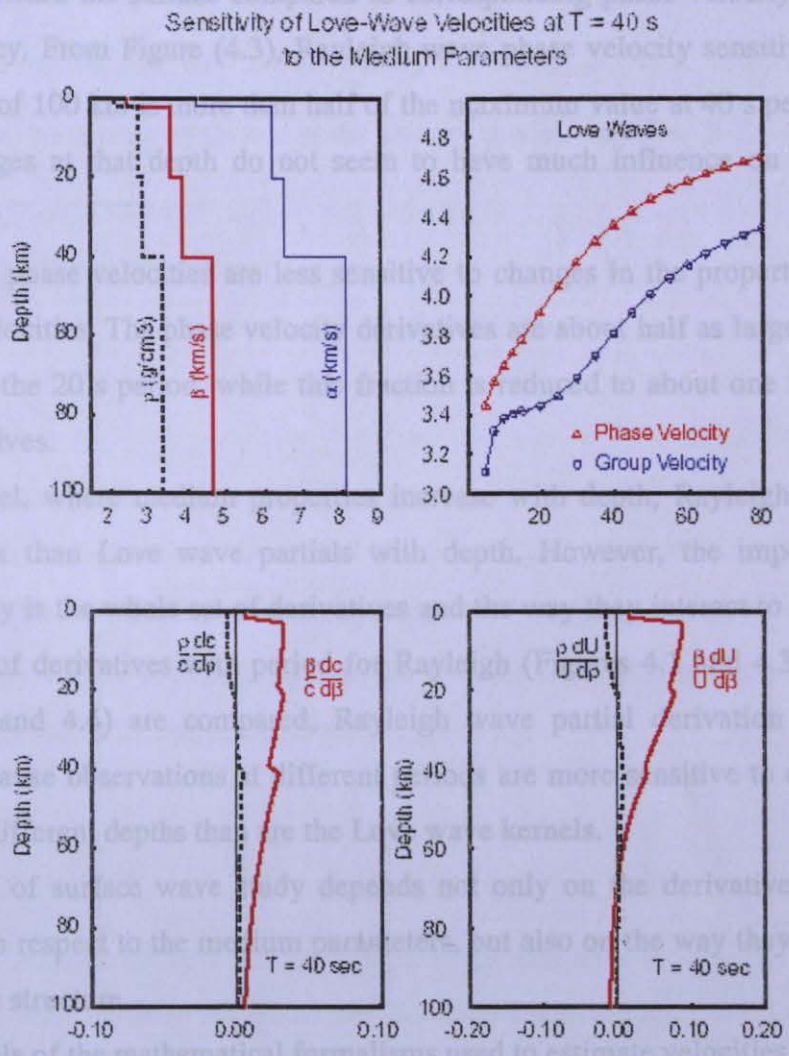

Figure 4.4. Partial derivatives of Love wave phase and group velocity at 40 s period with respect to S wave velocity and density. Upper panels show the model used on this analysis (left), and the corresponding Love wave phase and group velocities (right). Bottom panels show the partial derivatives of the surface wave phase velocity (left) and group velocity (right) with respect to the model parameters. The horizontal scale is different on bottom panels, and that these derivatives are dimensionless.

3) Love waves are much more sensitive to changes in S wave velocities than to changes on density, but they are completely insensitive to changes on Vp as we should expect from their genesis.

As Ritzwoller and Levshin (1998) pointed out, the sensitivity extent on group velocities is shallower than the sensitivity extent on phase velocities; that is, group velocity derivatives are

compressed toward the surface compared to corresponding phase velocity derivatives at the same frequency. From Figure (4.3), Rayleigh wave phase velocity sensitivity to changes on Vs at a depth of 100 km is more than half of the maximum value at 40 s period while S wave velocity changes at that depth do not seem to have much influence on the corresponding group velocity.

In general, phase velocities are less sensitive to changes in the properties of the medium than group velocities. The phase velocity derivatives are about half as large as group velocity derivatives at the 20 s period, while this fraction is reduced to about one fourth for the 40 s period derivatives.

For a model, where medium properties increase with depth, Rayleigh wave partials are more complex than Love wave partials with depth. However, the important thing in an inversion study is the whole set of derivatives and the way they interact to build a solution. If the variation of derivatives with period for Rayleigh (Figures 4.1 and 4.3) and Love waves (Figures 4.2 and 4.4) are compared, Rayleigh wave partial derivation kernels are more complete, because observations at different periods are more sensitive to changes in seismic properties at different depths than are the Love wave kernels.

Resolution of surface wave study depends not only on the derivatives of surface wave velocities with respect to the medium parameters, but also on the way they interact to resolve features of the structure.

Some details of the mathematical formalisms used to estimate velocities from surface wave observations, are as follows; it is assumed that we are looking for the actual structure of our model, starting from an initial guess that is close enough to the solution so the first order Taylor's expansion is adequate. In other words, it is assumed that our problem is linear. In this case, the equations that relate observations to the models parameters are;

$$\begin{bmatrix} \delta d_1 \\ \delta d_2 \\ . \\ . \\ . \\ \delta d_n \end{bmatrix} = \begin{bmatrix} \frac{\delta d_1}{\delta m_1} \frac{\delta d_1}{\delta m_2} \cdots\cdots \frac{\delta d_1}{\delta m_m} \\ \frac{\delta d_2}{\delta m_1} \cdots\cdots \\ \cdots\cdots \\ \cdots\cdots \\ \cdots\cdots \\ \frac{\delta d_n}{\delta m_1} \cdots\cdots \frac{\delta d_n}{\delta m_m} \end{bmatrix} \begin{bmatrix} \delta m_1 \\ \delta m_2 \\ . \\ . \\ . \\ \delta m_m \end{bmatrix} \qquad (4.5)$$

where δd_i represents the difference between the i^{th} observation and the estimates obtained from our initial model, $\partial d_i / \partial m_j$ are the partial derivatives of the i^{th} observation with respect to the j^{th} model parameter evaluated at the starting model, and δm_j is the difference between the actual j^{th} model parameter and its starting value.

Equation (4.5) can be written as;

$$\delta d = G\delta m \tag{4.6}$$

where characters represent vectors (lowercase) or matrices (uppercase), o refers to observations, G to partial derivatives, and m to the model parameters.

Solving equation (4.6) means finding a matrix $G^{\dagger}$ such that, $G^{\dagger}G = I$ the identity matrix. Usually the matrix G is ill conditioned, so the product $G^{\dagger}G$ will not give the identity matrix but a approximation to it. The solution will be given by;

$$\delta m^{est} = G^{\dagger}\delta d \tag{4.7}$$

Then, it is considered how the Earth's structure and data are related. In the absence of noise, the difference between the initial and true model is given by;

$$\delta d = G\delta m^{true} \tag{4.8}$$

Replacing δd from equation (4.8) into equation (4.7);

$$\delta m^{est} = G^{\dagger}G\delta m^{true} = R\delta m^{true} \tag{4.9}$$

where the matrix R is called the model resolution matrix (Menke,1984). The rows of R can be considered as windows through which each of the model parameters are seen from the observation's perspective. If the i^{th} row is a delta function, we could estimate the i^{th} model parameter perfectly well. On the other hand, if values on the resolution matrix are spread in a row we cannot resolve the actual value of the corresponding parameter no matter which

technique we are using to obtain them, and the solution will correspond to a weighted average of the true model parameters.

To illustrate the resolving capabilities of surface wave observations, the resolution matrix of a theoretical inverse problem will be considered. The model in Figures (4.1) to (4.4) are used to estimate the resolution matrix for the S wave velocity using Rayleigh and / or Love wave group velocities with periods between 5 s and 80 s as the observations, and I will define resolution kernel will be defined as each row of the resolution matrix.

The model, as explained previously, was discretized with 2 km layer thicknesses. Figure (4.7) shows the model, the theoretical Rayleigh and Love wave velocities, and some rows of the model resolution matrix.

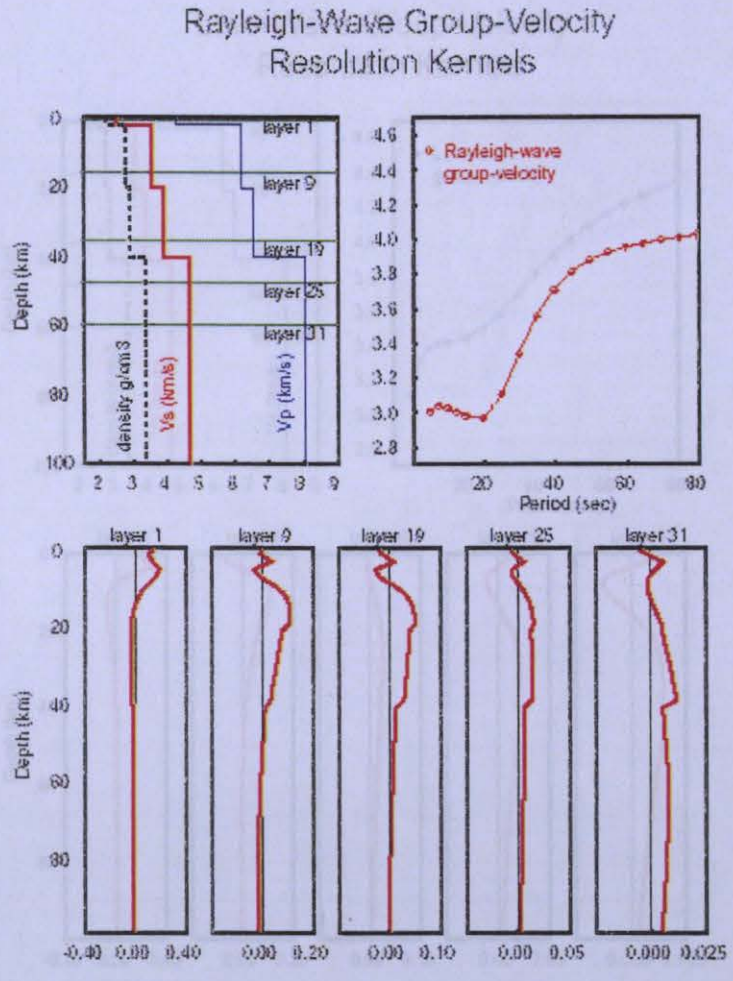

Figure 4.5. Model resolution kernels for the inversion of the S wave velocities, using Rayleigh wave group velocities as the observations. Upper panels correspond to the model (left) and theoretical group velocities (right). Lower panels show the resolution kernels of the inverse problem at selected layers indicated by the four horizontal lines in the upper left panel.

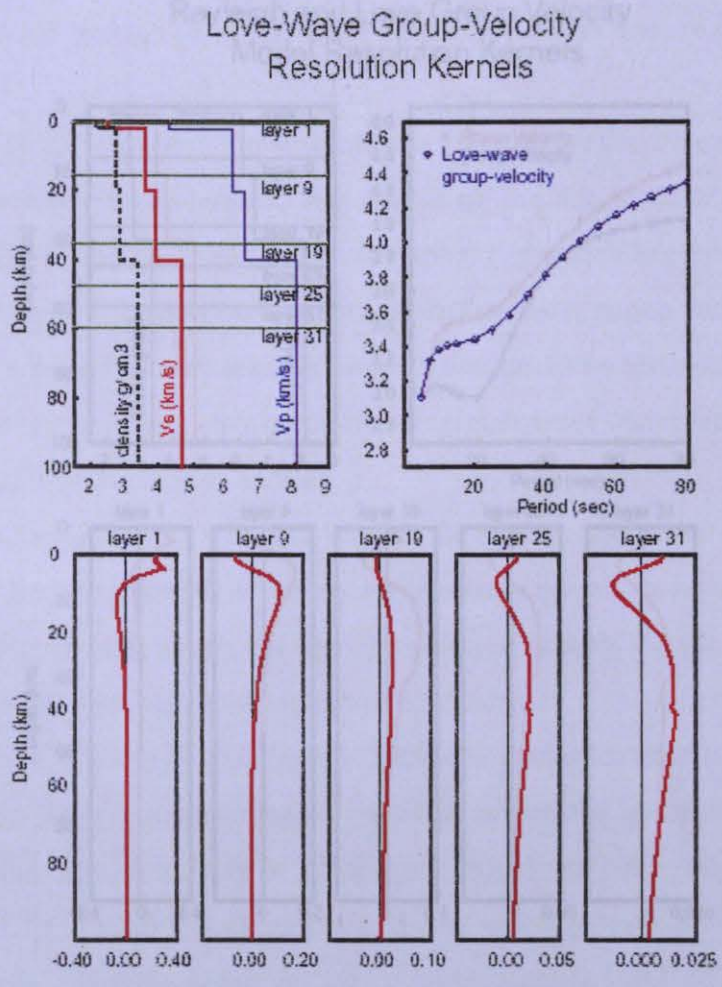

Figure 4.6. Model resolution kernels for the inversion of the S wave velocities, using Love wave group velocities as the observations. Upper panels correspond to the model (left) and theoretical group velocities (right). Lower panels show the resolution kernels of the inverse problem at selected layers indicated by the four horizontal lines in the upper left panel.

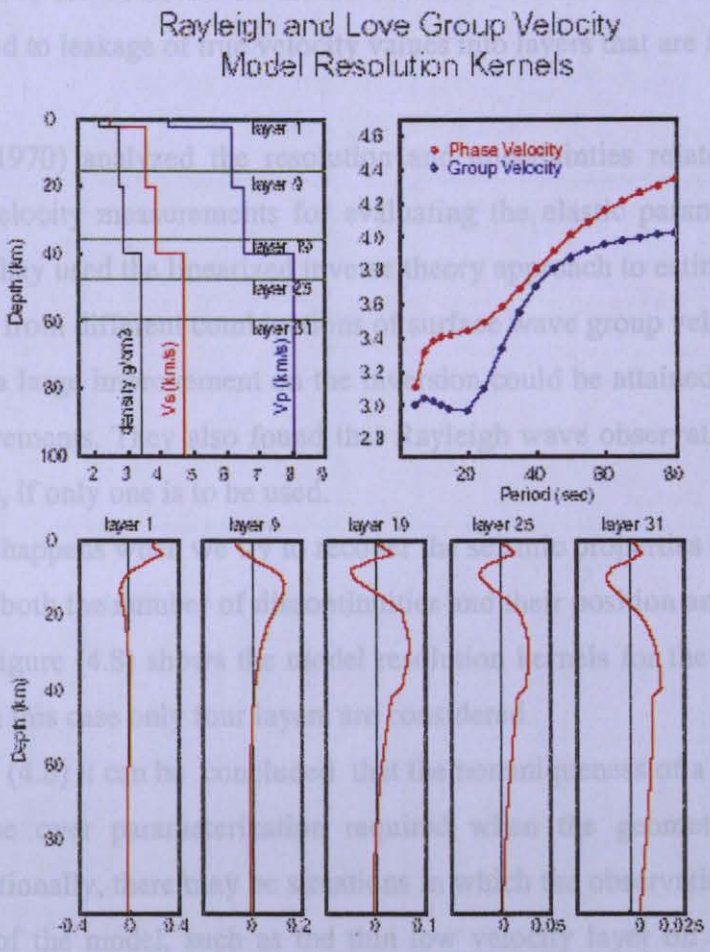

Figure 4.7. Model resolution kernels for the inversion of the S wave velocities, using Rayleigh and Love wave group velocities as the observations. Upper panels correspond to the model (left) and theoretical group and phase velocities (right). Lower panels show the resolution kernels of the inverse problem at selected layers indicated by the four horizontal lines in the upper left panel.

Some conclusions can be made ;

1) Due to the high model parameterization none of the resolution kernels resembles a delta function; therefore, not even the shallower layers can be uniquely resolved.

2) The resolution kernels spread out as they become deeper within the structure; this means that the shallower the layer the more accurate the estimation of S wave velocity can be.

3) Large sidelobes are observed on all the rows of the resolution matrix. This unfortunate situation can lead to leakage of true velocity values into layers that are far from those values.

Der et al. (1970) analyzed the resolution and uncertainties related to the inversion of surface wave velocity measurements for evaluating the elastic parameters of the crust and upper mantle. They used the linearized inverse theory approach to estimate the resolution of S wave velocities from different combinations of surface wave group velocity observations, and concluded that a large improvement on the inversion could be attained by using higher mode velocity measurements. They also found that Rayleigh wave observations are more valuable than Love wave, if only one is to be used.

To see what happens when we try to recover the seismic properties of the layered structure when we know both the number of discontinuities and their position another synthetic test has been applied. Figure (4.8) shows the model resolution kernels for the model used in Figures (4.5) to (4.7). In this case only four layers are considered.

From Figure (4.8) it can be concluded that the nonuniqueness of a surface wave inversion comes from the over parameterization required when the geometry of the structure is unknown. Additionally, there may be situations in which the observations see little or nothing of some parts of the model, such as the thin low velocity layer on top of the structure on previous example, when the group velocity observations start at 5 s. These conclusions arise from the fact that model resolution kernels resemble delta functions for three of the four layers of the model. The model resolution kernel of the top layer shows that what we obtain for the top layer velocity after the inversion is mostly a weighted average of velocities on the next two layers. This unfavorable situation comes from the truncation of small eigenvalues during the determination of the matrix $G\dagger$.

In summary, surface wave dispersion measurements are mostly sensitive to changes on S wave velocities, although P wave velocity variations may be important when they occur in shallow structures. Surface wave phase velocities carry less information than corresponding group velocities, and Rayleigh waves are more sensitive to model parameters than Love waves; yet, none of these observations could lead us to obtain an unique model of the structure, except when the geometry of the layers is known beforehand (if we try to recover the seismic properties of the layered structure when we know both the number of discontinuities and their position) and when the observations carry enough information to resolve all the details that the actual model requires.

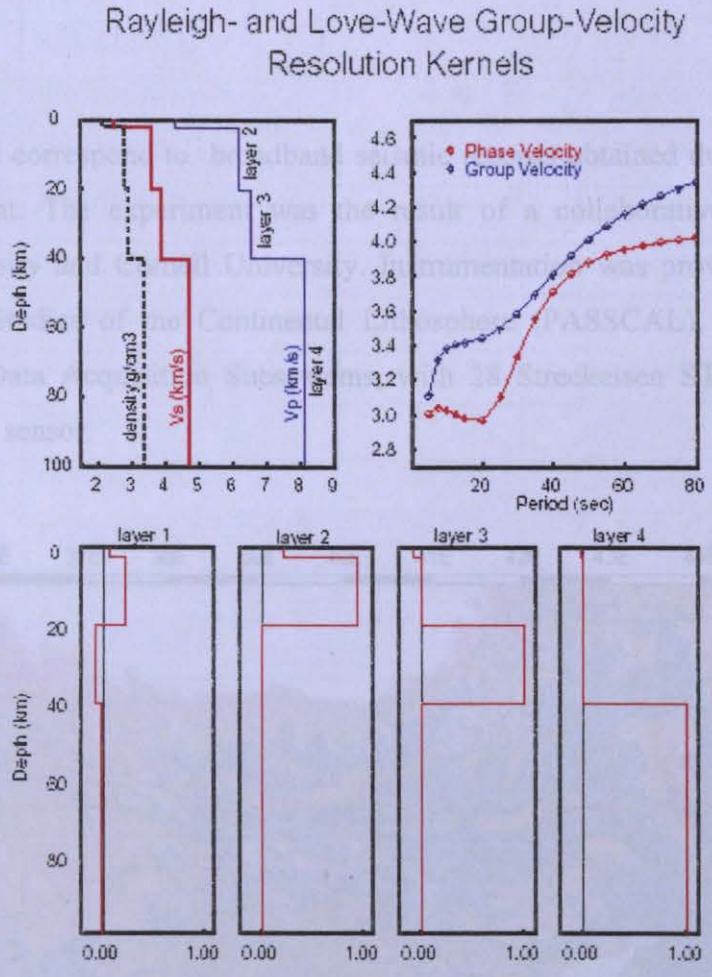

Figure 4.8. Model resolution kernels for the inversion of the S wave velocities, when both number of layers and their thicknesses are known, using Rayleigh and Love wave group velocities as the observations. Upper panels correspond to the model (left) and theoretical group and phase velocities (right). Lower panels show the resolution kernels of the inverse problem at each of the four layers of the actual structure.

5. SURFACE WAVE ANALYSIS AND RESULTS

5.1. Data

The data used correspond to broadband seismic records obtained during the 1999 - 2001 ETSE experiment. The experiment was the result of a collaborative effort between the Boğaziçi University and Cornell University. Instrumentation was provided by program for Array Seismic Studies of the Continental Lithosphere (PASSCAL), and consisted of 29 REFTEK 72A Data Acquisition Subsystems, with 28 Streckeisen STS-2 sensors and one Guralp CMG-3T sensor.

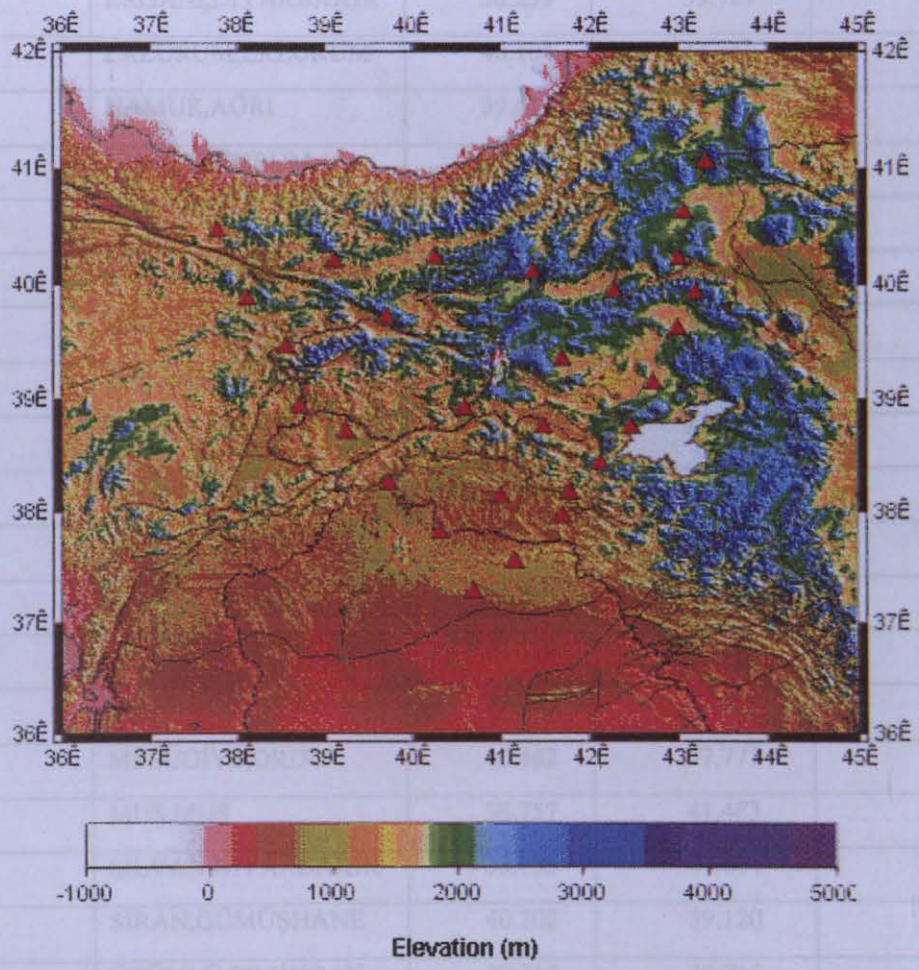

Figure 5.1. Map view of the Eastern Anatolian Plateau with topography. Symbols represent the locations of the temporary ETSE broadband seismic stations in Eastern Turkey used in this study that were deployed during the 1999-2001 Eastern Anatolian Seismic Experiment. Solid lines show the location of major faults.

STATION ID	LOCATION	LATITUDE (°N)	LONGITUDE (°E)	ELEVATION (m)
AGIN	AĞIN,ELAZIĞ	38.939	38.712	837
AHLT	AHLAT,BİTLİS	38.748	42.477	1614
BNGL	BİNGÖL,BİNGÖL	38.920	40.598	968
BTLS	BİTLİS,BİTLİS	38.431	42.124	1695
BYBT	BAYBURT,BAYBURT	40.235	40.266	1662
BYKN	BAYKAN,SİİRT	38.166	41.782	819
CMCY	CUMAÇAY,AĞRI	39.920	43.196	2031
DGRL	DOĞRUYOL,KARS	41.056	43.326	2037
DGSU	DOĞANSU,AĞRI	39.131	42.729	1623
DYBR	DİYARBAKIR	37.823	40.318	678
ERGN	ERGANİ,DİYARBAKIR	38.259	39.729	861
EZRM	ERZURUM,ERZURUM	40.104	41.363	1830
HAMR	HAMUR,AĞRI	39.613	42.992	1710
HINS	HINIS,ERZURUM	39.349	41.697	1640
HRPT	HARPUT,ELAZIĞ	38.704	39.246	1380
HRSN	HORASAN,ERZURUM	39.945	42.287	1773
ILIC	ILIÇ,ERZİNCAN	39.454	38.570	1281
IMRL	İMRANLI,SİVAS	39.880	38.119	1596
KARS	KARS,KARS	40.622	43.068	1860
KOTK	KOTEK,KARS	40.222	43.009	1365
KRLV	KARLIOVA,BİNGÖL	39.375	40.987	1842
KTLN	KURTALAN,SİİRT	37.953	41.707	791
KYPR	KAYAPINAR,BATMAN	37.559	41.169	1231
MRDN	MARDİN,MARDİN	37.290	40.698	669
MSDY	MESUDİYE,ORDU	40.462	37.777	1104
MUSH	MUŞ,MUŞ	38.757	41.483	1506
SILN	SİLVAN,DİYARBAKIR	38.135	41.004	870
SIRN	SİRAN,GÜMÜŞHANE	40.202	39.120	1485
UZML	ÜZÜMLÜ,ERZİNCAN	39.713	39.715	1485

Table 5.1. ETSE station locations.

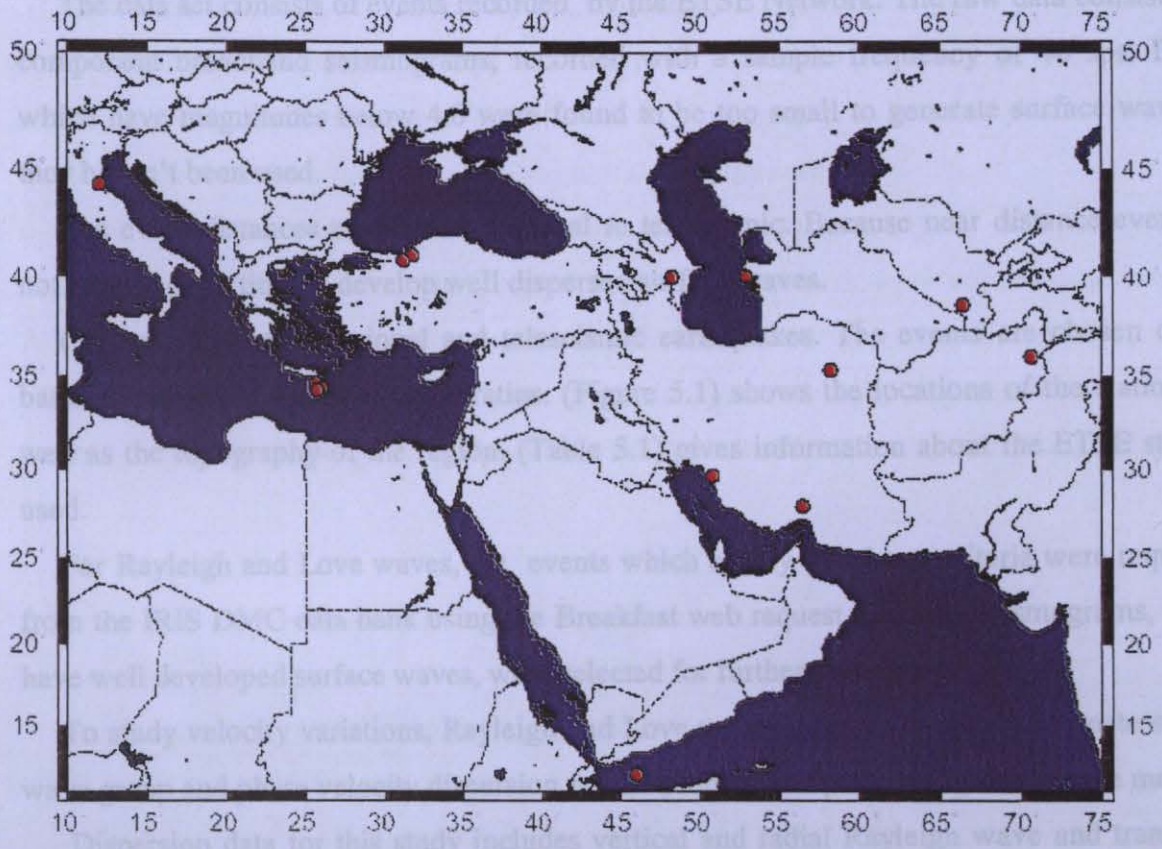

Figure 5.2. Figure shows the location of earthquakes (red circles) and the stations (white triangles).

Table 5.2. List of Earthquakes Used in this Study

NO	DATE	ORIGIN TIME UT	LATITUDE (°N)	LONGITUDE (°E)	MAGNITUDE
1	26 012000	23:00:19.9	40.02	52.90	5.5
2	02 02 2000	22:58:01.5	35.29	58.22	5.1
3	10 02 2000	01:35:01.9	12.01	45.95	5.0
4	14 02 2000	06:38:27.4	11.90	46.06	5.0
5	22 02 2000	11:55:25.6	34.60	25.60	5.1
6	05 03 2000	09:40:06.0	27.95	56.47	5.6
7	10 03 2000	22:01:45.9	34.36	26.03	5.1
8	21 03 2000	14:07:40.8	39.95	48.23	5.1
9	05 04 2000	04:36:58.8	34.22	25.69	5.3
10	20 04 2000	08:41:29.5	38.62	66.44	5.5
11	03 05 2000	09:01:16.2	29.66	50.80	5.0
12	10 05 2000	16:52:09.8	44.31	12.00	5.0
13	12 05 2000	23:10:29.9	35.97	70.66	6.2
14	12 11 1999	16:57:19.55	40.76	31.16	7.5

The data set consists of events recorded by the ETSE Network. The raw data consists of 3 component broadband seismograms, recorded with a sample frequency of 40 sps. Events which have magnitudes below 4.0 were found to be too small to generate surface waves so they haven't been used.

The event distances range from regional to teleseismic. Because near distance events do not have enough time to develop well dispersed surface waves.

(Figure 5.2) shows regional and teleseismic earthquakes. The events are chosen on the basis of adequate signal to noise ratios. (Figure 5.1) shows the locations of the stations, as well as the topography of the region. (Table 5.1) gives information about the ETSE stations used.

For Rayleigh and Love waves, the events which satisfy the above criteria were requested from the IRIS DMC data bank using the Breakfast web request method. Seismograms, which have well developed surface waves, were selected for further processing.

To study velocity variations, Rayleigh and Love waves were analyzed to estimate surface wave group and phase velocity dispersion for the propagation paths using one station method.

Dispersion data for this study includes vertical and radial Rayleigh wave and transverse Love wave component seismograms. Group and phase velocity dispersion curves are calculated for the events recorded from 23 October 1999 to 9 August 2001 in the ETSE network.

5.2. Data Preperation

The first step is acquiring the waveforms. Data requests to individual networks can be constructed in a variety of ways, the easiest is to create an electronic mail request for the waveforms. Once the data are retrieved they are organized into groups by recording station.

To perform surface wave study, three component (vertical, north south and east west) broadband signals are required. In this effort, signals are used from events with magnitude M $\geq$ 4, regional and teleseismic earthquakes, recorded between 1999 and 2001 ETSE experiment.

Before doing any analysis of the seismogram, the instrument response must be removed. This is done by deconvolving the instrument from the seismogram. But because of the nature of surface wave analysis, we do not necessarily need information of the instruments as long as the instrument responses of the three components are matched. So it was not necessary to remove the instrument response before doing the processing.

Each pair of horizontal component signals (north south and east west components) are rotated to their corresponding radial and transverse directions (Figure 5.3). Once the radial and transverse component of motion are obtained, the seismograms were then decimated and trend and taper analysis have been applied to the seismograms.

Finally, each three component signal are reviewed to remove signals that contained low signal to noise ratios and / or when any of the three components were not recorded properly. After the removal of noisy and incomplete signals, surface waves are calculated.

Using the methodology discussed, the group and phase velocity dispersion curves for the fundamental mode Rayleigh and Love waves are calculated using one station method (Figure 5.4).

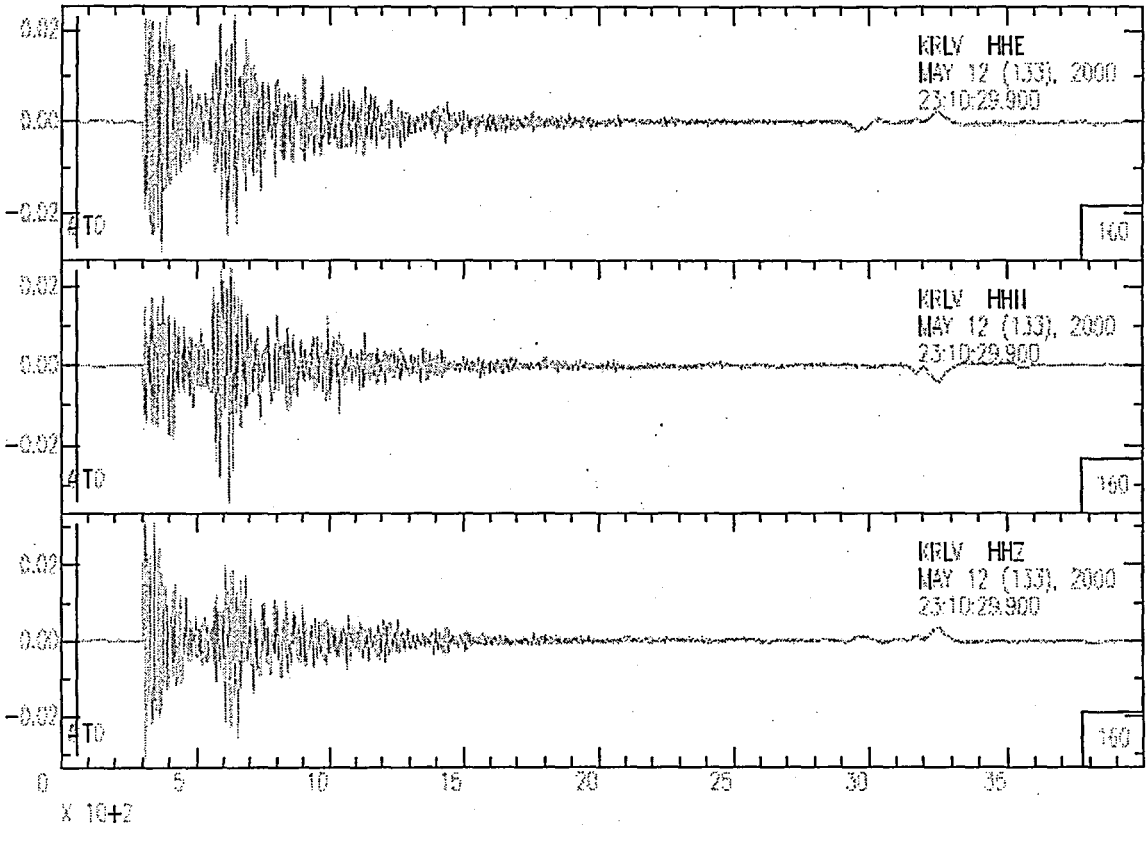

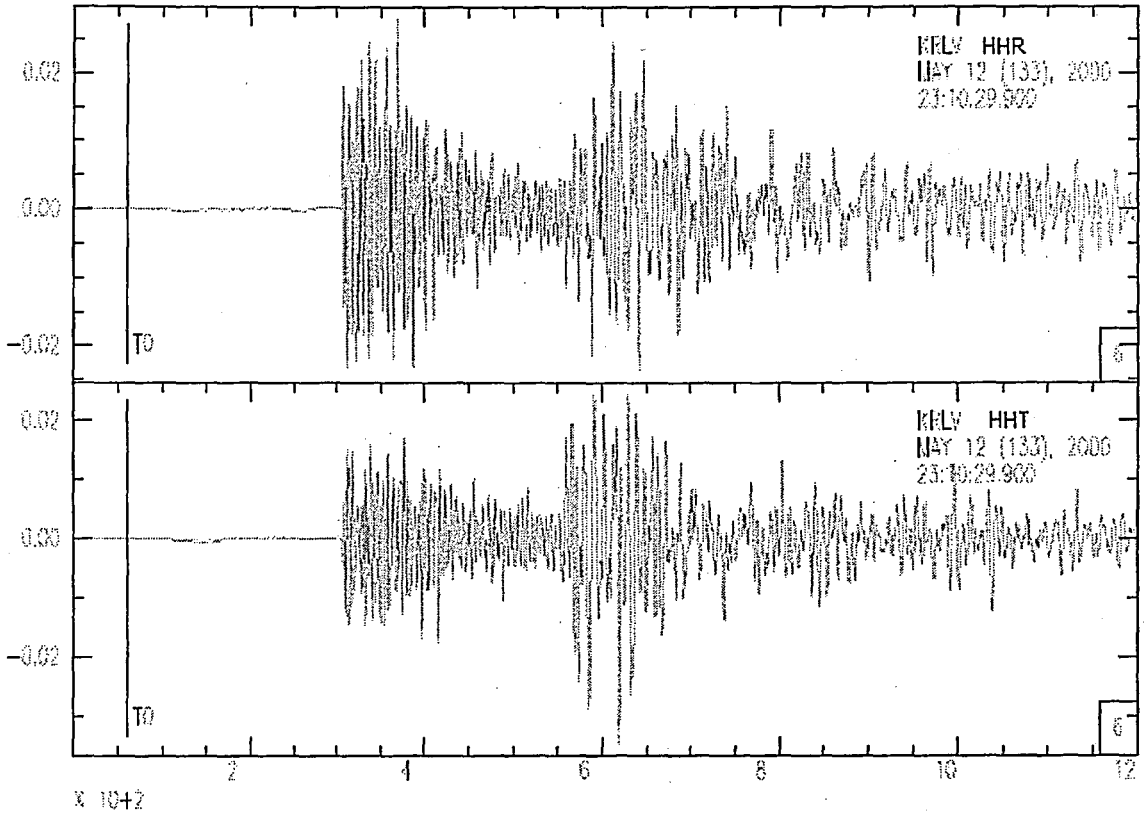
KELV HHR
MAY 12 (133), 2000
23:10:29.900
0.02
0.00
-0.02
T0
KELV HHT
MAY 12 (133), 2000
23:10:29.900
0.02
0.00
-0.02
T0
2
4
6
8
10
12
x 10+2

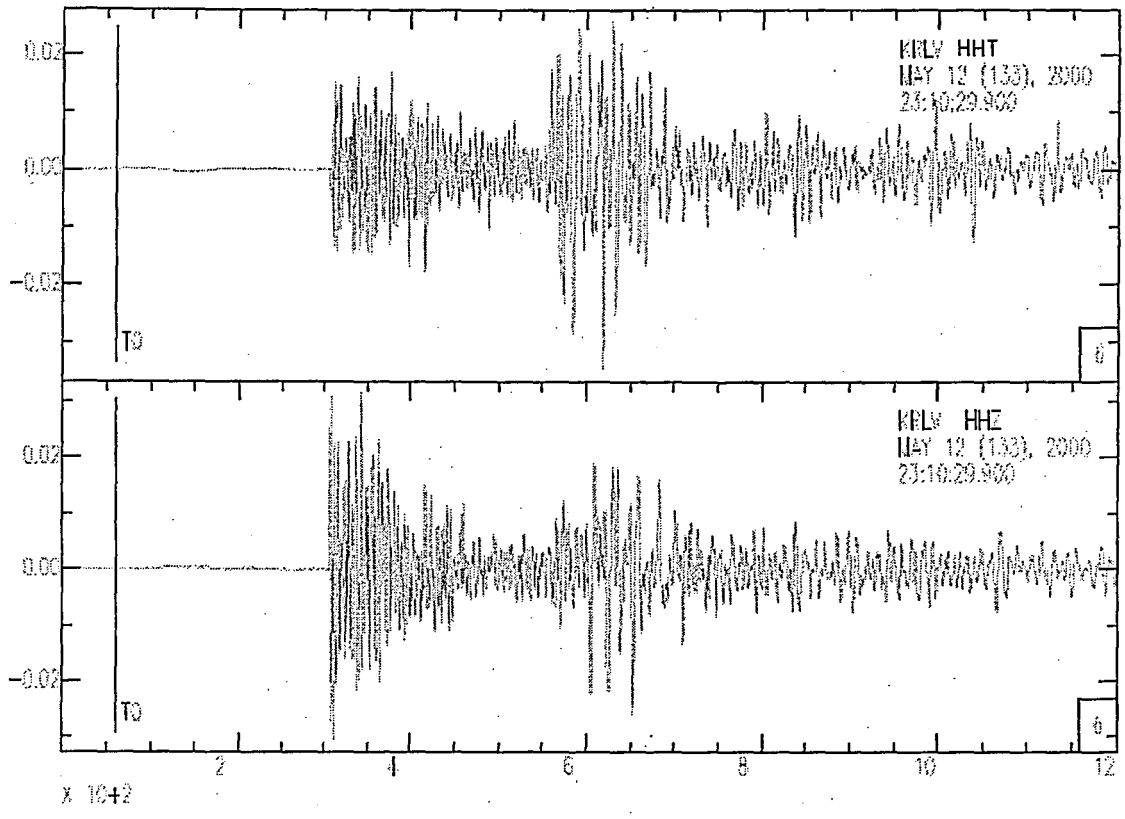

Figure 5.3. An example of the actual (raw) (the east-west component (HHE), the north-south component (HHN), and the vertical component (HHZ)) seismogram at the top, and rotated seismogram (the radial component (HHR), and the tangential component (HHT)), in the middle, used to compute the surface waves. The figure at the bottom is the phase matched filtered seismogram of (the radial component (HHT), and the vertical component (HHZ) seismograms). (?)

5.3. Results

Dispersion curves are sensitive to velocity averages rather than to specific details. Therefore, velocity models obtained by inverting surface wave dispersion curves are strongly dependent on the initial assumptions of layer thicknesses and the location of first order velocity discontinuities. Since the surface waves from different periods travel at different velocities, their analysis can give a constrain to the earth structure.

In this study, the group and phase velocities of fundamental mode Rayleigh and Love waves are obtained using Computer Programs in Seismology code (Herrmann and Ammon,

2002). (Figure 5.4) shows the location of ETSE stations, earthquakes used and the ray paths that the dispersion curves are obtained.

Rayleigh wave phase velocity is measured between 10 and 85 second periods. Phase velocity is 2.75 km/s for 10 second period and it is 3.9 km/s for 85 second period (Figure 5.5). On the other hand, Love wave phase velocity is measured between 10 and 50 second periods. Phase velocity is 2.8 km/s for 10 second period and 4.40 km/s for 50 second period (Figure 5.6).

Results from different period ranges imply a different S wave velocity disribution within the region.

Starting models used for the surface wave inversions include both a 1-D model from a 12 ton dam shot recorded by ETSE (Gürbüz et al., 2004) and the models from the original receiver function inversions.

During the inversion, rapid velocity changes of the layers make the inversion unstable. By using Differential Smoothing Technique (Constable et al., 1987) this kind of unstability problem in the inversion can be solved. In this technique; lots of thin layers are given during the initial modelling. By imposing a restriction into the equations, it doesn't allow the rapid velocity changes between the layers as much as it can be. At the end of the inversion, a smoothed earth structure is obtained (Constable et al., 1987). This method has been used while obtaining the S wave velocity structure in this study.

According to the results of S wave velocity versus depth inversion, it is found that between 20 and 30 km depth there is a low velocity layer, which has S wave velocity of approximately 3.4 km/s. The thickness of the crust is calculated as 45 km. Velocity gradually increases between 30 km and 45km (Figure 5.7) and (Table 5.3) .

It can be seen from the result of inversion that, the upper crust is well defined and there is a crust mantle transition in between.

S wave velocities in the middle of the array, where there is a triple junction, we find a low velocity zone. The thickness of the crust varies and variation in thickness of the crust can be attributed to the complexity of the region.

Thickness of the crust, S wave velocity and depth of LVZ that we found are in good agreement with the previous studies.

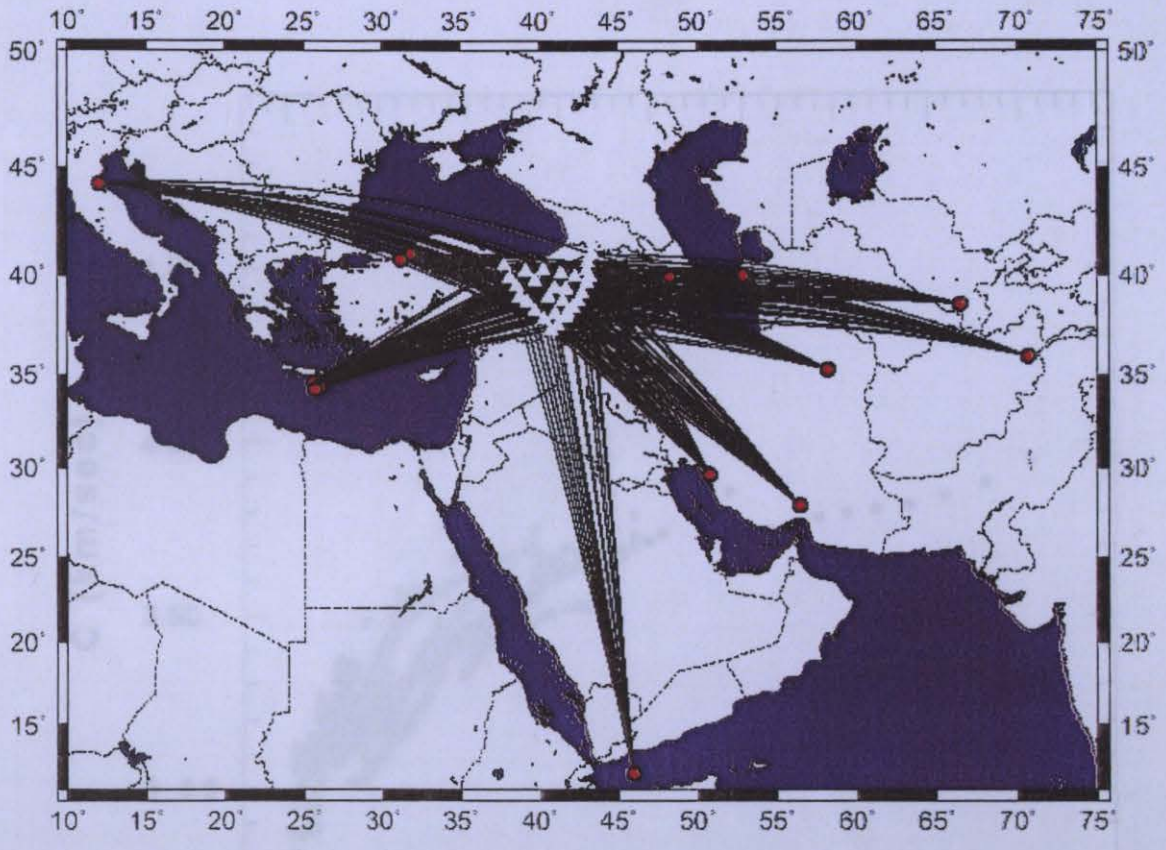

Figure 5.4. Figure shows the location of earthquakes (red circles) whose records were used to obtain dispersion curves on the Eastern Anatolian Plateau and the stations (white triangles).

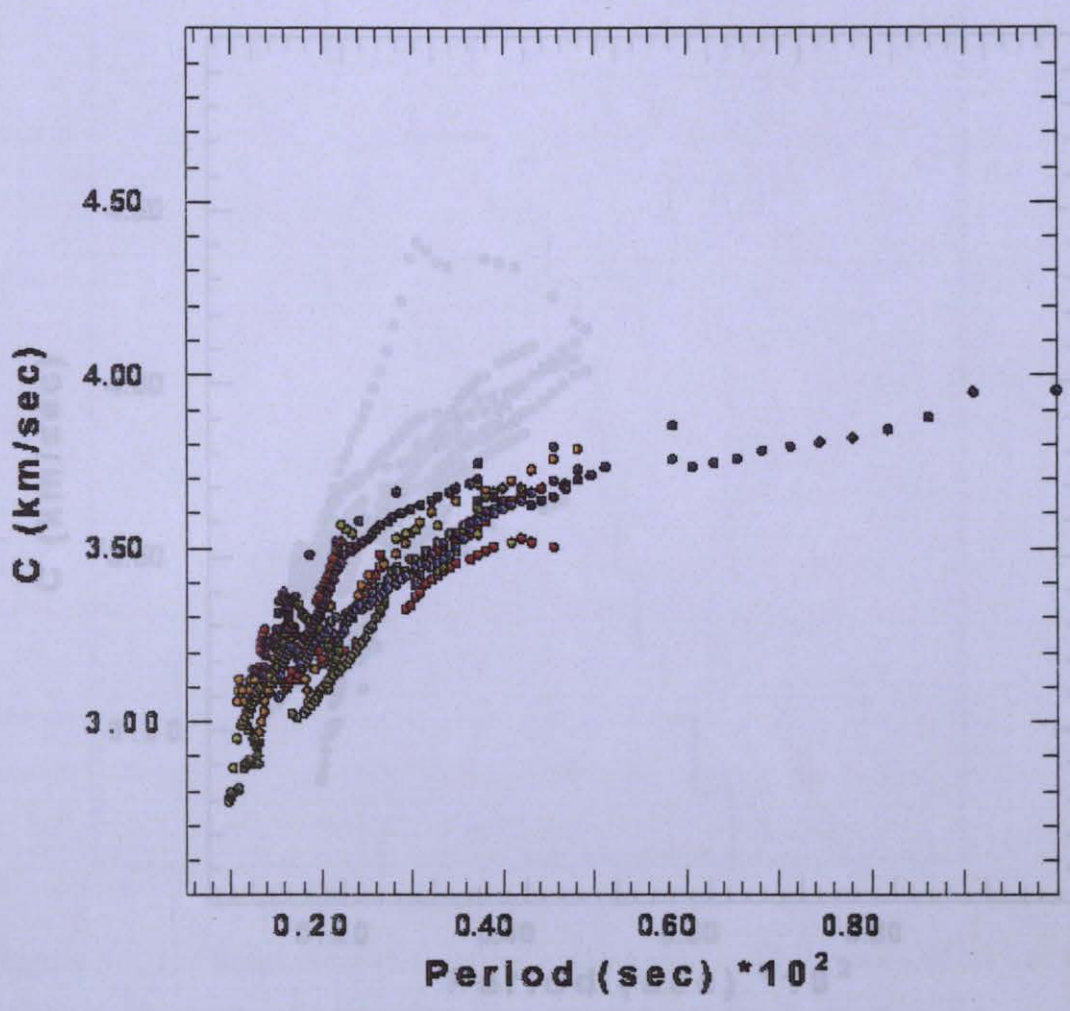

Figure 5.5. Rayleigh wave phase velocity curves. The different colors correspond to different earthquakes.

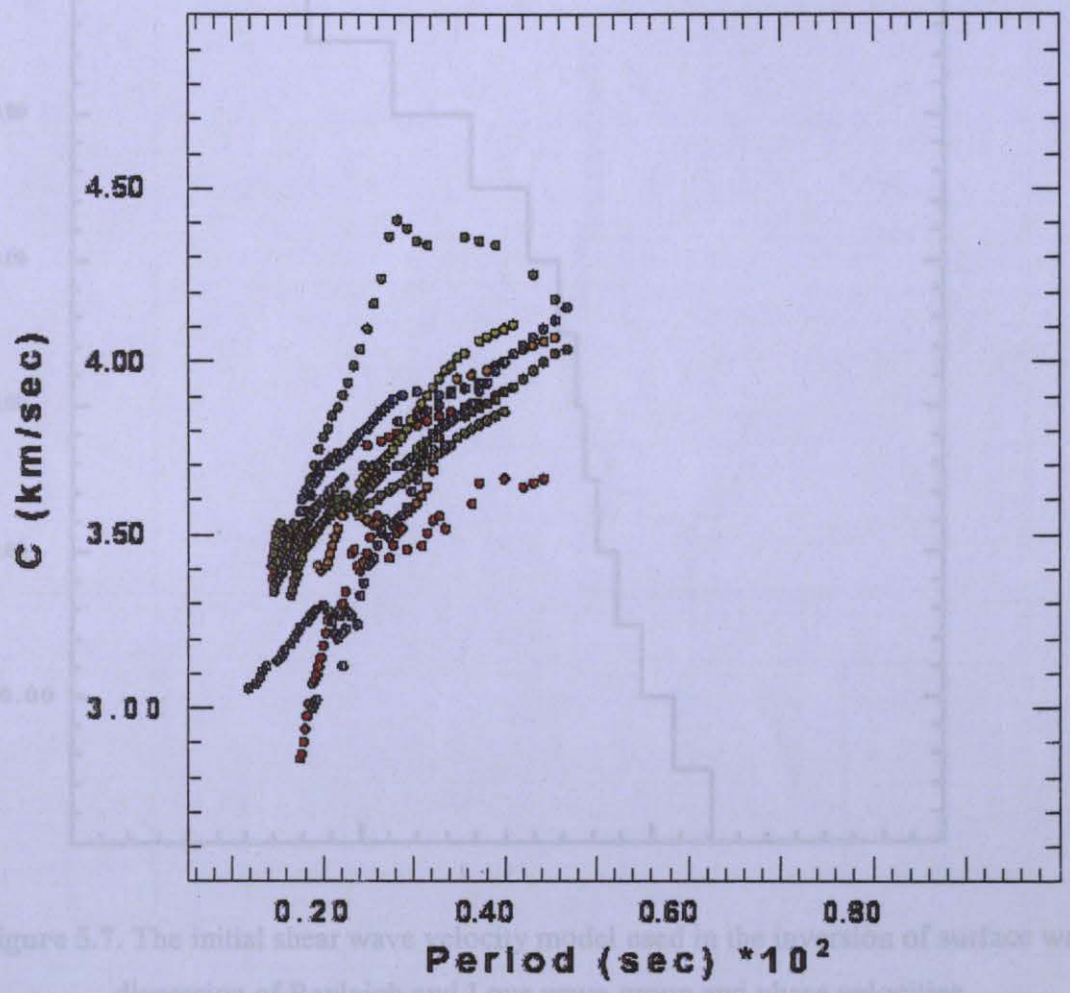

Figure 5.6. Love wave phase velocity curves. The different colors correspond to different earthquakes.

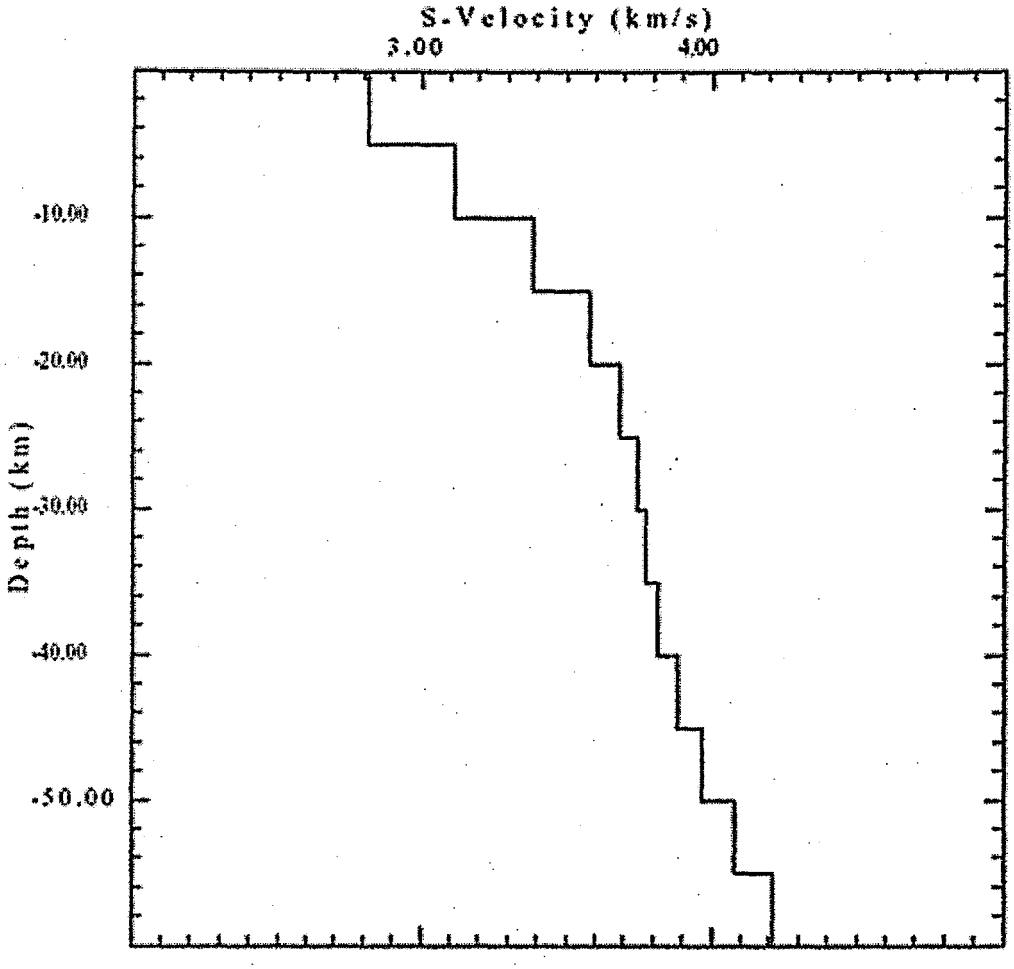

Figure 5.7. The initial shear wave velocity model used in the inversion of surface wave dispersion of Rayleigh and Love wave group and phase velocities.

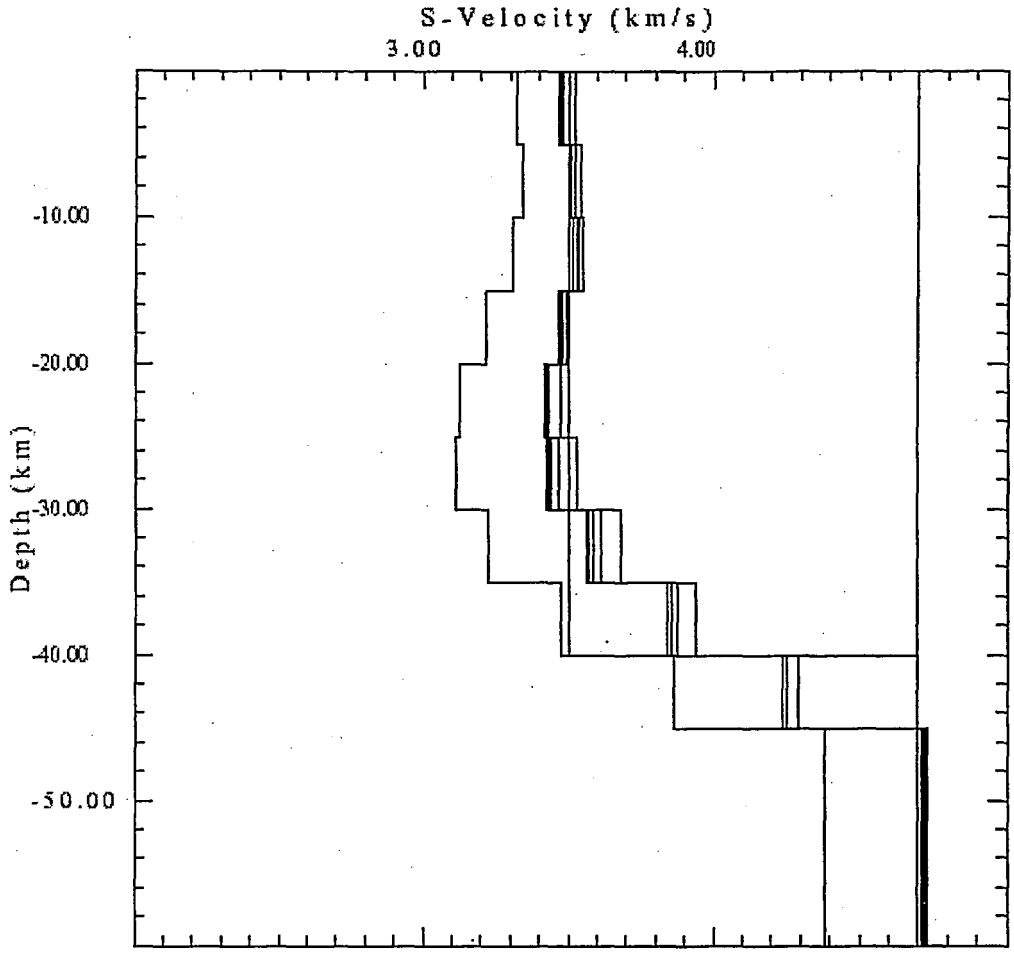

Figure 5.7. The final shear wave velocity model inverted from surface wave dispersion of Rayleigh and Love wave group and phase velocities.

D(KM)	H(KM)	VP(KM/S)	VS(KM/S)	RHO(GM/CC)
5	5	5.876	3.452	2.6753
10	5	5.9892	3.5186	2.6979
15	5	6.0621	3.5614	2.7187
20	5	5.9738	3.5095	2.6948
25	5	5.8389	3.4305	2.6678
30	5	5.8271	3.4234	2.6655
35	5	6.054	3.5568	2.7163
40	5	6.5365	3.8402	2.8592
45	5	7.2162	4.2395	3.0488
50	0	8.0291	4.727	3.3201

Table 5.3. Inversion results from group and phase velocities of Rayleigh and Love waves, where H is the layer thickness.

6. DISCUSSION AND CONCLUSIONS

One of the aim of the Eastern Turkey Seismic Experiment (ETSE) was to investigate the crustal and upper mantle velocity structure beneath the northernmost Arabian plate and the Anatolian Plateau and also the Eurasian Arabian plate margins across the Bitlis suture and East and North Anatolian Fault zones in order to constraine geodynamic models for young continent continent collision. ETSE was composed of a 29 station broadband PASSCAL array which was deployed from October 1999 until August 2001 for a period of two years. Broadband data available through the Eastern Turkey Seismic Experiment (ETSE) provide an opportunity for studying the high resolution velocity structure of the region.

We investigated the crust and upper mantle structure of Eastern Turkey where the Anatolian, Arabian and Eurasian Plates meet, forming a complex tectonic regime. Analysis of surface wave data is an important tool for determining the average shear wave velocity structure beneath the region. Well recorded regional and teleseismic surface wave data were used to calculate phase and group velocities of Rayleigh and Love waves.The velocity structure beneath the region was investigated by using different period ranges. We obtained S wave velocity model by making Love and Rayleigh wave dispersion measurements using the ETSE stations with one station method.

Since the surface waves from different periods travel at different velocities, hence their displacements vary with depth, their analysis can give a constrain to the earth structure.

The group and phase velocities are obtained using Computer Programs in Seismology code (Herrmann and Ammon, 2002), where the Rayleigh and Love waves are selected from the vertical, radial and tangential displacements, respectively.

Zor et al. (2003) found an average 46 km thick crust in the Anatolian Plateau using inversion of receiver functions. Receiver functions are sensitive to the velocity contrast of interfaces and the relative travel time of converted and reverberated waves between those interfaces. The interpretation of receiver functions alone, however, may result in an apparent depth velocity trade off (Ammon et al., 1990).

The receiver function profile along the western transect of the ETSE array indicates that there is no significant crustal thickening across the East Anatolian Fault Zone (EAFZ). This implies that the northward convergence of the Arabian plate is being largely accommodated by the westward extrusion of the Anatolian plate. The profile does suggest,

the presence of a crustal root near the northern part of the Anatolian Plateau and across the North Anatolian Fault (Zor et al., 2003)

Results from Sn attenuation tomography and Pn travel time tomography imply a fundamental change in the properties of the uppermost mantle in the vicinity of the Bitlis suture and EAFZ. Observations of very low Pn velocities and very high Sn attenuation beneath the easternmost Anatolian Plateau are best interpreted to indicate that the mantle lid beneath the Eastern Anatolian Plateau is anomalously hot and that the lithospheric mantle is very thin (Gök et al., 2003).

Shear wave splitting analysis indicates that there is no significant change in upper mantle polarization anisotropy across the Bitlis suture or the EAFZ. There also appears to be some correlation between very slow mantle lid velocity and large splitting lag times across the eastern portion of the Anatolian Plateau (Sandvol et al., 2003)

Results of this study from different period ranges imply a different S wave velocity disribution within the region. Starting models used for the surface wave inversions include both a 1-D model from a 12 ton dam shot recorded by ETSE (Gürbuz et al., 2004) and the models from the original receiver function inversions.

Rayleigh wave phase velocity is measured between 10 and 85 second periods. Phase velocity changes between 2.75 km/s for 10 second period and 3.9 km/s for the 85 second period. On the other hand, Love wave phase velocity is measured between 10 and 50 second periods. Phase velocity changes between 2.8 km/s for 10 second period and 4.40 km/s for 50 second period.

According to the results of S wave velocity versus depth we found that between 20 and 30 km depth there is a low velocity layer which has S wave velocity of 3.4 km/s. The thickness of the crust is calculated as 45 km.

S wave velocities in the middle of the array, where there is a triple junction, we find a low velocity zone. The thickness of the crust varies and variation in thickness of the crust can be attributed to the complexity of the region.

Zor et al.(2003) found a regional LVL with depth and thicknesses of average 15–25 km and approximately 10 km, respectively. Stations showing LVL are located in regions dominated by Neogene and Holocene volcanism and probably are underlain by partially molten uppermost mantle obtained from the study of Sn and Pn phases (Gök et al., 2000; Al-Lazki et al., 2003). Meanwhile, the absence of Lg and Sn arrivals crossing the middle portion of the network indicate strong attenuation in the crust as well as in the uppermost

mantle (Gök et al., 2000). The presence of the LVLs in the middle portion of the network is consistent with the presence of the young basaltic volcanics as well as the absence of Lg and Sn arrivals in the region.

Thickness of the crust, S wave velocity and depth of LVZ that is found are in agreement with the previous studies mentioned above.

Dispersion curves are sensitive to velocity averages rather than to specific details. Therefore, velocity models obtained by inverting surface wave dispersion curves are strongly dependent on the initial assumptions of layer thicknesses and the location of first order velocity discontinuities. It is more powerfull using joint invrsion of receiver functions and surface wave dispersion curves.

The results of ETSE studies yield a picture of the lithospheric structure and deformation beneath the northern Arabian plate and the Anatolian plateau. This picture and its interpretation are critical to improving our understanding of how continental collision works. Tectonic environment makes the East Anatolian plateau and Bitlis suture an excellent natural laboratory to study the early stages of continental collision, its consequences and evolution of continental lithosphere.

REFERENCES

Abramowitz, M. And I. A. Stegun, 1965, Handbook of mathematical functions, Dover Publications, Inc., New York, 73, 1395-1406.

Aki, and P. G. Richards, 1980, Quantitative seismology: Theory and methods, W. H. Freeman and Company, San Francisco.

Al-Lazki, Ali I., Seber, D., Sandvol, E., Türkelli, N., Mohamad, R. and Barazangi, M., 2003, Tomographic Pn velocity and anisotropy structure beneath the Anatolian Plateau (Eastern Turkey) and the surrounding regions, Geophys. Res. Lett., 30 (24), 6, 1-4.

Allen, C., 1975, Geological criteria for evaluating seismicity, Geol. Soc. Am. Bul., 86, 1041–1057.

Ambraseys, N. N., 1970, Some characteristic features of the North Anatolian Fault Zone, Tectonophysics, 9, 143–165.

Ammon C. J. and G. Zandt, 1993, Receiver structure beneath the southern Mojave Block, California, Bull. Seism. Soc. Am., 83, 737-755.

Ammon, C. J., 1991, The isolation of receiver effects from teleseismic P waveforms, Bull. Seism. Soc. Am., 81, 2504-2510.

Barka, A., and K. Kadinsky-Cade, 1988, Strike slip fault geometry in Turkey and its influence on earthquake activity, Tectonics, 7, 663– 684.

Ben-Menahem, A., and S. J. Singh, 1981, Seismic waves and sources, Dover Publications, Inc., New York.

Bhattacharya, S. N., 1983, Higher order accuracy in multiple filter technique, Bull. Seism. Soc. Am., 73, 1395-1406.

Bloch, S., A. L. Hales, 1968, New techniques for the determination of surface wave phase velocities, Bull. Seism. Soc. Am., 58, 1021-1034.

Bloch, S., A. L. Hales, and M. Landisman, 1969, Velocities in the crust and upper mantle of southern Africa from multimode surface wave dispersion, Bull. Seism. Soc. Am., 59, 1599-1629.

Braile, L. W., and G. R. Keller, 1975, Fine structure of the crust, inferred from linear inversion of Rayleigh wave dispersion, Bull. Seism. Soc. Am., 65, 71-83.

Brune, J. N., and J. Dorman, 1963, Seismic waves and Earth structure in the Canadian shield, Bull. Seism. Soc. Am., 53, 167-210.

Brune, J. N., J. E. Nafe, and J. E. Oliver, 1960, A simplifed method for the analysis and synthesis of dispersed wave trains, J. Geophys. Res., 65, 287-304.

Constable, S. C., R. L. Parker and C. G. Constable, 1987, Occam's inversion: A practical algorithm for generating smooth models from electromagnetic sounding data, Geophys., 52, 289-300.

Der, Z., R. Masse and M. Landisman, 1970, Effects of observational errors on the resolution of surface waves at intermediate distances, J. Geophys. Res., 75, 3399-3409.

Dziewonski, A. and D. L. Anderson, 1981, Preliminary reference Earth model, Phys. of Earth and Planet Int., 25, 297-356.

Dziewonski, A. M., and A. L. Hales, 1972, Seismology: Surface waves and Earth oscillations. Methods in computational physics, Vol 11. Academic Press, New York, 70-72.

Dziewonski, A., S. Bloch, and M. Landisman, 1969, A technique for the analysis of transient seismic signals, Bull. Seism. Soc. Am., 59, 427- 444.

Ewing, W. M., W. S. Jardetsky, and F. Press, 1957, Elastic waves in layered media, McGraw Hill, New York.

Gök, R ., Sandvol, E., Türkelli, N., Seber, D., and Barazangi, M., 2003, Sn attenuation in the Anatolian and Iranian Plateau and surrounding regions, Geophys. Res. Lett., 30 (24), 5, 1-4.

Gök, R., N. Türkelli, E. Sandvol, D. Seber, and M. Barazangi, 2000, Regional wave propagation in Turkey and surrounding regions, Geophys. Res. Lett., 27(3), 429- 432.

Gürbüz, C., N. Türkelli, T. Bekler, R. Gök, E. Sandvol, D. Seber, and M. Barazangi, 2004, Location and calibration using Eastern Turkey broadband seismic network: Analysis of the Ağrı Dam explosion, Bull. Seism. Soc. Am., 94, 1166-1171.

Haskell, N.A., 1953, The dispersion of surface waves on multilayered media, Bull. Seism. Soc. Am., 43, 17-34.

Hempton, M. R., 1985, Structure and morphology of the East Anatolian Transform Fault Zone near Lake Hazar, southeastern Turkey, Geol. Soc. of Amer. Bull., 96, 233–243.

Herrin, E., and T. Goforth, 1977, Phase matched filters: Application to the study of Rayleigh waves, Bull. Seism. Soc. Am., 67, 1259-1275.

Herrmann, R. B., 1973, Some aspects of band pass filtering of surface wave, Bull. Seism. Soc. Am., 63, 663-671.

Herrmann, R. B., 1987, Computer programs in seismology, Saint Louis University, St. Louis. MO.

Jackson, D. D., 1972, Interpretation of inaccurate, insufficient and inconsistent data, Geophys. J. Roy. Astron. Soc., 28, 97-110.

Julia, J., C. J. Ammon, R. B. Herrmann, and A. M. Correig, 2000, Joint inversion of receiver function and surface wave dispersion observations, Geophys. J. Int., 143, 1-19.

Keilis-Borok, 1986, Seismic surface waves in a laterally inhomogeneous Earth, V. I. ed., Klumer Academic Publishers, Boston.

Keskin, M., J. A. Pearce, and J. G. Mitchell, 1998, Volcano stratigraphy and geochemistry of collision related volcanism on the Erzurum-Kars Plateau, North Eastern Turkey, J. Volcanol. Geotherm. Res., 85, 355–404.

Keskin,M., 2003, Magma generation by slab steepening and breakoff beneath a subduction accretion complex: An alternative model for collision related volcanism in Eastern Anatolia, Turkey, Geophys. Res. Lett., (30) 24, X, 1-4.

Kovach, R.,1978, Seismic surface waves and crustal and upper mantle structure, Rev. Geophys. and Space Phys., 16, 1-13.

Larson, E. W., and G. Ekstrom, 2001, Global models of surface wave group velocity, Pure Appl. Geophys., 158, 1377-1400.

Lay T., and T. C. Wallace, 1995, Modern global seismology, Academic Press, San Diego.

Love, A. E. H., 1911, Some problems of geodynamics, Cambridge University Press, Cambridge, San Diego, 160-178.

McMechan, G. A. and M. J. Yedlin, 1981, Analysis of dispersive waves by wave field transformation, Geophysics, 53, 869-874.

McMechan, G. A. and R. Ottolini, 1980, Direct observation of a $(p-\tau)$ curve in a slant stacked wave field, Bull. Seism. Soc. Am., 70, 775-789.

Menke, W., 1984, Geophysical data analysis: Discrete inverse theory, Academic Press, Inc.

Mitchell, B. J., and R. B. Herrmann , 1979, Shear velocity structure in the eastern US from the inversion of surface waves group and phase velocities, Bull. Seism. Soc. Am., 69, 1133-1148.

Molnar, P.,1988, A review of geophysical constraints on the deep structure of the Tibetan Plateau, the Himalaya and the Karakoram, and their tectinic implications, Phil. Trans. R. Soc. London, 326, 33-88.

Mueller, S., 1977, A new model of the continental crust, In Geophysical Monograph 20: The Earth's Crust, Heacock, J. G., ed., Amer. Geophys. Union, Washington, D.C., 289-317.

Nataf, H. C., I. Nakanishi, and D. Anderson, 1986, Measurments of mantle wave velocities and inversion for lateral heterogeneities and anisotrophy-III. inversion, J. Geophys. Res., 91, 7261-7307.

Örgülü, G., M. Aktar, N. Türkelli, E. Sandvol, and M. Barazangi, 2003, Contribution to the seismotectonics of the Eastern Anatolian Plateau from moderate and small size events, Geophys. Res. Lett., 30 (24), 3, 1-4.

Percival, D. B., and A. T. Walden, 1993, Spectral analysis for physical applications: Multitaper and conventional univariate technique, Cambridge University Press, Cambridge.

Pilant, W. L., and L. Knopoff, 1970, Inversion of phase and group slowness, J. Gephys. Res., 15, 2135-2136.

Press, F., M. Ewing, and J. Oliver, 1956, Crustal structure and surface wave dispersion in Africa, Bull. Seism. Soc. Am., 46, 97-103.

Ritzwoller M. H., and A. L. Levshin, 1998, Eurasian surface wave tomography: Group velocities, J. Geophys. Res., 103, 4839-4878.

Russell, D. R., 1987, Multichannel processing of dispersed surface waves, Ph. D. Dissertation, Saint Louis University, St. Louis, MO.

Sandvol, E., N. Türkelli, and M. Barazangi, 2003, The Eastern Turkey Seismic Experiment The study of a young continent continent collision, Geophys. Res. Lett., (30) 24, 4, 1-4.

Sato, Y., 1955, Analysis of dispersed surface waves by means of the fourier transform, 1, Bull. Earthquake Res. Inst. Tokyo Univ., 33, 33-47.

Sato, Y., 1956, Analysis of dispersed surface waves by means of the fourier transform, 2, Synthesis of movement near the origin, Bull. Earthquake Res. Inst. Tokyo Univ., 34, 9-18.

Sato, Y., 1958, Attenuation, dispersion and the wave guide of the G wave, Bull. Seism. Soc. Am., 48, 231-251.

Şengör, A. M. C., S. Özeren, E. Zor, and T. Genç, 2003, East Anatolian high plateau as a mantle supported, N-S shortened domal structure, Geophys. Res. Lett., 30 (24), 8, 1-4.

Takeuchi, H., and M. Saito, 1972, "Seismic surface waves" In methods in computational physics, Vol. 11: Seismology: Surface waves and Earth oscillations, B. A. Bolt, (ed.), Academic Press, New York, 217-295.

Turin, G. L., 1960, An introduction to matched filters, I. R. E. Trans., IT-6, 311-329.

Türkelli, N., E. Sandvol, E. Zor, R. Gök, T. Bekler, A. Al-Lazki, H. Karabulut, S. Kuleli, T. Eken, C. Gürbüz, S. Bayraktutan, D. Seber, and M. Barazangi, 2003, Seismogenic zones in Eastern Turkey, Geophys. Res. Lett., (30) 24, 2, 1-4.

Wiggins, R. A., 1972, The general linear inverse problem: implications of surface waves and free oscillations for Earth structure, Rev. geophys. Space Phys., 10, 251-285.

Yu, G. K. and B. J. Mitchell, 1979, Regionalized shear velocity models of the Pacific upper mantle from observed Love and Rayleigh wave dispersion, Geophys. J. R. Astr. Soc., 57, 311-341.

Zor, E., Gürbüz C., Türkelli, N, Sandvol., E., Seber, D., Barazangi, M., 2003, The crustal structure of the East Anatolian Plateau from receiver functions. Geophys. Res. Lett., (30) 24, 7, 1-4.